Corrosion of Titanium and Titanium Alloys in Aqueous Acid Electrolyte

By

Peter W.A. Reid

B.A.Sc., Queen's University, 2001

A Thesis Submitted in Partial Fulfillment of the Requirements for the Degree of:

Master of Applied Science

In

The Faculty of Graduate Studies

Metals and Materials Engineering

We accept this thesis as conforming to the required standard

The University of British Columbia

July 2003

In presenting this thesis in partial fulfilment of the requirements for an advanced degree at the University of British Columbia, I agree that the Library shall make it freely available for reference and study. I further agree that permission for extensive copying of this thesis for scholarly purposes may be granted by the head of my department or by his or her representatives. It is understood that copying or publication of this thesis for financial gain shall not be allowed without my written permission.

Department of Metals & Materials Engineering

The University of British Columbia
Vancouver, Canada

Date July 15/2003

DE-6 (2/88)

Abstract

The corrosion characteristics of three dilute Ti alloys (ASTM 1, 2, and 7) in aqueous sulphuric acid electrolytes were studied using open circuit potential measurements, potentiodynamic techniques, and long term immersion testing. The effects of acid concentration, alloying addition, temperature, and the iron and chloride content of the electrolyte were examined.

The open circuit potential measurements resulted in Ti grade 7 coming to a higher open circuit potential with the electrolyte at approximately 0.07 V_{SHE}, while the rest potentials for Ti grades 1 and 2 were approximately -0.50 V_{SHE}. The difference is believed to be the result of Pd alloying additions, which act as a catalyst for reduction reactions on the surface of the active Ti alloys during crevice corrosion. By decreasing the required over voltage for the reduction of species such as H^+ to occur, a more oxidizing overall mixed potential of the system is achieved.

Potentiodynamic scanning around the corrosion potential of titanium alloys in sulphuric acid (H_2SO_4) yielded maximum corrosion rates of 4.9×10^{-5} mm/yr (0.002 mpy). In all cases corrosion rates increased with lower pH and higher Cl^- content.

Potentiodynamic testing of the $[Fe^{3+}]/[Fe^{2+}]$ redox couple shows limiting currents to be controlled by concentration polarization, and the kinetics of the overall reactions were faster on the surface of the more noble Pt electrode. Slopes were on the order of 150-300 mV/decade,

with exchange current densities of 10^{-7} and 10^{-4} for Ti and Pt respectively. All corrosion potentials were in the range of 0.5 to 0.7 V_{SHE}.

During the long-term immersion testing, Ti grade 7 proved to be more corrosion resistant than the commercially pure alloys due to the formation of a visibly thicker oxide layer. Preferential attack, when visible, was initiated on metallic iron and iron oxide impurities in the alloys and was observed on all immersion coupons.

Table of Contents

List of Figures

List of Tables

Acknowledgements

The author wishes to acknowledge his supervisory committee Dr. Desmond Tromans, Dr. David Dreisinger and Dr. Akram Alfantazi for providing the opportunity to perform this research and for support and guidance along the way. In addition, a very special thank you to James Vaughan, MASc. candidate at the University of British Columbia, for all of his help, intuition, and general face slapping when required. Thanks for the rides.

A special thanks to Jim Grauman of TIMET for providing all of the alloys and raw sample material used in this study, and Greg Gamble for helping to put this work in perspective. The author would also like to acknowledge Mary Mager for her help with SEM work and software support, and Ross and Carl for machining all of the samples used in testing. Recognition should also go to the University of British Columbia for providing equipment and financial assistance and to Bé Wassink and Anita Lam for their much appreciated laboratory assistance.

And last, but most importantly, the author would like to thank his fiancée, best friend, and confidante Natasha for her tireless efforts and unyielding assistance with the rest of the world while her worse half toiled nightly in the laboratory (believe it or not).

1 Introduction

1.1 Objectives

Recent increases in the application of the High Pressure Acid Leach Process (HPAL) to extract Nickel and Cobalt from laterite ores has prompted the use of higher strength, erosion and corrosion resistant autoclave (AC) liners. As Ti is one of only a few affordable and formable materials able to resist the high-temperature corrosive slurries that occur in the HPAL process, there has been a renewed interest in the corrosion mechanisms of these alloys under these conditions. Although this investigation will concentrate on some of the specific effects of the HPAL environment during the leaching of laterite ores, additional observations will be made as to the more general corrosion characteristics of this particular material and some of its more commonly applied alloys.

1.2 Project Scope

The investigation focused on DC polarization testing: open circuit potential measurements and potentiodynamic scanning around the corrosion potential of titanium alloys in sulphuric acid (H_2SO_4), and long term immersion testing of commercially pure Ti Grade 2 and the corrosion-resistant Ti grade 7 in similar aqueous mineral acid solutions. The potentiodynamic experiments provide insight into the values of the corrosion potential, exchange current

density, Tafel behaviour, and the effects of acid concentration, chlorides and temperature on each of these electrochemical characteristics. Coupled with qualitative observations and weight loss measurements from the long-term immersion testing, an estimated corrosion rate can be calculated. In addition, the effects of iron on the oxidation and reduction kinetics of the electrochemical reactions occurring were examined using the same potentiodynamic methods. The oxidation and reduction reactions and their associated kinetics occurring on the wetted surfaces of the AC are affected by alloy composition. Thus the type and morphology of scale formed and surface potentials observed during these reactions are different for various grades of titanium.

Specifically, this study will address the effects of the following on the electrochemical behaviour of Ti in aqueous sulphuric acid electrolytes:

i. Sulphuric acid concentration;
ii. Metal refinement and alloy composition;
iii. Iron and chloride content of the electrolyte;
iv. Temperature.

2 Literature Review

2.1 Description of the High Pressure Acid Leach Process

One of the more recent developments in the hydrometallurgical extraction industry is the industrial scale application of the HPAL Process for extraction of Nickel and Cobalt from nickeliferrous-laterites found in Western Australia (WA) and Cuba. The process involves the injection of sulphuric acid and a ground slurry of laterite ore into an AC, such as that shown in Figure 1, and leaching of nickel and cobalt at elevated temperatures (250-270°C) and pressures of up to 50 atm.[1][2][3] Laterite ores typically have a very complex mineralogy, varying in grade from deposit to deposit; and consequently leaching conditions are unique to the mine. The scope of this investigation is primarily limited to the effects of the laterite HPAL process on autoclave materials of construction in contact with feed slurries, and thus discussion will be limited to those ores.

Figure 1: Picture of a titanium clad AC in Murrin Murrin.[4]

In reference to their composition and leaching properties, ore bodies used in the WA HPAL process are termed "dry" ores. Dry ores typically have an overall Fe content of at least 21.6 wt.% and usually contain only 1.4 wt.% nickel and 0.125 wt.% cobalt. The bulk of the ore consists of complex compounds that dissolve and reprecipitate during leaching.[1] In excess of 80% of the WA ore blend is composed of non-reducing constituents such as smectite clays (nontronite) and saprolite. A typical assay (see Table 1) of a WA laterite ore body would show approximately: 15% limonite ore, 40-45% smectite clays with secondary silica and minor amounts of chromite and magnetite, 40% saprolitic ore (Ni rich) and minor amounts of talc, magnesite, secondary silica and chromite.[2][3] The effect of the excess nontronite and serpentine minerals in the WA laterite ores results in an increased average acid consumption (approx. 500 kg/t dry ore) over that of other ores.[2]

Table 1: Typical Compositions of Australian Laterite Leach Feed.[2][3][4][7][8][9]

Element	Conc. In Ore (wt%)	Constituent	W.A. Diluted Bore Water (mg/l)
Ni	1.0 - 1.54	**Cl^-**	52000 - 200000
Co	0.069 - 0.13	**Na**	30000
Fe	20.8 – 45	**Mg**	4200
Cr	0.66 - 2.0	**SO_4**	5500
Al	1.71 - 5.00	**Ca**	400
Mn	< 0.32	**K**	93
Mg	0.55 - 4.62	**Al**	<1
Na	1.10		
Si	18.4	**TDS**	104000
Fe:Al	4.3:1	**PH**	6.6-7.2

Laterite ores do not require grinding for metal liberation and the leaching process is fairly insensitive to ore particle size. The ore preparation circuit is mainly used to disaggregate the slurry and prepare the ore for injection into the AC, the result being a highly abrasive mixture.

In addition, process water is often saline ranging from moderately low to very high concentrations of total dissolved solids (TDS). This is the case with WA leaching operations. To reach in excess of 95% extraction of Ni and Co, the level desired for financial optimization, it has been found in lab, pilot, and commercial operations that the concentration of sulphuric acid at room temperature, or "free acid" concentration, in the final solution must be in the range of 30 – 50 gpl (0.3 – 0.5 M). But at temperatures above 150°C some of the less stable sulphate ions combine with a proton to produce the more stable bisulphate ion, HSO_4^-. This suggests the majority of the free acid measured at room temperature is actually present as a bisulphate ion at 250°C in the leach solution, which in turn means that even more free acid is required to generate the necessary protons (H^+). This problem is amplified when using saline process water, which further increases the minimum quantity of acid required for leaching of Laterite ores.[3][8]

2.2 Titanium Characteristics and Applications

Until the middle of the 1960's, titanium was primarily employed in the aerospace industry. Since then its low density, its high corrosion- and abrasion-resistant properties, and improvements in manufacturing methods have expanded its use to other areas involving highly aggressive environments that would quickly destroy other materials. Titanium alloys have been more than satisfactorily applied to service in marine environments, refineries, desalination systems, pulp and paper industries, the chemical process industry (CPI), and many

hydrometallurgical applications over a wide range of temperatures and varying conditions of pressure and pH.

Table 2:Ti Alloy Designations, Compositions and Strengths.[10]

Common Alloy Designation	UNS Number	ASTM Grade	Nominal Composition (%)	Ultimate Strength (MPa)	Yield Strength (MPa)
Group I: Commercially Pure Titanium					
Grade 1	R50250	1	0.06 O	240	170
Grade 2	R50400	2	0.12 O	345	275
Grade 3	R50550	3	0.2 O	450	380
Grade 4	R50700	4	0.3 O	550	483
Group II: Low Alloy Content Titanium with Pd/Ru Additions					
Grade 2, Pd	R52400	7	0.12 O, 0.15 Pd	345	275
Grade 1, Pd	R52250	11	0.06 O, 0.15 Pd	240	170
Grade 2, low Pd	R52402	16	0.12 O, 0.05 Pd	345	275
Grade 1, low Pd	R52252	17	0.06 O, 0.05 Pd	240	170
Group III: Other α and Near-α Alloys					
Ti 5-2.5	R54520	6	5 Al, 2.5 Sn	828	793
Ti 3-2.5	R56320	9	3 Al, 2.5 V	620	483
Grade 12	R53400	12	0.3 Mo, 0.8 Ni	483	345
Ti 3-2.5, Low Pd	R56322	18	3 Al, 2.5 V, 0.05 Pd	620	483
Ti 3-2.5, Ru	R56323	28	3 Al, 2.5 V, 0.1 Ru	620	483
Ti 5111	R55111	32	5 Al, 1 Sn, 1 Zr, 1 V, 0.8 Mo	689	586
Group IV: α–β Alloys					
Ti 6-4	R56400	5	6 Al, 4 V	895	828
Ti 6-4 ELI	R56407	23	6 Al, 4 V, 0.13 O max	828	759
Ti 6-4 ELI, Ru	R56404	29	6 Al, 4 V, 0.1 Ru, 0.13 O max	828	759
Group V: β Alloys					
β–C	R58640	19	3 Al, 8 V, 6 Cr, 4 Zr, 4 Mo	793	759
β-C, Pd	R58645	20	3 Al, 8 V, 6 Cr, 4 Zr, 4 Mo, 0.05 Pd	793	759
β 21S	R58210	21	15 Mo, 2 Al, 2.7 Nb, 0.25 Si	793	759

2.2.1 Use of Ti and Its Alloys in the Chemical Process Industry

Titanium's more than 30-year history of applications in the CPI as piping, valves, heat exchangers and agitation equipment has tested this material under a wide variety of extreme service environments. However, the scope of this study has been limited to testing the alloys utilized primarily in the WA HPAL process and similar conditions, namely the ASTM designated grades 1, 2, and 7 (UNS R50250, R50400, and R52400 respectively). Grades 1 and 2 are recognized as unalloyed materials, although they usually have trace amounts of oxygen and iron present as impurities, with Grade 1 being slightly more refined. Although Ti grade 1, containing a typical Ti content of 99.8%, possesses the greatest ductility with excellent cold formability, it lacks strength in comparison to other grades.[11] In light of this, Ti grade 2 is the most widely used of all the commercially pure grades and represents approximately 95% of the overall Ti usage in the CPI.[11] From this base metal (with Ti content of typically 99.6%)[11], more exotic grades have been developed for better formability, strength, ductility, and corrosion resistance. Ti grade 7 is such a product, being equivalent to grade 2 in all physical and mechanical properties. However, by the addition of anywhere between 0.12 to 2.5 wt% Pd (average 0.15%) the result is a significant increase in crevice corrosion resistance above that of grades 1 or 2. Ti grade 7 can withstand up to 47% by weight acid concentration in the presence of sulphuric acid at room temperature, much improved over the mere 5 wt% H_2SO_4 capabilities of the commercially pure grades.[11]

The interiors of most of the six WA AC were built of grade 1 titanium clad (explosion bonded) to carbon steel. One of the other AC was constructed of grade 11 and another from

grade 17. Cladding thickness among the vessels ranges from 6 to 8 mm with the base steel thickness typically 100 mm.[1] Grades 2 and 7 can also be found within the AC agitation mechanisms and in weld repairs, not to mention T joints and elbows in piping to and from the vessels. A general rule for the application of Ti is that it should not be specified if it exhibits a general corrosion rate above 0.125 mm/yr.[1]

2.2.2 Explosion Bonding Techniques

Whereas Gr. 2 can be considered the workhorse of the non-aerospace industry, Gr. 1 is most often selected for applications requiring high formability.[10] This is why WA AC linings are made from Ti grade 1 sheet explosion bonded to the interior surface of a steel pressure vessel. Thus, there are no structural stresses imposed on the Ti metal itself and it can be viewed as more of a lining than a structural entity. In addition, the nature of the explosion bonding process (also known as explosion welding) is a "cold" welding process utilizing sound waves as the energy source for bonding. The gas expansion of the explosive detonation (V_d) accelerates the cladding plate across the "stand-off" gap resulting in an angular collision between the two materials at the specified collision velocity (V_p). The result is a wavy mechanical bond between the Ti and steel somewhat akin to a high angle grain boundary (see Figure 2).[12] Thus there is no alteration of the microstructures and, in theory, no residual stresses left in the cladding or the base material. This suggests the metals can be examined in this study as rolled and without having to be bonded to the steel substrate.

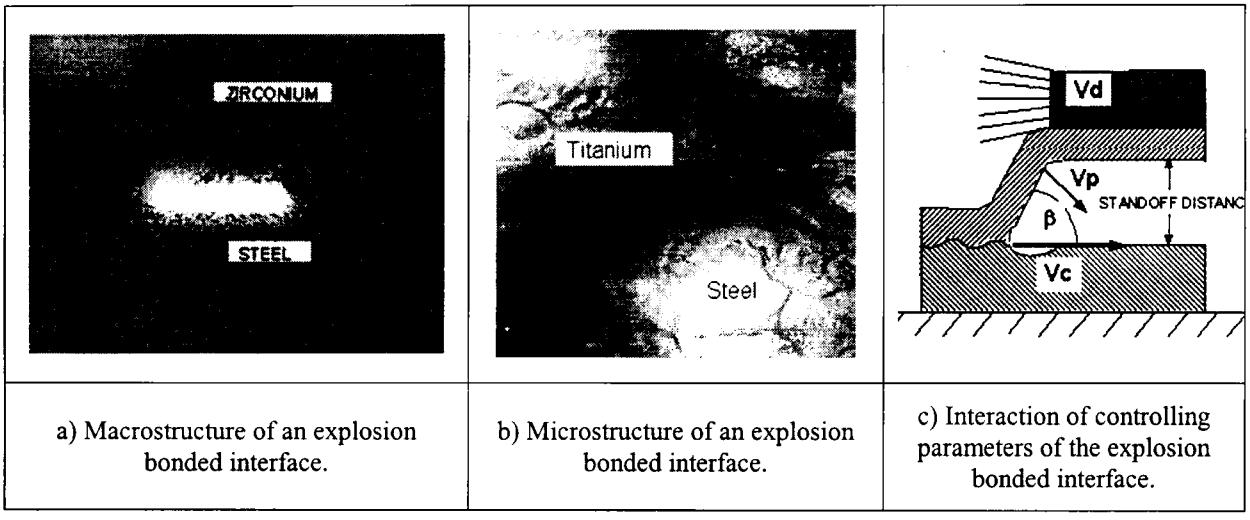

a) Macrostructure of an explosion bonded interface.

b) Microstructure of an explosion bonded interface.

c) Interaction of controlling parameters of the explosion bonded interface.

Figure 2: The metal bond and controlling parameters of the explosion bonding process, where V_p is the plate collision velocity and V_c is the impact point velocity, which is equal to V_d, the explosive detonation velocity.[12]

2.3 The Metal

Titanium and its alloys have become attractive alternatives to the heavier nickel and stainless steel alloys because of their unique physical and chemical properties. Physically, titanium exhibits minimum yield strengths greater than copper-nickel alloys and 316 stainless steel, around 275 MPa for commercially pure grades, while retaining a significantly lower elastic modulus of 110 GPa, providing improved shock properties and ease of fabrication. However, it is primarily the electrochemical properties of titanium that are of interest to this investigation.

Pure Ti undergoes an allotropic transformation from hcp (α) to bcc (β) when heated past 882.5°C.[13] Substitutional or interstitial solutes that increase the transition temperature are known as α stabilizers, while those alloying additions which decrease the transition temperature are β stabilizers and are generally the transition and noble metals. In most alloys, both the α and β phases are present and a third category must be created. For this reason, Ti alloys are classified as single phase α, single phase β, or two phase (α+β) based on their equilibrium structure at ordinary temperatures. Those classified as α alloys are known to possess satisfactory strength, toughness, creep resistance, and weldability, a property of the resulting hcp structure.[13] The β alloys are extremely formable, but because of their bcc structure are prone to the previously mentioned ductile-brittle transformation. Combining the properties of both phases in α+β alloyed Ti will exhibit good fabricability and high strength at reasonable temperatures. The Ti alloys currently used in high temperature, highly corrosive applications are alloyed with either oxygen alone as an impurity or oxygen plus a combination of noble and transition elements, and are therefore typically single-phase α or two-phase alloys. The binary phase diagrams for these materials can be found in Appendix B: Materials Characterisation.

Elements alloyed with Ti can be separated into two groups: those that improve alloy strength and those that improve corrosion resistance. Oxygen and iron improve the overall strength of the material, by stabilizing the α and β phases respectively as mentioned before, but impair or decrease the ductility. Alloying with other elements, such as V, Pd and Mo, shifts the metal's rest potential in a noble direction, increasing the resistance to corrosion.

Also, minor alloying additions of platinum group metals have been proven to significantly enhance crevice corrosion resistance.

There are numerous titanium alloys available commercially, but most can be categorized into a few main types based on alloy composition and mechanical properties as seen in Table 2. Those alloys of significance to high temperature, extractive metallurgy applications are mainly ASTM grades 1, 2, 7, 11, 12 and 17, which are used in piping, heat exchangers and autoclave interiors. These alloys are chosen on the basis of their formability, strength, corrosion- and erosion-resistant properties as well as their low maintenance and excellent service records in previous applications.

2.4 The Oxide

Alone, titanium is a very reactive material ($E^{o}_{Ti/Ti2+} = -1.63\ V_{SHE}$)[10] with a high affinity for oxygen and will oxidize instantly when subjected to even trace amounts of oxygen or water, resulting in a stable, adherent surface oxide layer. Films grown at faster rates are typically amorphous in structure and much stronger than those grown slowly, which form a crystalline microstructure, though they are not as stable in creviced situations.[10] [14] The uniform distribution of pores present in the amorphous coating serves to blunt cracks and improve toughness. Whether amorphous or crystalline, this layer protects the underlying metal and provides the specific erosion- and corrosion-resistant properties that are of use to industry. In

both cases, the oxide acts as an impenetrable barrier, impervious to most chemical process streams with mechanical strengths up to 2.5 GPa.[1] And if properly maintained with even a small supply of air or water (less than 2 ppm O_2, or H_2O), this barrier will instantly be repaired if harmed by mechanical damage or erosion.

TiO_2 can be found naturally and in abundance in the form of rutile and has to date been used extensively as white coloured pigment in various applications. Rutile is the high temperature phase of this oxide, following an irreversible transformation from the low temperature phase anatase, which occurs at approximately 700-900°C.[14] Rutile is also the more common titanium dioxide and is more stable than anatase by ~12 kJ/mol.[10] Although it may be the more common and more stable phase at room temperatures, the alternate anatase phase is considered to be metastable at all temperatures and is often found intermixed with rutile in polycrystalline materials.[14] Both phases are tetragonal in structure and hence there is little or no volume change associated with this transformation. TiO_2 may also take on the form of brookite, an orthorhombic structure again considered to be metastable at all temperatures, however it is considered a temporary transition phase and is rarely observed in practice. Occasionally, a perovskite structure may form as well; but this structure is still under investigation and deemed irrelevant to the context of this review.

It is generally agreed that the passive films of Ti consist of at least one of the forms of TiO_2 meaning they have a composite structure, which can include TiO (more evident in the early stages of formation). Passive films are resistant to breakdown by the action of aggressive ions such as chlorides, but their protectiveness can be breached through chemical dissolution in

reducing environments. Spatially localized film breakdown can occur through the action of aggressive ions, and via abrasion or erosion of the film itself.[18]

Electronically, Ti ions in TiO_2 have a Ti^{4+} ($3d^0$) electron configuration with the highest filled Ti orbital being the 3p, which is approximately 35 eV below the Fermi level. TiO_2 is a wide band-gap semiconductor whose valence band is predominantly O, and the conduction band is predominantly Ti 3d, 4s, 4p orbitals. The bulk band gap is approximately 3.1 eV.[13]

2.5 Corrosion of Titanium Alloys

2.5.1 General Corrosion Mechanisms

In most service conditions, the general corrosion rates for Ti alloys are negligible because of the tough surface oxide. Corrosion resistance can be further improved by heating in air (500-800°C) to increase the oxide thickness.[1][20] The breakdown of this film requires the presence of reducing, acidic conditions that are easily avoided by even trace elements of many oxidizing species found in most process conditions. Metal ion contaminants, such as Fe, Cu, Mn, Na, Sn and even Ti^{3+} and Ti^{4+} ions, act as corrosion inhibitors by creating oxidizing conditions that will stabilize the protective film in reducing media, such as the strong mineral acid H_2SO_4 found in HPAL processes. The presence of these ions effectively shifts the rest potential in a noble direction relative to the corrosion potential (E_{corr}) of the system. For example, the addition of 100 ppm of Cu^{2+} has been found empirically to reduce the corrosion

rate of grade 2 more than a thousand fold in 20% sulphuric acid at 100°C.[1] In addition, dissolved oxygen in the process slurry from air sparging further reduces corrosion rates by maintaining the metal ions in their highest oxidation states. To date, titanium is also the only structural metal in use that has no history of direct attack from microbiologically induced corrosion.[10]

Hydrogen absorption is possible at high temperatures, in process streams or slurries with a maximum of 2% oxygen or moisture content.[10] Should concentrations of dissolved oxygen exceed this level, the metal is passivated and the properties of the protective oxide layer will again prevail. But in alkaline environments with basic conditions (pH > 12), temperatures in excess of 80°C and potentials less noble than –700 mV SCE, Ti can be embrittled due to H uptake and diffusion and will form titanium hydrides.[21] Fortunately, *massive* hydriding requires the simultaneous occurrence of three separate conditions involving temperature, chemical composition and kinetics.[23] First, the temperature must be above 80°C for hydride formation. Secondly, the pH of the environment must be less than 3 or greater than 12, strongly acid or basic conditions. Finally, for hydriding to occur, a source or mechanism for generating atomic hydrogen must be present. The passive film was found to help protect the underlying Ti from absorption of electrolytic hydrogen at potentials positive of a certain threshold potential (-0.6 V_{SHE}), close to the flat band potential of the semiconducting oxide film.[22]

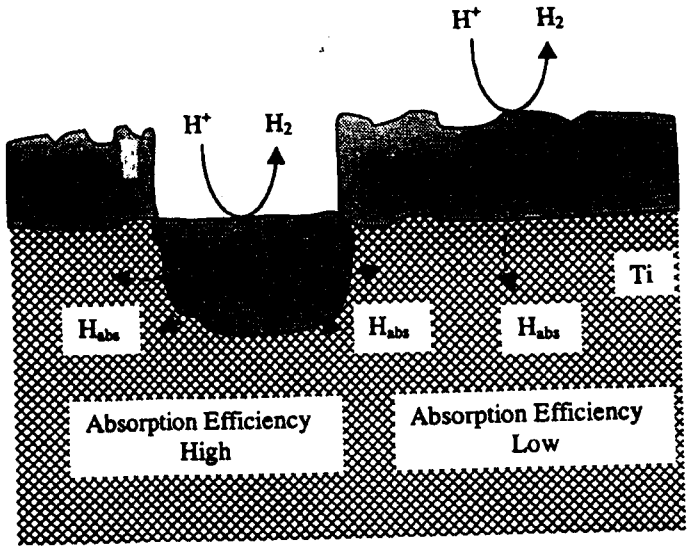

Figure 3: Pictoral representation of H absorption on the Ti surface. The left shows the case when no oxide is present, while the right has a thick oxide on the metal surface.[23]

Although *massive* hydriding is a rare occurrence in most service conditions, it is quite common to observe this phenomenon on a smaller scale in association with crevice corrosion. The oxide surface layer formed during initial oxidation may block dissolution but does not prevent the diffusion of hydrogen into the metal. At high temperatures, hydride precipitates may produce very thin films, in the form of platelets, with significant diffusion and penetration of hydrides into the metal wall. Hydride sheets create local stresses causing H embrittlement leading to micro-crack formation, especially in regions where the passivation is not homogeneous, such as that shown on the left side of Figure 3.[23] The cracks can subsequently lead to mechanical failure, or more often to sites for the initiation of crevice corrosion, hence titanium hydrides are often observed in the metal surrounding micro crack openings.

2.5.2 Crevice Corrosion of Titanium Alloys

Although titanium hydriding is the major cause of localized crevice corrosion, which most often occurs in narrow fissures where oxygen levels are low and a stagnant electrolyte solution is present, crevices can also be the result of adhering process stream deposits or scales. Scales support acidic reducing conditions within the crevice between the metal and the deposit by diffusion or simple migration if the scale is porous. The result is usually irregular shaped open mouth pits with high aspect ratios. It should be noted that commercially pure Ti is resistant to crevice corrosion below 80°C, while corrosion resistant grades, such as Ti grade 7, can extend this temperature to 260°C.[1][11][24][25] The severity of the attack on the material depends on many factors including the crevice geometry, solution composition and temperature, alloy composition, and the occurrence of an accompanying reduction process for hydrogen evolution. Ti alloys are more susceptible to pitting and crevice corrosion at elevated temperatures when the chloride ion concentration (in the form of NaCl) is increased.[18][38]

Initially, metal within the crevice will oxidize and consume dissolved oxygen or other oxidants at a rate faster than can be maintained by diffusion from the bulk solution. The interior of the crevice will become anodic while the surrounding surface is essentially cathodic. While the reduction process outside the crevice continues, the metal inside is dissolved into solution without being able to form the protective oxide, as shown in Figure 4. After sufficient oxidation within the crevice has occurred to alter local crevice chemistry, Cl^- ions will diffuse from the bulk solution to maintain charge neutrality and will increase the concentration of Ti^{3+} and Ti^{4+} ions by raising the passive current density of the alloy surface within the crevice.

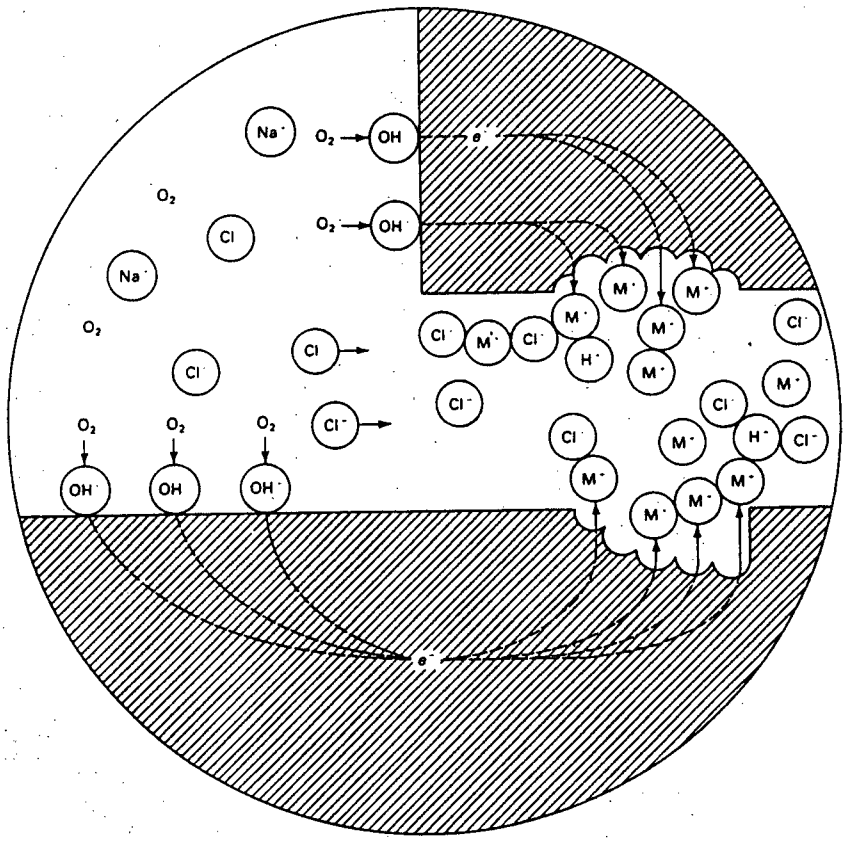

Figure 4: Pictoral representation of crevice corrosion. Dissolution of metal ions within the crevice draws negatively charged Cl ions into the crevice to preserve mass and charge balance. The unstable chloride and oxychloride intermediate compounds formed are subsequently hydrolysed to form free acid, lowering the pH of the crevice.[70]

Ti cations will then react to form unstable chlorides and oxychlorides that can be hydrolyzed to form titanium oxides like rutile, again raising the acidity in the process according to electrochemical equation 1 below.[10]

$$2Ti + O_2 + 2H_2O = 2TiO_2 + 4H^+ + 4e^- \quad (1)$$

This is regarded as the initiation phase: when the diffusion of oxygen into crevice is slower than its depletion through cathodic reaction. During this phase three stages occur: deoxidation, hydrolysis (or acidification) and the formation of a crevice solution with properties critical for corrosion of the material (also known as the activation stage). The next phase to occur is the propagation phase causing extensive attack involving a rapid increase in the corrosion current, and the onset of rapid corrosion until the accumulation of corrosion products at the mouth of the crevice induces a resistance large enough to halt the reaction. The initiation phase occurs much more rapidly than the propagation phase.

The role of oxygen solubility in the crevice corrosion of Ti is complex. As temperature increases, the solubility of oxygen decreases gradually until a minimum is reached, altering the rate of mass transfer and the kinetics of the dissolution and reduction reactions. Past the minimum, as the temperature continues to increase, the solubility of oxygen increases again and will be even greater at temperature (~225°C), speeding the external cathodic reaction rate. However, the presence of other dissolved species in solution, such as chlorides or sulphates, will limit the overall solubility of oxygen in solution because of a decrease in the molar volume of the solvent, in this case water.[14] Thus the resulting solubility is difficult to predict without empirical information. It has been found that at $T > 80°C$ (close to the minimum level of oxygen solubility) Ti is subject to attack via crevice corrosion in the presence of Cl, Br, I, F or sulphate-containing aqueous solutions.[39] From this information, the author suggests the reduction of oxygen to be a minor factor in the crevice corrosion of Ti, and instead the effects of hydrogen reduction should be taken into consideration as the cathodic half of the corrosion

reaction. As suggested by McKay and Mitton, the reduction of H^+ in the crevice can account for as much as 90% of the total corrosion.[15]

2.6 Scale Formation in the HPAL Process

As mentioned previously, conditions within HPAL processes typically operate with between 30 and 50 gpl H_2SO_4 (0.3 and 0.5 M H_2SO_4) at temperatures of 250-270°C and total atmospheric pressures around 5 MPa. During the process, scale is deposited on internal surfaces. This scale is comprised of mainly of hematite (Fe_2O_3), jarosite ($XFe_3(SO_4)_2(OH)_6$, X = H_3O^+, Na^+, K, etc.) and alunite ($XAl_3(SO_4)_2(OH)_6$, X = H_3O^+, Na^+, K^+, etc.) (Figure 5). Scale growth rates ranged from 167 mm/yr in the first AC to 13 mm/yr in the last AC during a bench scale test performed in a series of AC leaching WA laterites. This was significantly greater than growth rates found for "wet" equatorial tropical laterites during the same testing, which were shown to produce scale at a rate of 90 mm/yr and <1 mm/yr for first and last AC respectively.[2] Major mineralogical components of the scale were members of the alunite group, hematite and amorphous silica. Scale deposited on the static AC surfaces during leaching of WA laterite was found to have a higher degree of porosity relative to that deposited on agitator blades. Temperature, acid concentration, location within the AC, whether it is a moving or static surface, process water salinity, and hydrodynamics, as well as the initial ore composition can each dramatically affect scale morphology and physical characteristics.

Figure 5: Scale deposits formed on AC agitator and lid from WA laterites. (122 hrs @ 250°C, 0.3 M free H_2SO_4)[2]

At temperatures of 250-280°C, Fe is re-precipitated from solution, mainly as hematite [Fe_2O_3], with some as jarosite [$HFe_3(SO_4)_2(OH)_6$] unless in saline waters where natrojarosite may be present [$NaFe_3(SO_4)_2(OH)_6$] as a significant component. As the salinity can often affect the acid consumption and nature of precipitate by-products formed, it is carefully controlled within the process.[3][8] The precipitation of the hematite layer adjacent to the AC

walls occurs via the hydrolysis of iron (III) sulphate as generated by the leaching of laterites and is represented by:

$$Fe_2(SO_4)3 + 3H_2O \rightarrow Fe_2O_3 + 3H_2SO_4 \qquad (2)$$

While in the presence of NaCl, such as in the WA laterite process, the formation of natrojarosite and natroalunite from leach liquors can be represented as:

$$3X_2(SO_4)_3 + 2NaCl + 12H_2O \rightarrow 2Na(X)_3(SO_4)_2(OH)_6 + 2\,HCl + 5H_2SO_4 \qquad (3)$$

Where $X = Fe^{3+}$ or Al^{3+}.

The scale formed is typically reddish brown in appearance, no doubt from the presence of Fe^{3+}, and is visibly crystalline. At a given temperature, scales formed on static and agitating surfaces are similar, meaning hydrodynamics plays a minor role in influencing scale composition. Temperature can also affect the amount of hematite present.[2] However, in regions of high acidity, scale formation can be a problem. As the pH decreases the morphology of the scale precipitates gradually changes from platelets to spheres, improving the solid/liquid separation properties of the residue by forming smaller pores.[9][7]

2.7 Previous Studies on Ti Alloys

Curently, the published investigations into the behaviour of Ti and its alloys in aqueous sulphuric acid environments are somewhat limited. To date many of the corrosion studies of this alloy have involved applications in alkali conditions such as pulp and paper leaching, acid conditions in radioactive waste containment vessels, or simulated bodily fluids studied in Ti implant research.

J.J. Noel studied the corrosion resistant behaviour of titanium and several of its dilute α-phase alloys in aqueous solutions by altering temperature, pH, and solution composition.[22] The barrage of experiments included open circuit potential measurements, DC electrochemical polarization scanning, and electrochemical impedance spectroscopy. Following electrochemical testing, analyses were performed on corroded samples using X-ray Photon Spectroscopy (XPS), optical microscopy, and Auger Electron Spectroscopy (AES).

N.T. Thomas and K. Nobe at the University of California also studied the anodic and cathodic behaviour of Ti in 1 N sulphuric acid in the absence and presence of chlorides in aqueous media. Employing rotating electrodes made from Ti 65A (0.023%C, 0.25%Fe, 0.01% N_2, 0.2% O_2), rotating at tangential velocities of 6.6 cm/sec, they performed anodic polarization experiments potentiostatically as well as galvanic polarization experiments to study the HER Electrode potentials. More specifically, the anodic behaviour of titanium in sulphuric acid solutions of pH from 0.25-2.00, as well as the effect of chlorides on the HER

occurring on the surface of the electrodes was examined. Solutions were deaerated with pre-purified nitrogen before experimental runs and the temperature of the cell was maintained at 24 °C. The Standard Calomel Electrode (SCE) was the electrode of choice.[40]

In addition, Hua et al studied Alloy 22 and Ti Grade 7 using standard methods for immersion testing over a period of four to eight weeks. They found that imperfections (precipitates, inclusions, stringers, pores etc.) inherited form materials processing often served as the sites of preferential dissolution, or "traps" for corrosion products. In this case, however, the samples were mounted using the multiple crevice assembly method described in ASTM G78-98.[68]

Testing methods chosen for this study included a combination of those listed above. By measuring the resulting open circuit potentials of different alloys in the same environment and combining this with potentiodynamic polarization in cathodic and anodic regions it is possible to evaluate the electrochemical behaviour of the Ti alloys both qualitatively and quantitatively. During DC polarization testing, exposed surfaces of the alloys were subjected to 3 and 4 month, long-term immersion testing to simulate AC conditions during HPAL leaching. From these results, weight loss data and calculated penetration rates can be ascertained. Finally, anodic and cathodic scanning performed on Pt and Ti rotating electrodes in the presence of ferric and ferrous ions at different concentrations produced information on the kinetics of the reactions occurring at the interface between the metal and electrolyte.

3 Experimental

3.1 Development of E-pH Diagrams

Development of the experimental E-pH diagrams was accomplished using the standard equations (eq. 6 - 9).

$$E = E^{o} - 2.303\frac{RT}{nF}\log K \tag{4}$$

Where R in this case is the gas constant (8.314 J/K mol), F is Faraday's constant (96485 C/mol) and K is the equilibrium constant dependant on the activities of species solution, such as the dissociation of sulphuric acid for example:

$$K = \frac{a_{prod}}{a_{reac}} \tag{5}$$

$$pH = -\log[a_{H+}] \tag{6}$$

$$\Delta G = -nFE = -RTln(K) \tag{7}$$

Where a_{prod} is the product of the activities of the species produced, a_{react} is the product of activities of the reactants, and a_{H+} is the activity of dissolved hydrogen ions. Extrapolation to

higher temperatures, when heat capacity quadratics were unavailable, was calculated using methods described by the Criss-Cobble theory[37] The electrochemical and thermodynamic data are included in Appendix A: Thermodynamic Data for E-pH Diagrams.

The E-pH diagrams shown in Figure 6 and Figure 7 were calculated at room temperature with sulphur ion activity taken to be unity and metal ion activities of 10^{-3} and 10^{-6} respectively. The result of decreasing metal ion activity is to shift the regions of Ti^{3+} stability into higher pH regions and to increase the stability of the hydrated oxide in the presence of reducing acids. Also, a lower metal activity allows for the formation of $HTiO_3^-$ at higher pH, but alkaline conditions were never reached in this study so this region was not investigated.

The E-pH diagrams developed suggest that as potential is increased one stable hydride and three dissolved species can exist in aqueous sulphate solutions in the range of potential and pH used for this testing. Ti ions hydrolyze through the following reactions [10]:

$$Ti^{4+} + 2H_2O \rightarrow [TiO_2]^{2+} + 2H^+ \quad (8)$$

$$Ti^{4+} + 4H_2O \rightarrow Ti(OH)_4 + 4H^+ \quad (9)$$

Boundaries between these regions of stability for hydride and metal cation, metal cation and oxide cation, and the oxide cations occur at approximately -0.75 V_{SHE}, 0.3 V_{SHE} and 1.8 V_{SHE} respectively. Perhaps of most interest are the transitions from the metal ion to oxy-cation complexes and the oxidation of these complexes to the TiO_2^{2+} ion above 1.8 V_{SHE}. In terms of

the electrolyte itself, the SO_4^- ion is stable at all pH above 0.5 V_{SHE} with hydrogen sulphide as the major species present below this potential.

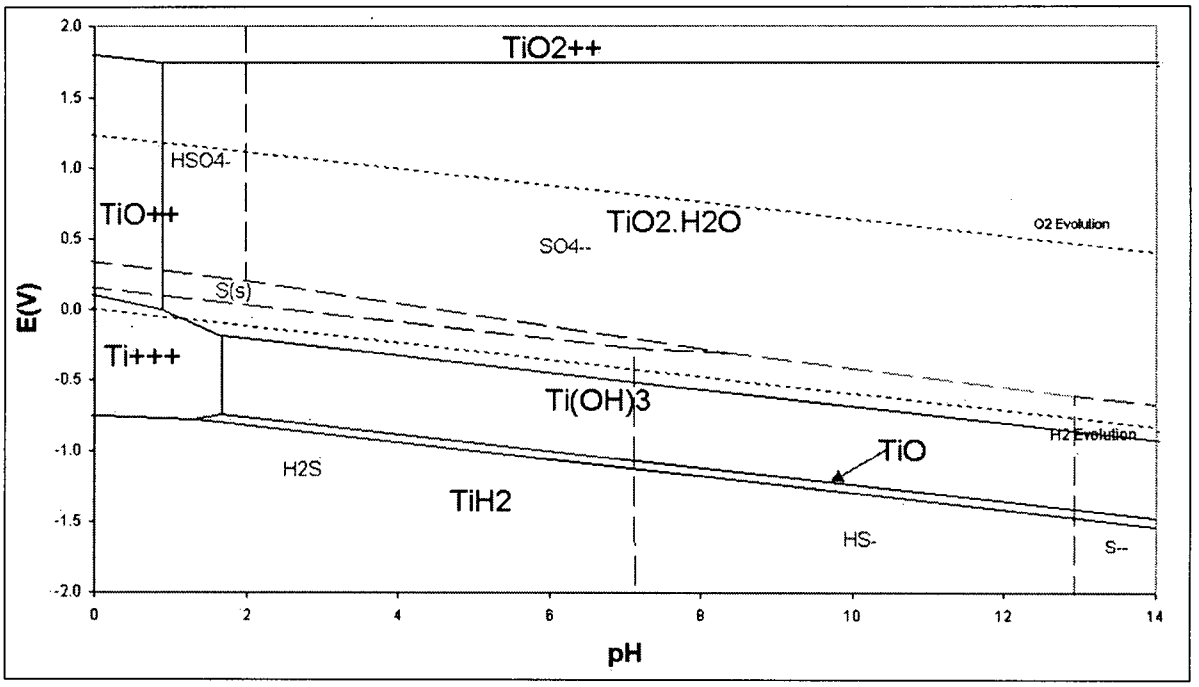

Figure 6: E-pH diagram for Ti-S-H_2O system at room temperature. Metal ion activity of 10^{-3}, sulphur activity of 1.

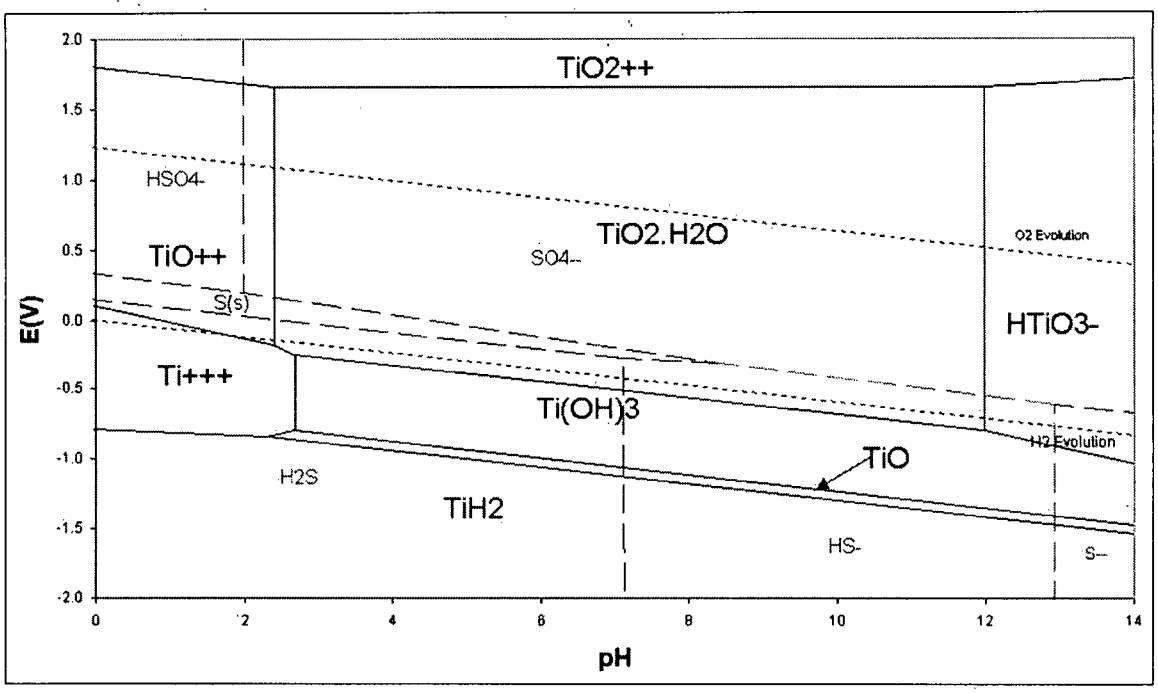

Figure 7: E-pH diagram for Ti-S-H_2O system at room temperature. Metal ion activity of 10^{-6}, sulphur activity of 1.

Figure 8 depicts the extrapolation of the E-pH data into 200°C, temperatures similar to those in the HPAL process. The increase in temperature would appear to have the same effect as decreasing metal ion activity and shifts the pH regions of ion stability further to the right into higher pH. The effects of this in the HPAL process would be difficult to determine given the decrease in acidity at higher temperatures from the formation of bisulphate ions.[60]

Temperature, however does not appear to have a large effect on the potentials in the pH regions of interest. Between pH = 0 and pH = 1, the slopes of the phase boundaries are not greatly affected. This also holds true for the effects of metal ion activity.

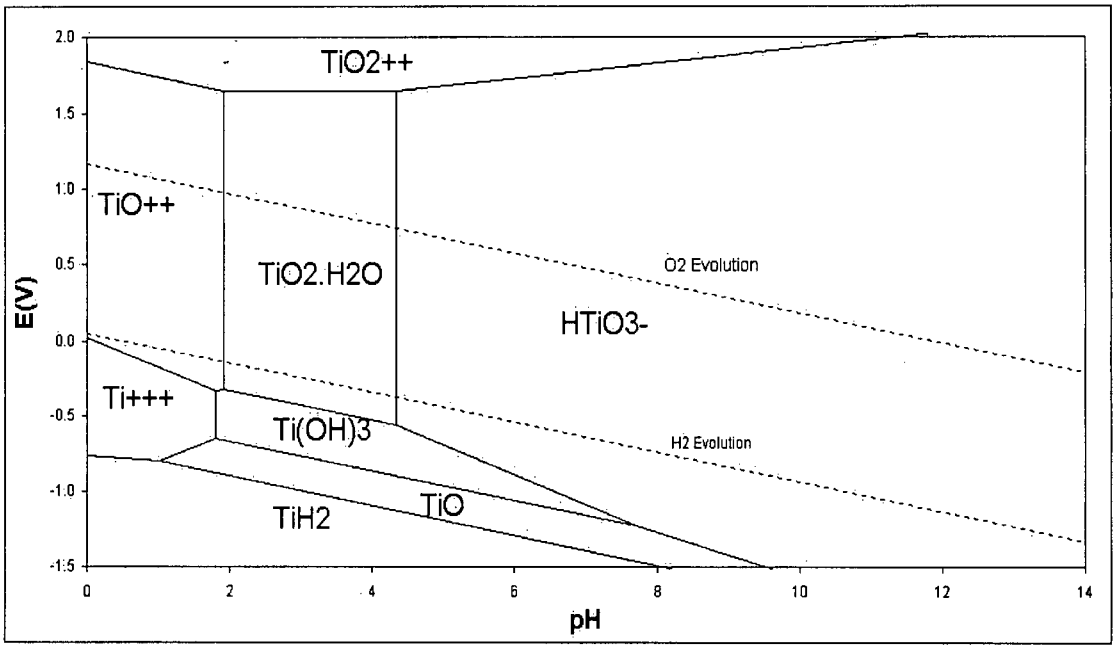

Figure 8: E-pH diagram for the Ti-H_2O system at 200°C. Metal ion activity of 10^{-6}. Extrapolations made using empirical formulas when available and the Criss-Cobble Theory. [38]

3.2 Materials Characterization

The specific titanium samples used for testing were provided by the Titanium Metals Corporation (TIMET) and included the commercially pure ASTM grades 1 and 2, and ASTM grade 7; the latter designed to be highly crevice corrosion resistant. The samples were sheared or punched (using a 5/8" diameter punch) from cold rolled sheets, which had been already reduced by approximately 50% and annealed. Each grade was characterized using XPS, X-ray Diffraction (XRD) and Scanning Electron Microscopy (SEM) techniques. All grades were confirmed to be α structured alloys (hcp). For Ti grades 2 and 7, Energy Dispersive X-ray

Spectroscopy (EDS) maps of Fe and Pd concentrations were also performed. The raw data from these examinations can be found in Appendix B: Materials Characterisation.

Figure 9 and Figure 10 show the result of progressively etching and taking XPS scans of the Ti layers to reveal the concentration of major constituents as a function of depth. As expected, the concentration of Ti increases with etch depth while oxygen concentration decreases. In addition, there appears to be a point approximately 4 μm into the surface where the concentration of Ti and the concentration of O are equal. This is probably the point where the oxide meets the metal surface as the oxygen concentration approaches a steady value with depth. There was no change in the concentration of iron in the commercially pure alloys as the depth was increased, and the iron content in Ti grade 7 was below detection limits. Similarly, the concentrations of Pd expected in Ti grade 7 are below XPS detection limits. This work was performed by the CANMET laboratories using a PHI model 5700 S XPS with PHI ACCESS and MULTIPAC software for data collection and processing (curve-fitting). As XPS can approximate the level of element speciation (chemical forms and oxidation states) at or near the surface of these materials, the surface oxide was found to contain primarily TiO_2.

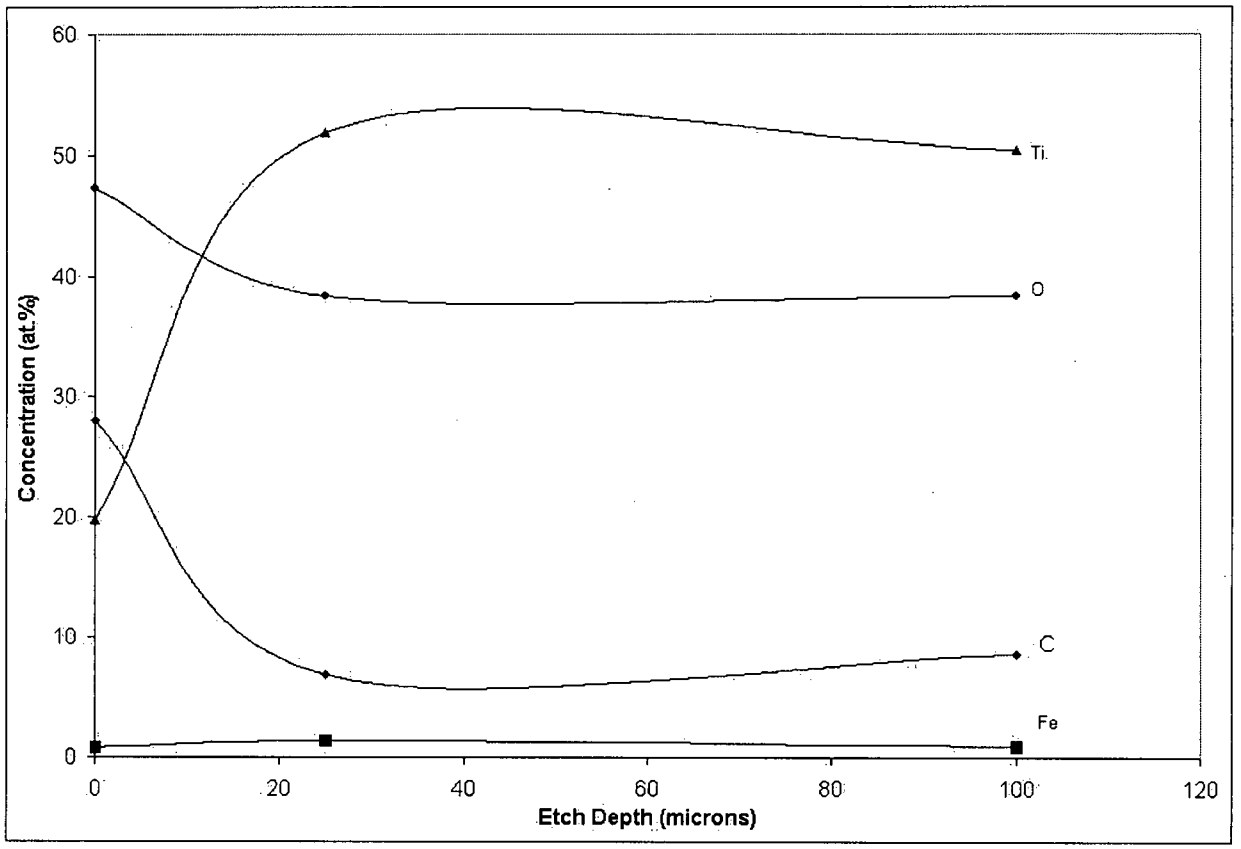

Figure 9: XPS depth profile of Ti grade 2 main constituents.

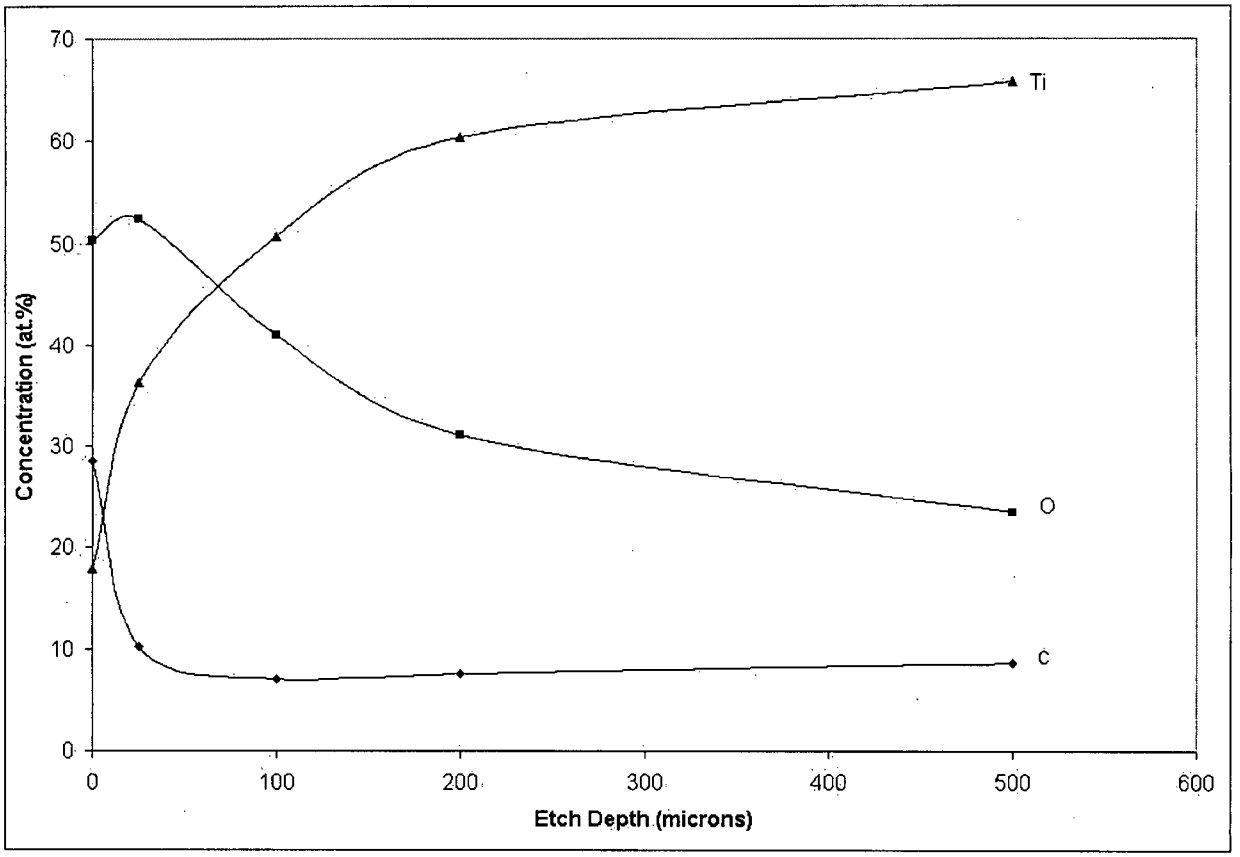

Figure 10: XPS depth profile of Ti grade 7 main constituents.

XRD samples were tested without preparation, as received. A 5 cm x 5 cm specimen was sheared from the stock material and mounted directly to the XRD. In addition to the three grades, grade 1 was subjected to a minor heat treatment at 800°C for 6 minutes in air to thicken the oxide layer in order to determine the position of the additional rutile peaks to avoid any misreading of the 2θ results. XRD results are depicted in Figure 11. Data was collected using a Siemens Diffraktometer model D 5000, and compared to the International Centre for Diffraction Database (Data Sets 1-49 and 70-86). All examinations were performed at 40 mA and 40 kV excitation voltage.

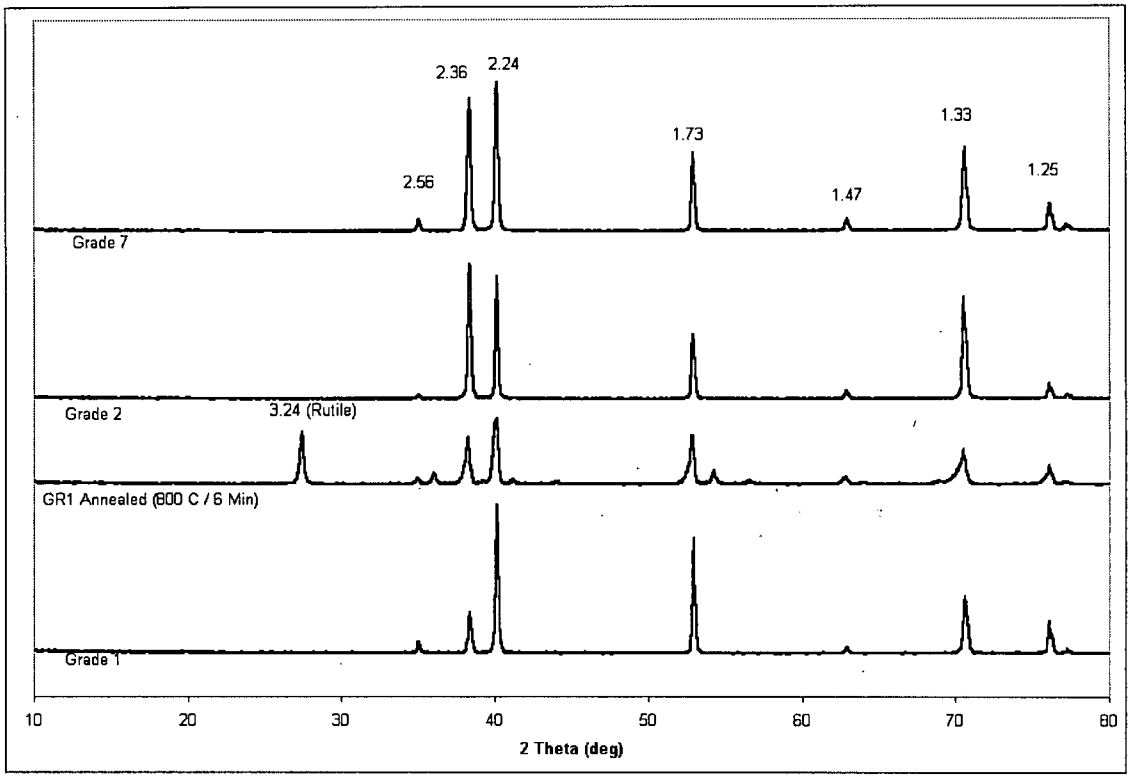

Figure 11: XRD spectra and d-spacings for Ti grades 1, 2, 7 and grade 1 after annealing at 800°C for 6 min in air.

Samples were prepared for SEM analysis by mechanically grinding to 1200 grit SiC paper, polishing to 1 μm diamond paste then electrochemically etching at below -30°C in a solution containing 300 ml methyl alcohol, 175 ml *n*-butyl alcohol, and 30 ml of 60% perchloric acid.[29] During polishing, samples were cooled in a liquid nitrogen bath to -30°C to avoid the formation of hydride precipitates at the grain boundaries, or the formation of a brown anodic film on the surface.[30] The potential of the sample surface was maintained at 20-30V and an optimum current density of approximately 0.1 A/cm^2 was applied for 15 minutes until the sample showed visible signs of grain boundary etching. This should have etched approximately 25-30 μm from the surface. Since the potential is known to fluctuate with

temperature, the procedure was controlled via current density to ensure proper results would be obtained. The results of the SEM analyses, using a Hitachi S-3000N microscope mated to Quartz-one software, are shown in Figure 12.

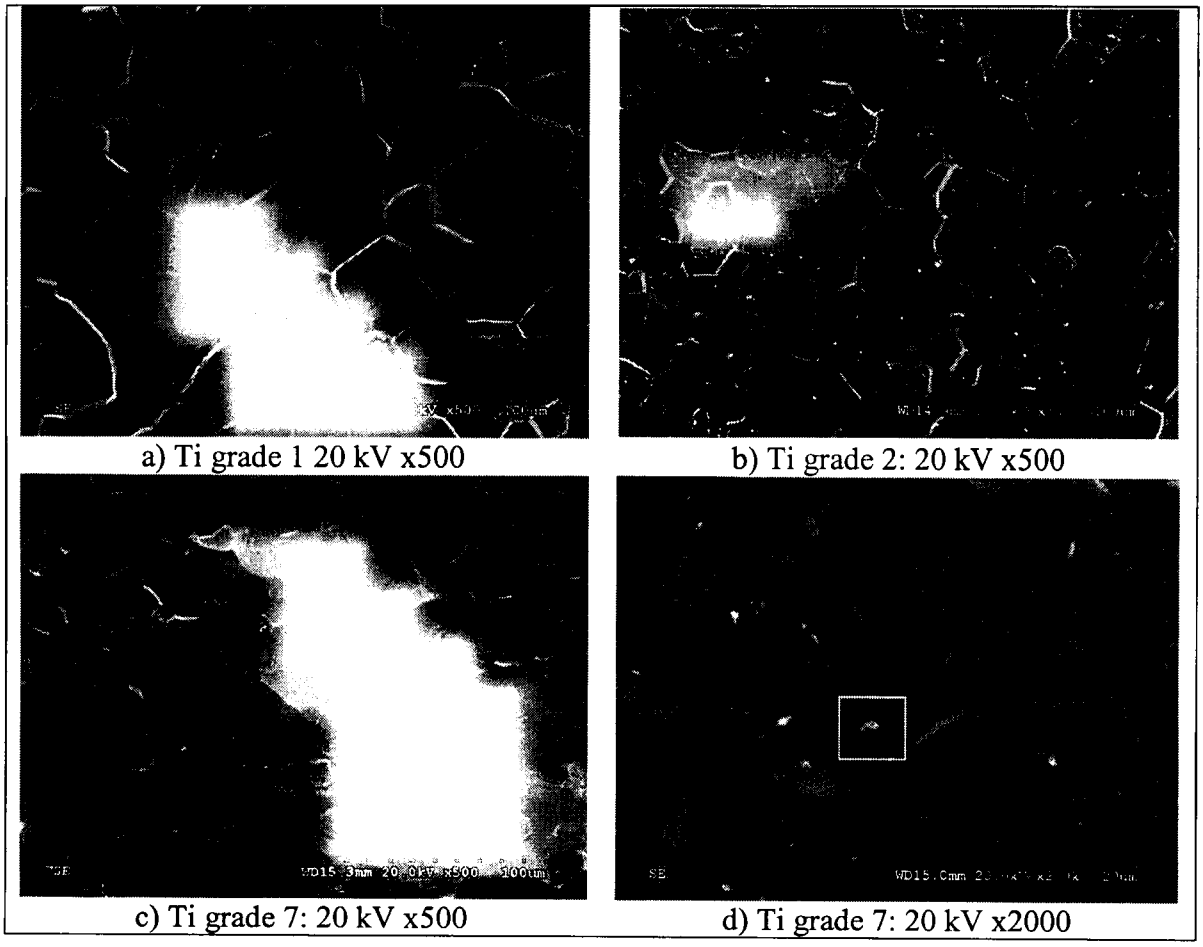

Figure 12: SEM micrographs: a) grade 1, b) grade 2, c) grade 7, d) Pd rich intermetallic particles on Ti grade 7, segregated particle highlighted by white box. Samples etched electrochemically at below -30°C in a solution containing 300 ml methyl alcohol, 175 ml *n*-butyl alcohol, and 30 ml of 60% perchloric acid.

The ASTM standard E112 was used to determine the average grain size of the materials for comparison with standard sizes for these metals in industrial situations. From these

micrographs, it would appear the average grain size ranged from 10 to 30 microns. The results are consistent with previous investigations of similar industrial metals in service.[1][10][21][22]

3.3 Long Term Immersion Testing

3.3.1 Specimen Preparation

Titanium sheets of grades 2 and 7 were cut into ~2.5 x 1.3 cm samples. A hole was drilled in the top of each sample for subsequent mounting. Samples were then individually measured for length, width and thickness, using Vernier callipers, and labelled by engraving a number into the top of each sample to either the right or left of the mounting hole. Finally, samples were cleaned, degreased, dried and weighed to a precision of +/-0.005g.

Initially the specimens were cleaned with acetone, rinsed with deionized water (DI) and dried in the low temperature furnace for 60 minutes. However, when recording weight loss data during testing samples were simply rinsed with DI water and acetone and dried in a desiccator for at least 4 hours as per standard ASTM practice G 31.[32]

Each immersion test was carried out in a 600 ml beaker capped with a no. 14 rubber stopper. Bolted to the underside of each stopper was a square, high density polyethylene sample tree designed to separate samples from each other physically and electrically by mounting samples one to a side with nylon screws.

3.3.2 Test Conditions

The samples were cleaned dried and weighed once a week for the initial 4 weeks and then once every two weeks for the duration of the 3 and 4-month tests. The suggested time for an immersion test is:[32]

$$\text{Hours} = 2000/\text{Corrosion Rate in mpy} \qquad (10)$$

As 4 months is equal to 2832 hours (3 months = 2256 hrs), as long as the corrosion rate exceeds 0.71 mm/y (or 0.89 mpy) this length of time should be sufficient to meet the suggested standard. Due to the low predicted corrosion rates in the less acidic tests, they were immersed for an extra month (118 days total). As well, the stronger solutions were weighed more frequently under the assumption of increased corrosion rates. However, after 3 months of immersion, no significant change in mass was occurring in these highly acidic conditions and the solutions were refreshed.

The six different solution conditions that were tested simultaneously at room temperature are described in Table 3. Solutions varied in H_2SO_4 concentration (0.1M, 1M and 5 M), to mimic both the minimum free acid in the HPAL process and possible crevice conditions, and Cl^- ion concentration (0 or 10 gpl). The chlorine ions were introduced in the form of sodium chloride (NaCl). The dimensions, initial weight and calculated densities of each sample are also reported in Table 3. There was no agitation and the containers were sealed air tight except when the samples were removed for weighing. ASTM standards require a minimum of 20

ml/cm^2 of exposed sample area. As the samples were only immersed 1.5 cm lengthwise in 800 ml of solution, these criteria were easily met.

Table 3: Test conditions, samples dimensions and calculated densities for long term immersion tests.

H_2SO_4 M	Cl- 10 g/L	Ti Grade	Length cm	Width cm	Thick cm	S.A. cm^2	Vol. cm^3	Mass (g)	Density (g/cm^3)
0.1	no	2	2.485	1.260	0.125	7.12	0.39	1.6928	4.38
1	no	2	2.540	1.265	0.125	7.30	0.40	1.73	4.36
5	no	2	2.540	1.290	0.125	7.43	0.40	1.7817	4.40
0.1	yes	2	2.550	1.260	0.125	7.30	0.40	1.7344	4.37
1	yes	2	2.500	1.290	0.125	7.32	0.40	1.7477	4.39
5	yes	2	2.540	1.260	0.125	7.27	0.40	1.7261	4.37
0.1	no	7	2.560	1.280	0.195	7.97	0.63	2.6865	4.26
1	no	7	2.485	1.265	0.195	7.67	0.61	2.585	4.27
5	no	7	2.560	1.270	0.195	7.92	0.63	2.6739	4.27
0.1	yes	7	2.485	1.295	0.195	7.83	0.62	2.6748	4.32
1	yes	7	2.465	1.280	0.195	7.69	0.61	2.5955	4.27
5	yes	7	2.560	1.315	0.195	8.16	0.65	2.8126	4.34

3.3.3 Calculation and Reporting of Corrosion Rates

The weight lost with respect to time data will translate directly to average penetration rates for titanium in the various solutions. Assuming localized or internal corrosion is not present in this situation, the average corrosion rate (R) in mpy can be calculated by:

$$R = X\frac{\Delta m}{At\rho} \qquad (11)$$

Where Δm is the mass lost in grams to the nearest 0.001 g, A is the surface area of the sample in cm^2, t is the exposure time in hours, ρ is the calculated density in g/cm^3, and X is the conversion factor from cm/hr to mpy (3.45×10^6).

3.4 DC Polarization Testing

3.4.1 Open-Circuit Potential Measurements and Potentiodynamic Polarization Experiments

Samples were tested as punched from the Ti sheet stock using a 5/8" diameter punch. Each was abraded to 600 grit SiC paper, rinsed with DI water, degreased with acetone, rinsed again and dried. They were then cleaned ultrasonically for 3 min and dabbed dry.

Using a model K47 "Corrosion Cell System" (Figure 13) and a model K105 "Flat Sample Holder" (Figure 14), both procured from Princeton Applied Research (PAR), the circular Ti specimen was immersed in electrolyte and protected from crevice corrosion by a specially designed Teflon© washer (PAR part no. MP1239). Two high-density graphite rods were used as counter electrodes. The reference electrode chosen was the Hg/Hg_2SO_4 (PAR part no. G0093) and the final opening on the corrosion test cell was for the inert gas line (N_2) used for purging. The potentiostat used was the PAR model 273A connected and operated by computer with M352 data analysis software.

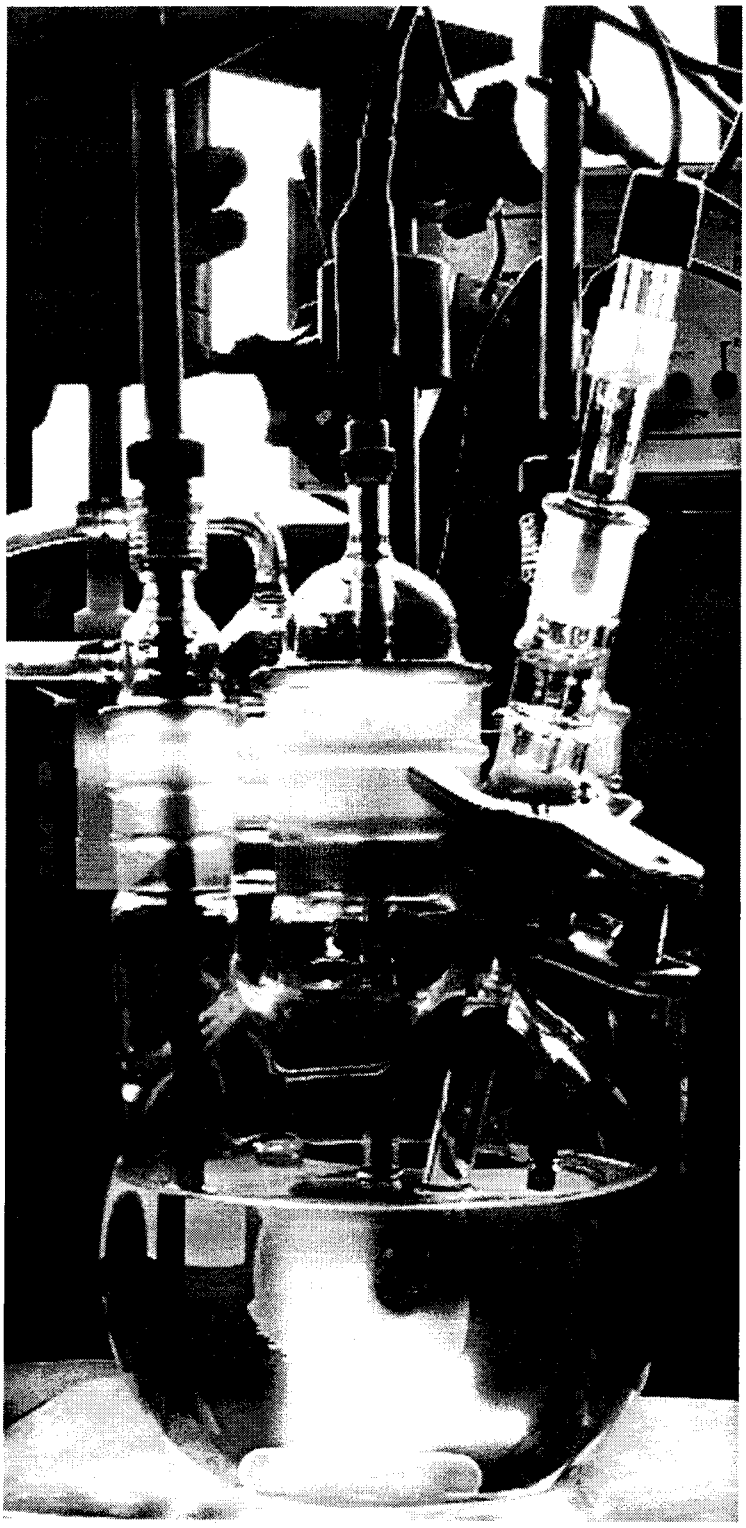

Figure 13: Model K47 corrosion cell manufactured by PAR.

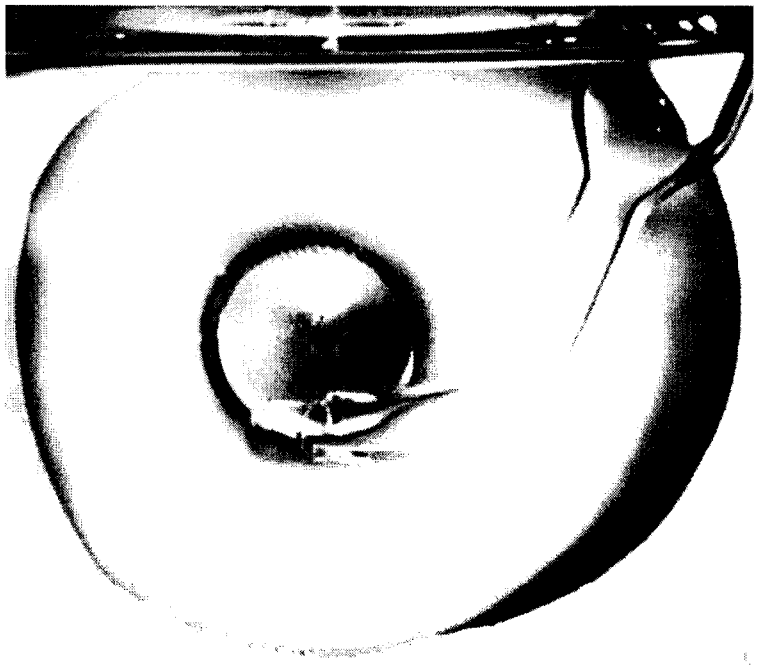

Figure 14: Close-up of flat specimen holder (PAR K105). Note the tip of the Luggin probe directly in front of the flat specimen, a glass frit was used to separate the solutions.

Polarization solutions consisted of different dilutions of sulphuric acid made from reagent grade acid and DI water. The following concentrations were employed: 0.3M, 1M, and 5M H_2SO_4 ($-0.7<pH<1$). The effect of chloride ions in the solution was examined using NaCl addition to the 5 M H_2SO_4. The temperature of the solutions was kept to within +/-2°C throughout testing using an Oakton "Stabletemp" water bath. In addition, the effect of temperature was tested at 50°C using 0.3M H_2SO_4 solution. Some of the experiments were performed in the absence (or near absence) of oxygen. This was achieved by purging the electrolyte with medical grade nitrogen for a minimum of 15 minutes immediately prior to testing and throughout the potentiodynamic scans.

After a stable open circuit potential was observed the potential scan was initiated with a scan rate of 0.5 mV/s. The results of each test were plotted on a semi log scale with log current on the abscissa and potential on the ordinate.

3.4.2 The Effect of Electrode Material on the RedOx Characteristics of Iron

In testing the effect of surface material on the reduction and oxidation behaviour of ferric and ferrous ions, common constituents of the HPAL slurries, two rotating disc electrodes (RDE) were used as the working electrodes and again the Hg/Hg_2SO_4 reference electrode was connected. One working electrode was a platinum RDE, from Pine Instrument Company (part no. AFMTI34DCPTT), with a surface area of 0.283 cm^2. The surface was used as received, already polished to 0.5 μm diamond. The other working electrode consisted of a 99.7% metals basis Ti rod procured from Alfa Aesar (stock # 10394) coated in epoxy resin, mechanically ground to 1200 grit on SiC paper then polished to 1 μm diamond paste. The surface area was 1 cm^2. Previous studies on high purity Ti monocrystals (entirely α phase) showed similar corrosion rates to grade 2 so the Ti electrode made from pure Ti bar stock can be expected to show similar behaviour as it's industrial counterparts.[35]

Ferric and ferrous ions were added to 0.3M H_2SO_4 electrolytes in the form of ferric sulphate and ferrous sulphate salts. The dependant variable was the ratio of ferric to ferrous ions, and consisted of $[Fe^{3+}]/[Fe^{2+}] = 1, 0.1, 0.01$.

Experiments were performed in a two-chamber cell (Figure 15) with each chamber separated by a 0.125 mm thick Nafion proton exchange membrane, from Alfa Aesar (stock # 42179). The membrane allows the flow of ions from the anodic half of the cell to the cathode portion, without allowing evolved gasses from the graphite counter electrode to enter the anodic chamber.

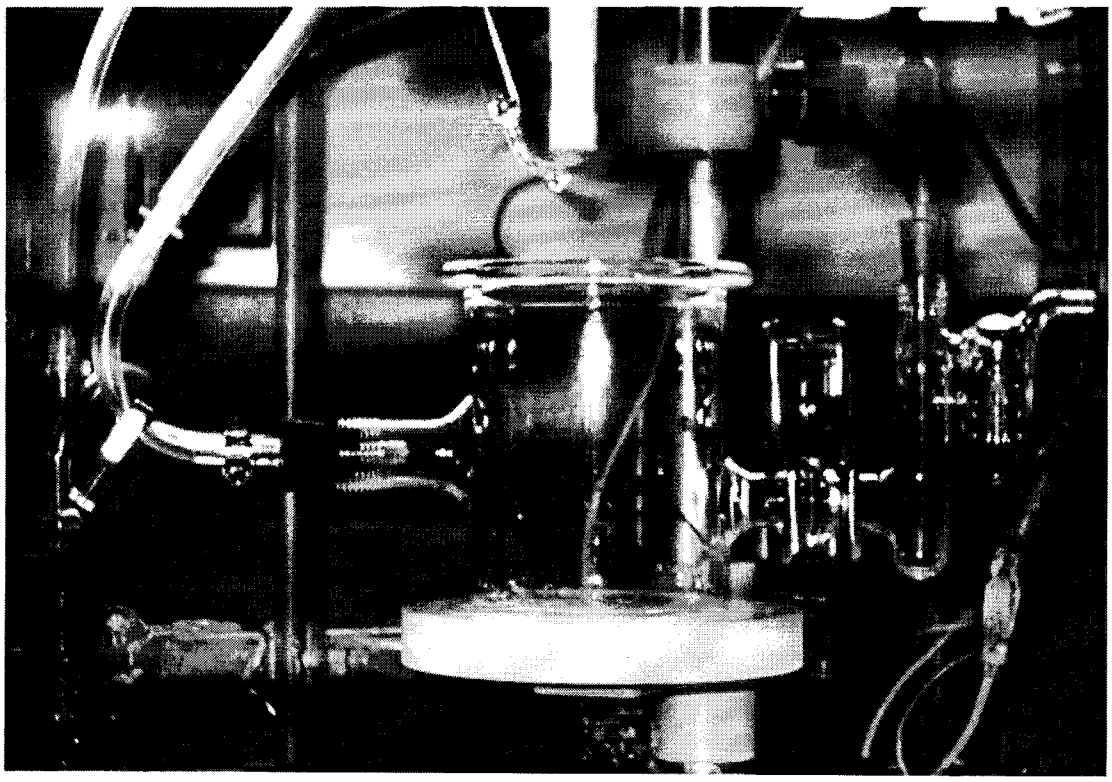

Figure 15: Two-chamber test cell separated by a Nafion membrane.

For each test, the Pt or Ti RDE was rotated with a frequency of 1000 rpm at room temperature in the iron containing solution, and the surface potential scanned to +/-1 V of the open circuit potential.

4 Results and Discussion

4.1 Long Term Immersion Testing

4.1.1 Weak Acid Tests

When samples were removed from the weaker acid solutions, the portion of the surface that had been immersed was different from the original material, as seen in Figure 16. Samples of Ti grade 7 had a brown colour while samples of Ti grade 2 had simply lost their lustre and maintained a greyish appearance. The film on Ti grade 7 is similar to the brown anodic films that can form during improper electropolishing of the metallographic samples. As expected, the samples immersed in the weak acid solutions (0.3M and 1M) lost very little overall mass as shown in Figure 17. Only grade 2 in 1M sulphuric acid with 10 gpl Cl^- addition, corresponding to the more susceptible alloy immersed in the most aggressive of the 4 month tests, showed any appreciable change in mass, and only during the initial days of the testing. Most of the samples actually gained mass throughout the testing suggesting an insoluble oxide product formed quickly on the surface of the alloys and sufficient oxidizing species were present in the system.

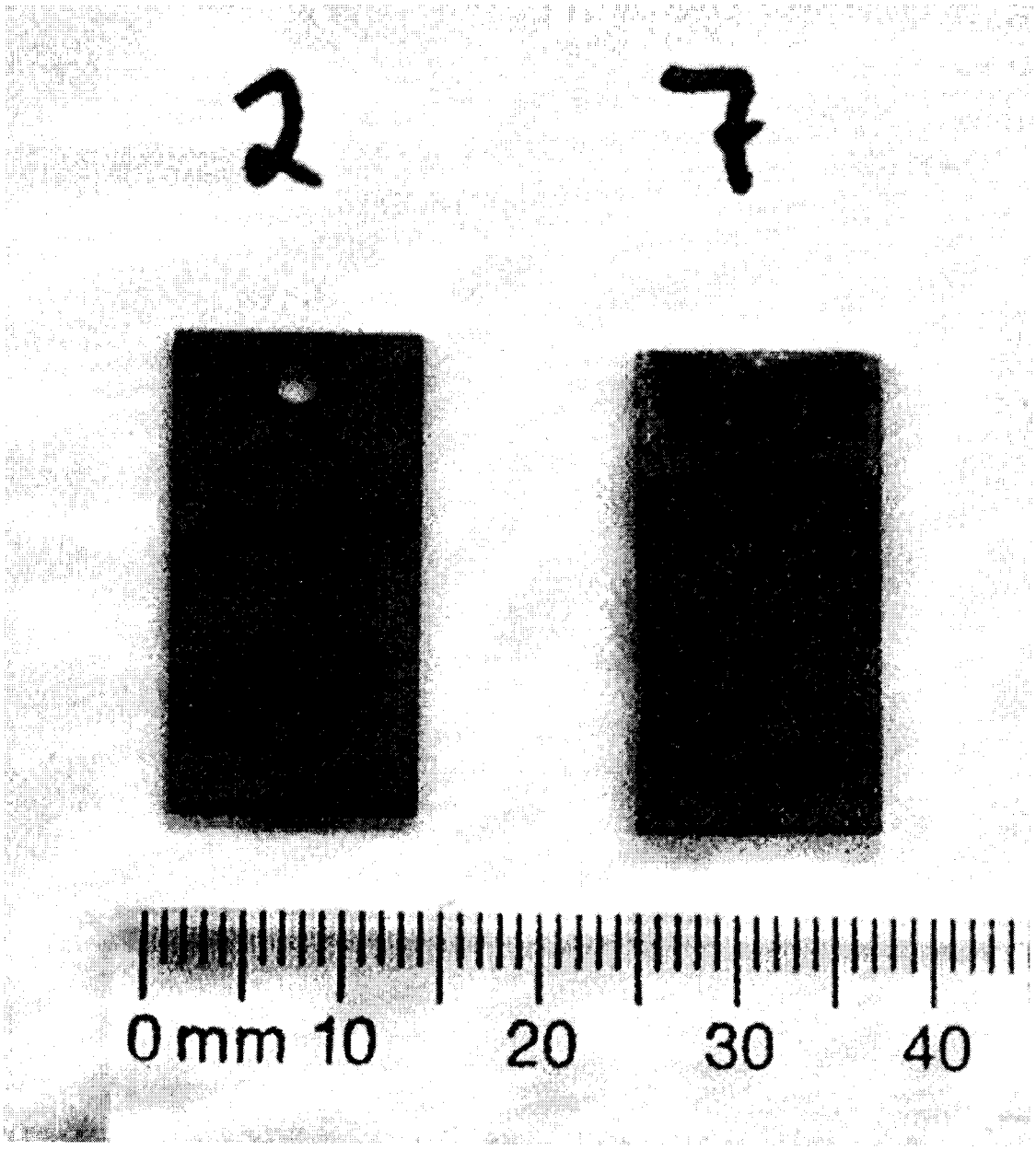

Figure 16: Photograph of Ti grades 2 and 7 immediately following removal from test solutions.

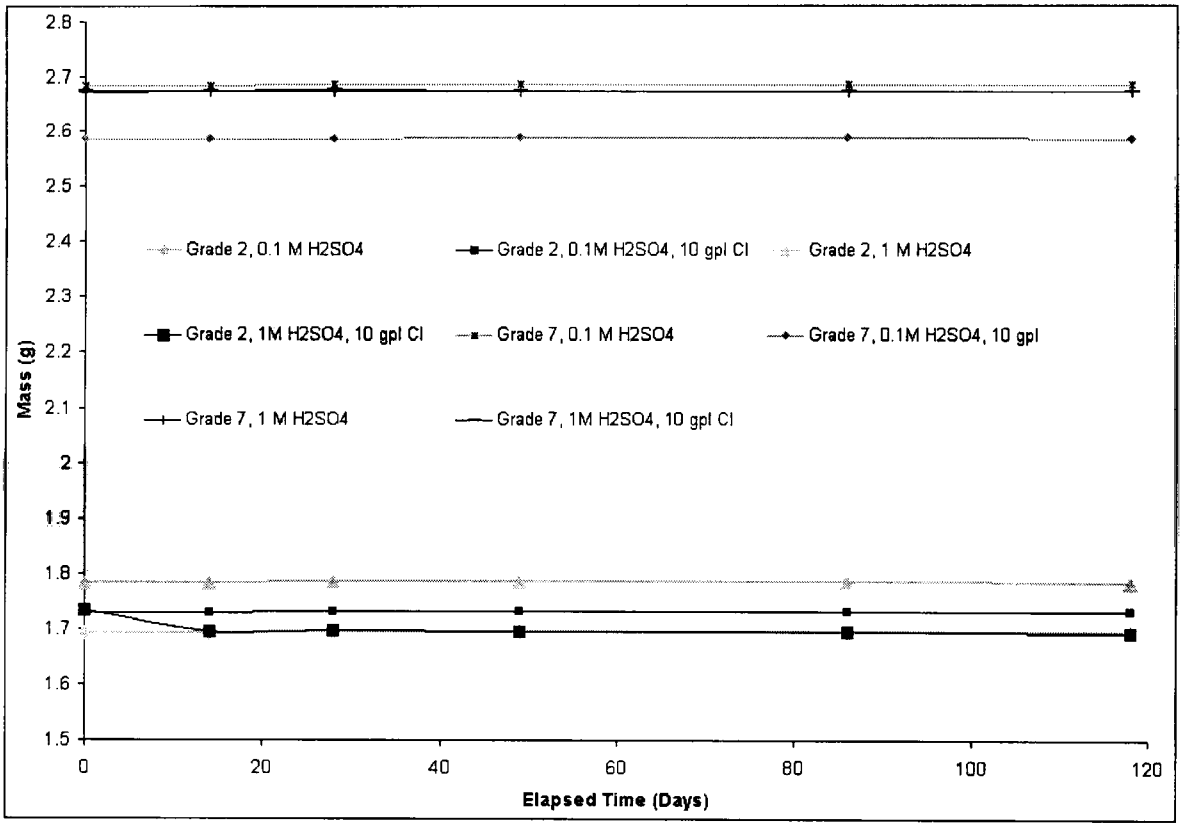

Figure 17: Mass lost on Ti grades 2 and 7 immersed in 0.1 M and 1 M solutions of H_2SO_4 for 118 days. Some solutions contained 10 gpl Cl^- additions in the form of NaCl.

Upon further analysis using SEM techniques, it was discovered that although no appreciable loss in mass was recorded, all samples were attacked locally by all solutions. Figure 18 and Figure 20 show the magnified grade 2 surfaces after immersion in 0.1M and 1M H2SO4 respectively, at 500X. The as-received surface had been etched and numerous cusps and dimples were present, indicating a general corrosion of the surface. The topography of the attack was quite impressive, covering the surface with numerous peaks and valleys. Samples of Ti grade 2 in the chloride containing solutions (Figure 19 and Figure 21) show slightly more aggressive attack, especially at grain boundaries. In both chloride solutions, selective grain

boundary corrosion was so severe that grain fallout had occurred. Notably, the sample in the weakest solution also succumbed to regions of localized attack over the entire surface. Regions similar to that shown in Figure 19 could be found scattered randomly on the exposed area showing much deeper layers of metal being affected. The Cl^- ions would appear to have more of an effect on preferential grain boundary attack than on the grains themselves.

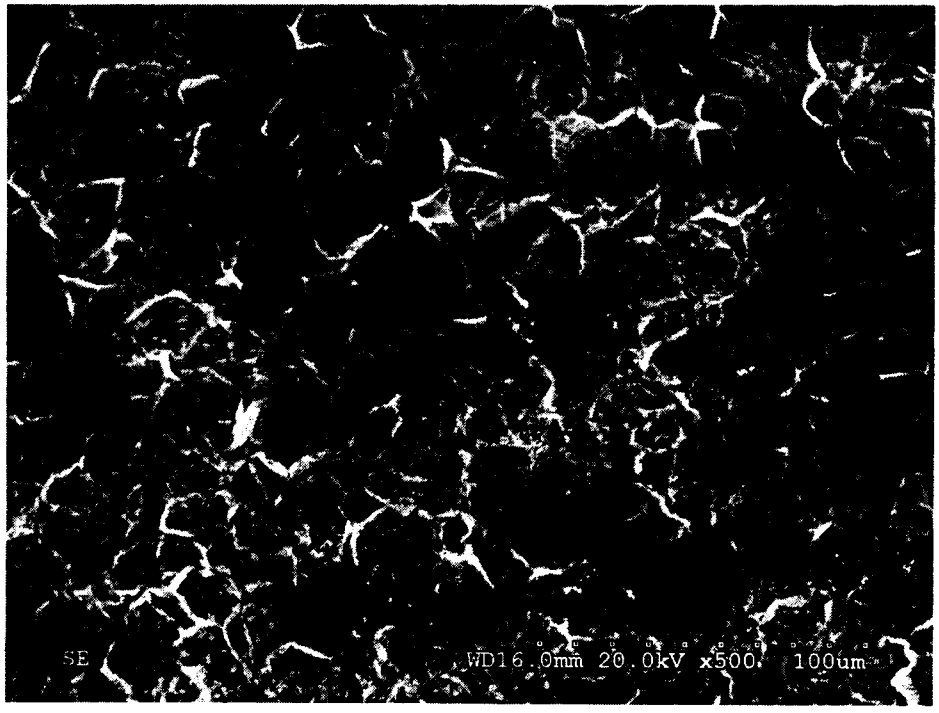

Figure 18: SEM micrograph, Ti grade 2. Sample 2.1after 118 days immersion in 0.1M H_2SO_4. 20 kV, 500 x magnification.

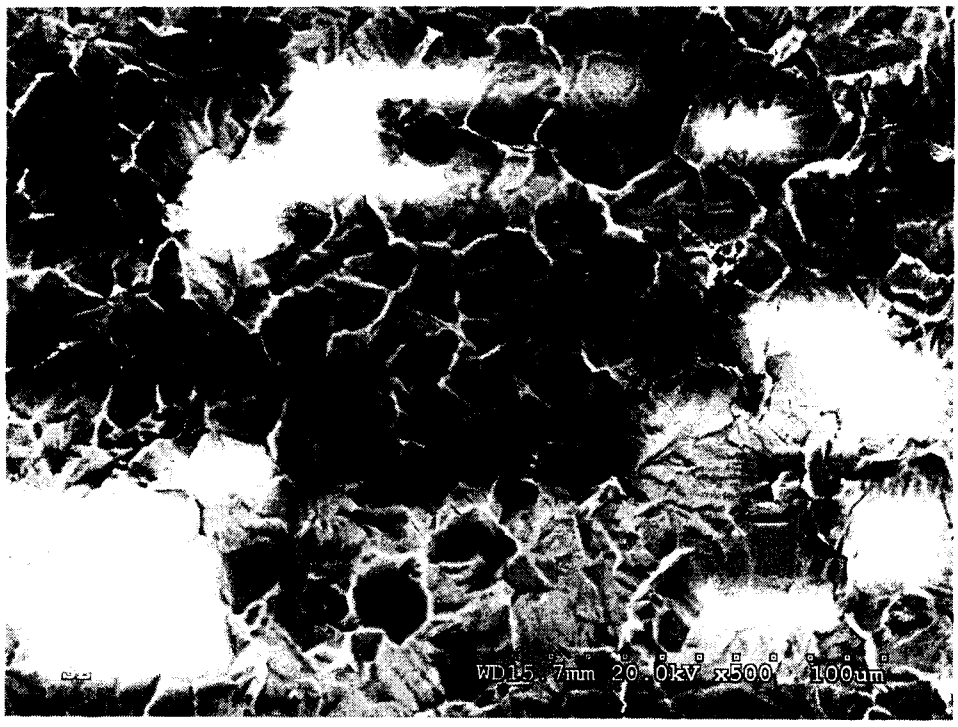

Figure 19: SEM micrograph. Ti grade 2. Sample 2.2 after 118 days immersion in 0.1M H_2SO_4 with 10 gpl Cl additions. 20 kV, 500 x magnification.

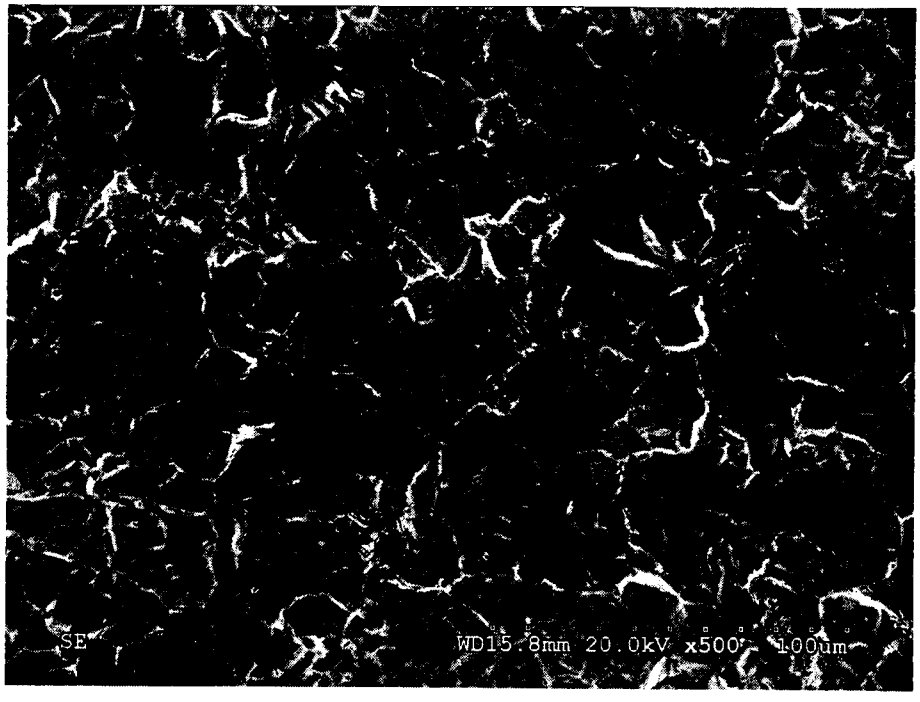

Figure 20: SEM micrograph. Ti grade 2. Sample 2.3 after 118 days immersion in 1M H_2SO_4. 20 kV, 500 x magnification.

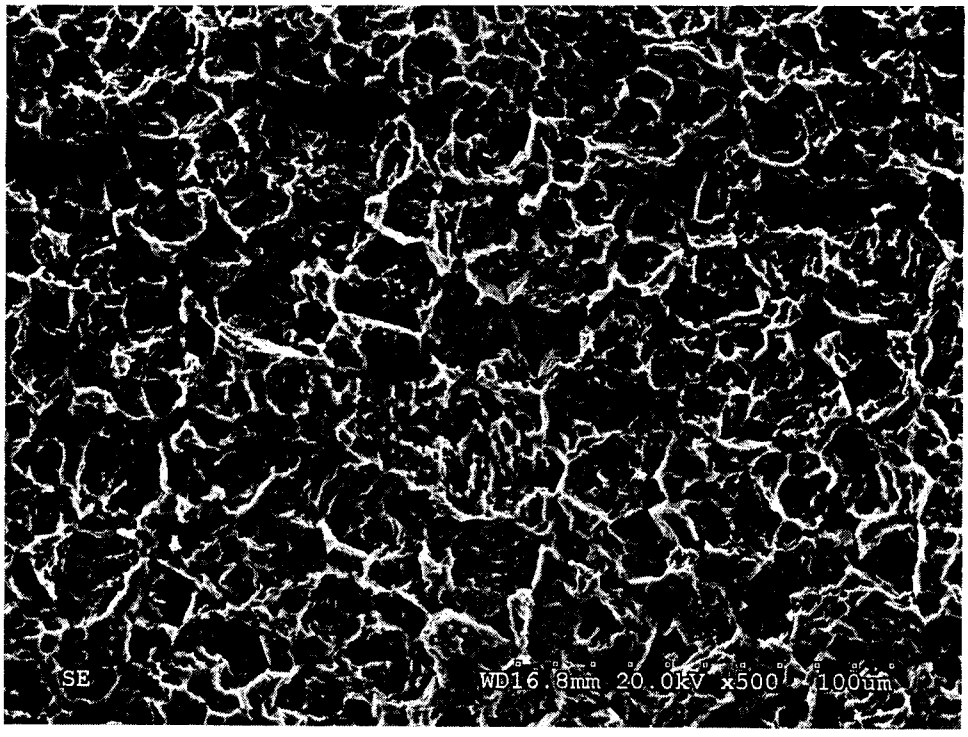

Figure 21: SEM micrograph. Ti grade 2. Sample 2.4 after 118 days immersion in 1M H_2SO_4 with 10 gpl Cl addition. 20 kV, 500 x magnification

It would appear the conditions of the 4-month testing were not sufficiently aggressive enough to severely damage the grade 7 alloy. All samples cut from this alloy gained a small amount of mass during testing, and when examined by SEM showed only small, localized pits of corrosion. It is unclear as to the reason for the formation of the pits in the weaker acid solution, but the author proposes two theories. First, it is possible the more noble Pd additions in this alloy, as seen in Figure 12d, resulted in galvanic attack to the surrounding Ti metal and thus the chunks of Pd additions simply "fell" out. Or, in a similar fashion, the presence of Fe impurities as shown in the EDS mapping, Appendix B: Materials Characterisation, were

subject to preferential attack by galvanic coupling and thus leave behind the small pits as they were dissolved. Closer examination of the Ti grade 2 micrographs revealed similarities in both pit characteristics and distribution, leading the author to believe it is the latter as there is no Pd present in the commercially pure samples, even as impurities.

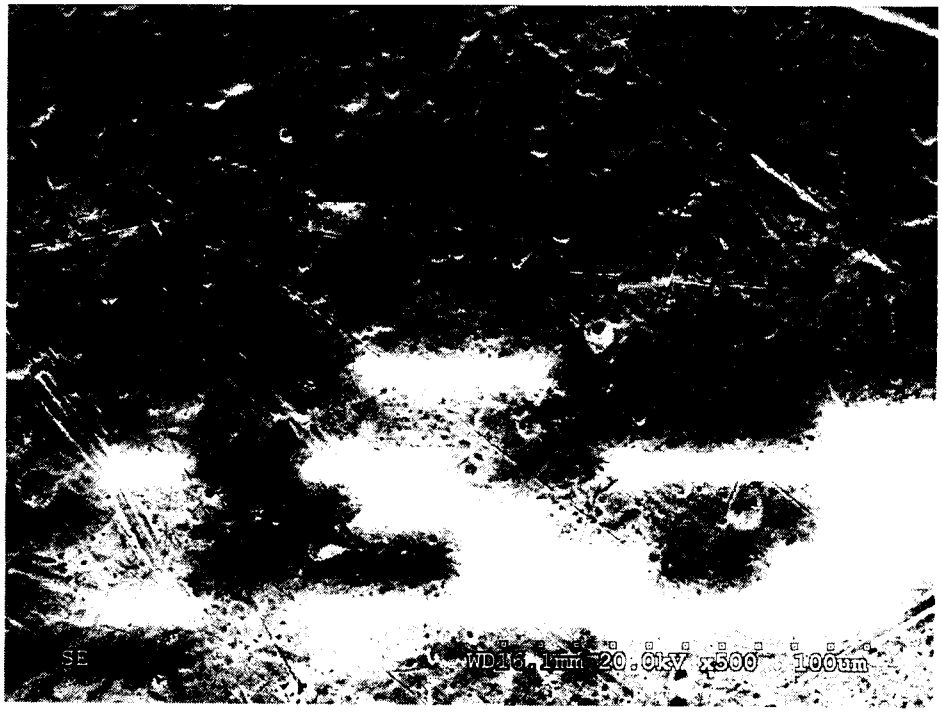

Figure 22: SEM micrograph. Ti grade 7. Sample 7.1 after 118 days immersion in 0.1 M H_2SO_4. 20 kV, 500 x magnification.

Figure 23: SEM micrograph. Ti grade 7. Sample 7.2 after 118 days immersion in 0.1 M H_2SO_4 with 10 gpl Cl addition. 20 kV, 500 x magnification.

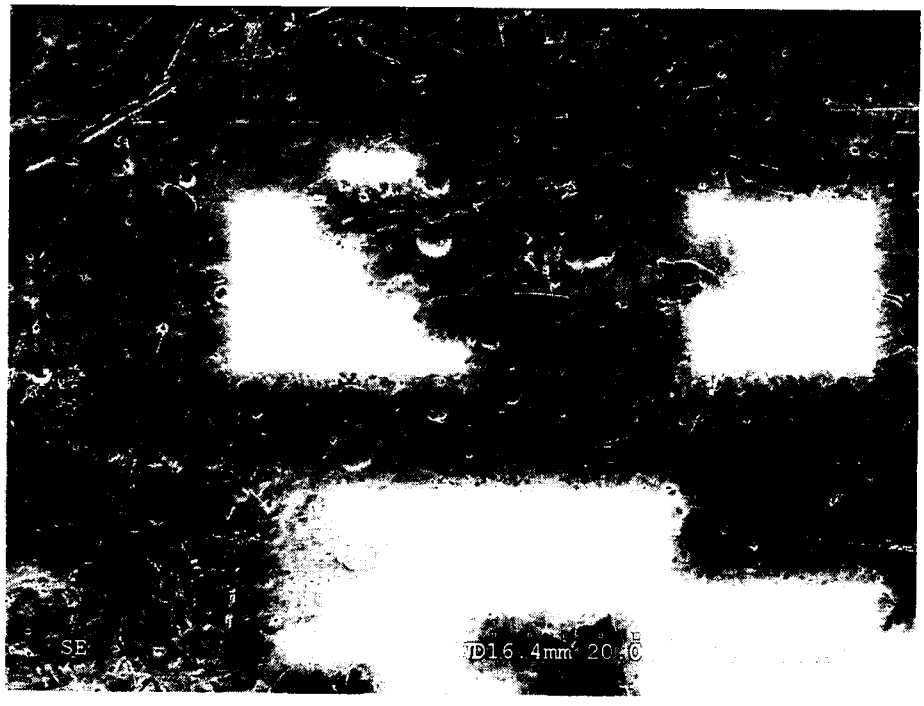

Figure 24: SEM micrograph. Ti grade 7. Sample 7.3 after 118 days immersion in 1 M H_2SO_4. 20 kV, 500 x magnification.

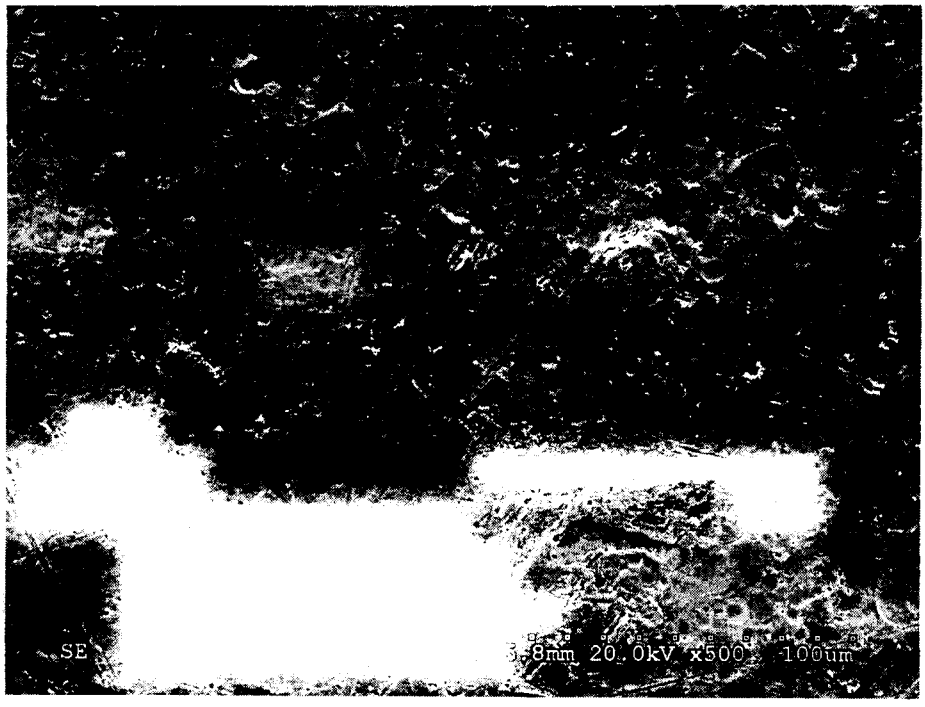

Figure 25: SEM micrograph. Ti grade 7. Sample 7.4 after 118 days immersion in1 M H_2SO_4 with 10 gpl Cl addition. 20 kV, 500 x magnification.

4.1.2 Strong Acid Tests

The results of the higher acid concentration testing were somewhat different as shown in Figure 26. Although there was little change in weight loss, similar to the previously discussed testing for the corrosion resistant alloy (Ti grade 7), the effect of the more aggressive solutions on the commercially pure alloys was immediately apparent. After immersion in both chloride and non-chloride solutions the mass of the grade 2 samples decreased sharply over the first week. At this point the solution without chlorides ceased corrosion for several weeks until about halfway through the testing when it again lost approximately 5% of its mass, after 12.5

mL of fresh solution was added to maintain the same waterline on the hanging samples. Meanwhile, the chloride-containing solution showed a steady decrease in mass over the same time period, again demonstrating the effect of Cl^- ions in solution. As with the longer immersion tests, there was little change in mass for the more corrosion resistant grade 7 alloys, until the point when the solution was refreshed and the sample subjected to chlorides lost an additional 5% in the first week. The increased dissolution in fresh solution would suggest there is some time required before a dissolution-free state is achieved again, most likely for the production of sufficient inhibiting Ti cations.

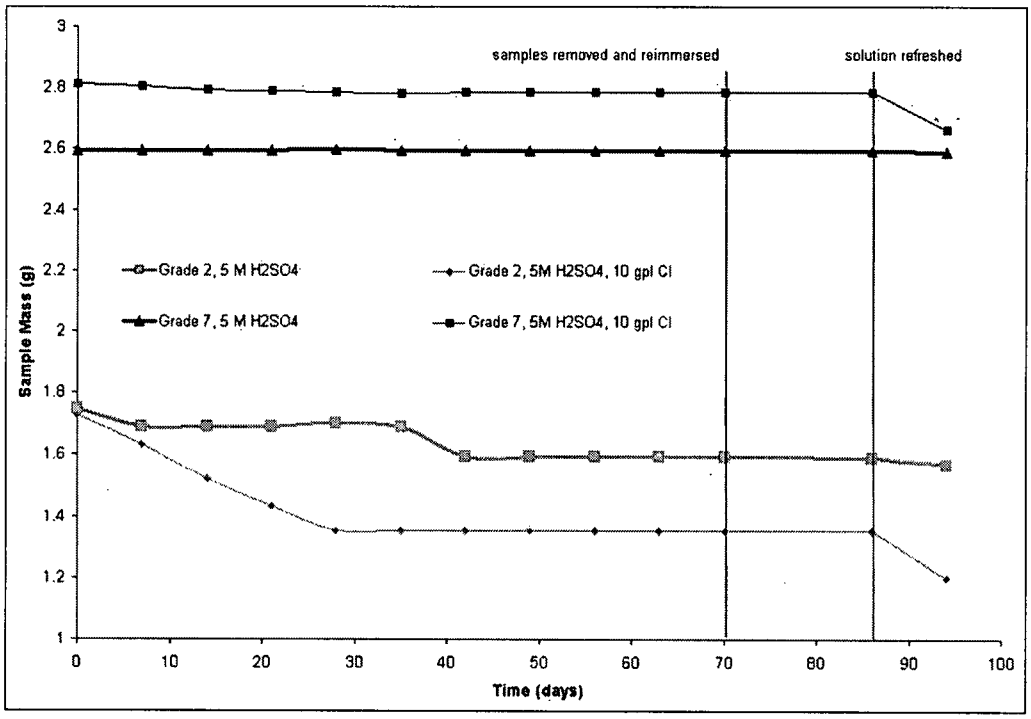

Figure 26: Mass lost on Ti grades 2 and 7 immersed in 5 M H_2SO_4 for 94 days. Some solutions contained 10 gpl Cl^- additions in the form of NaCl.

SEM micrographs of the 3-month immersion tests on Ti grade 2 are shown in Figure 27 and Figure 28. After 94 days immersion in 5M sulphuric acid, both of the grade 2 samples had been heavily attacked and exhibited both general dissolution and the same grain fallout as described previously, in this case much more severely, due to an effect of increased acid concentration. In crevice corrosion situations, the local chemistry is such that the pH can be lower than that of the bulk solution. However, from the conditions within the HPAL process, a crevice would be required to create such a low pH, especially at higher temperatures. This situation could worsen if a porous scale trapped stagnant solution with even 0.3 M chloride dissolved next to the outer surface of the liner.

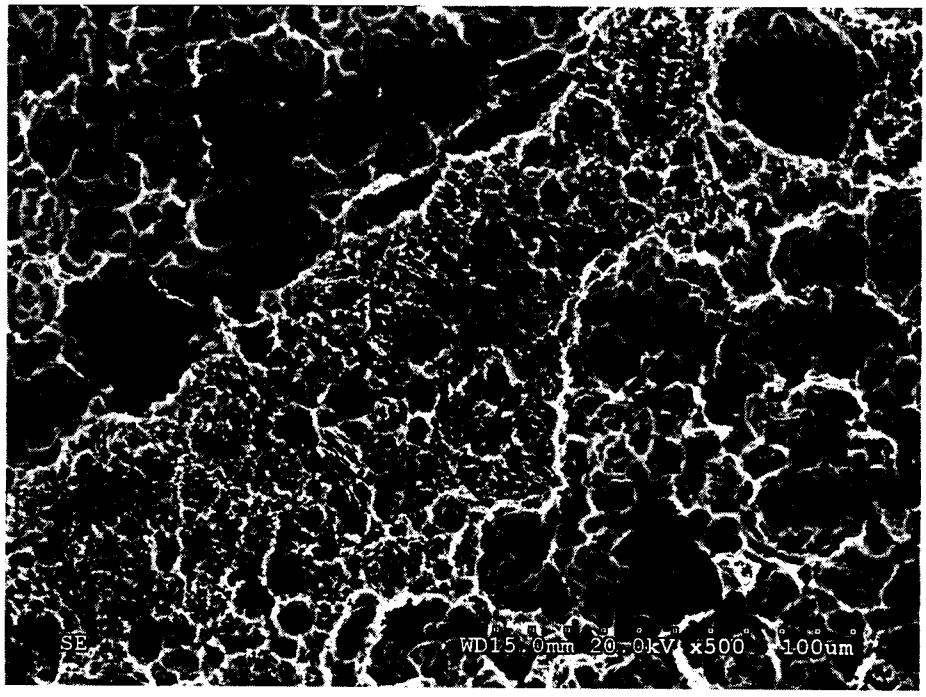

Figure 27: SEM micrograph. Ti grade 2. Sample 2.5 after 94 days immersion in 5 M H_2SO_4. 20 kV, 500 x magnification.

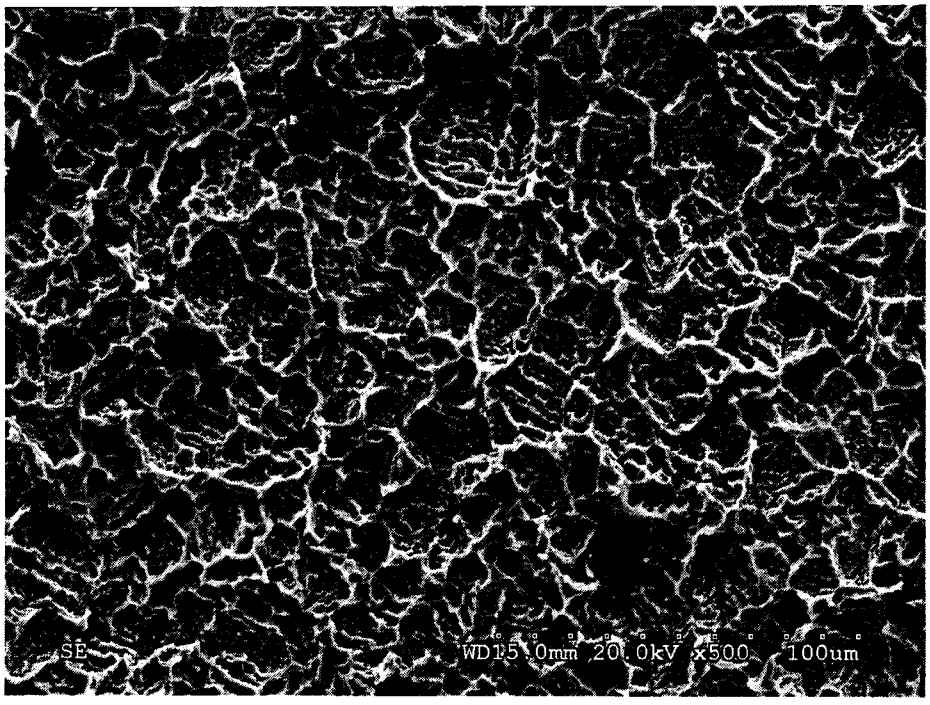

Figure 28: SEM micrograph. Ti grade 2. Sample 2.6 after 94 days immersion in 5 M H_2SO_4 with 10 gpl Cl addition. 20 kV, 500 x magnification.

These results coincide with previous studies by Tromans and Been on Ti alloys in corrosion conditions involving hydrogen peroxide.[35] They too discovered small pits formed mainly along grain boundaries with fewer small pits on the grain surface. As the corrosivity of the solution increased, the pits became more defined, and again, grain boundary corrosion was present causing grain dropout. In this case, the explanation was the same in that selective grain boundary corrosion was caused by the high chemical free energy nature of the grain boundaries due to the decrease in the average number of nearest neighbour atoms in this region.[35]

Surprisingly, Ti grade 7 did not show any decrease in mass following the immersion testing until the solution was refreshed, and then only the chloride containing solution had an effect.

After SEM examination (Figure 29 and Figure 30), the reason for this became apparent: grade 7 had built up a thick oxide layer that had protected it from further dissolution. It is possible Ti^{4+} ions from the corrosion of the grade 2 specimens present in the immersion tests acted as inhibitors, protecting the alloys by promoting oxide growth at the metal surface. The time required to form the oxide may be reasonably short given the solutions were only massed weekly.

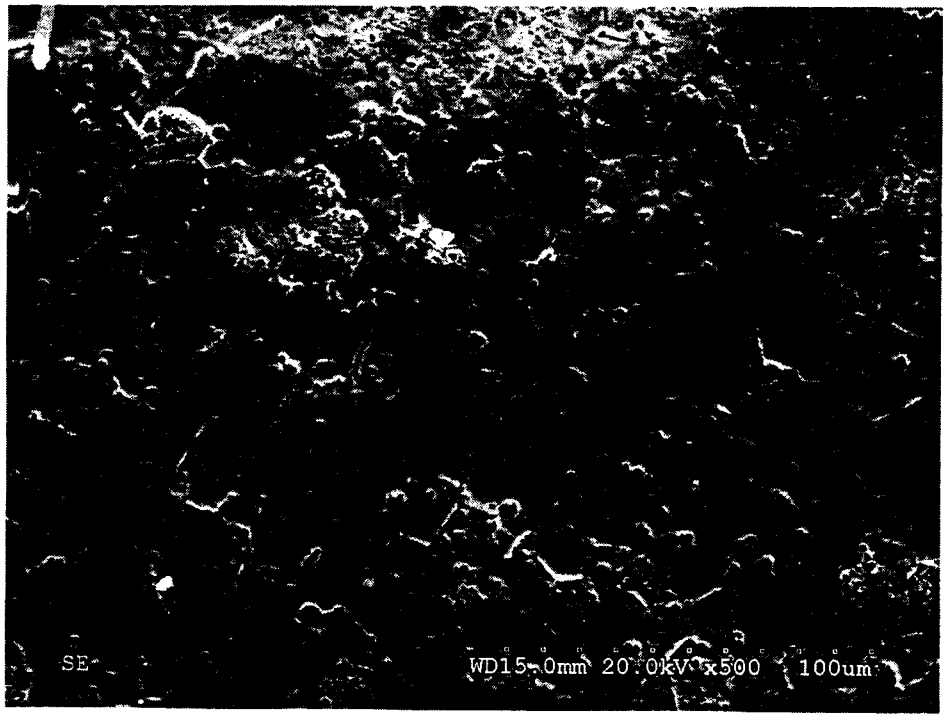

Figure 29: SEM micrograph. Ti grade 7. Sample 7.5 after 94 days immersion in 5 M H_2SO_4. 20 kV, 500 x magnification.

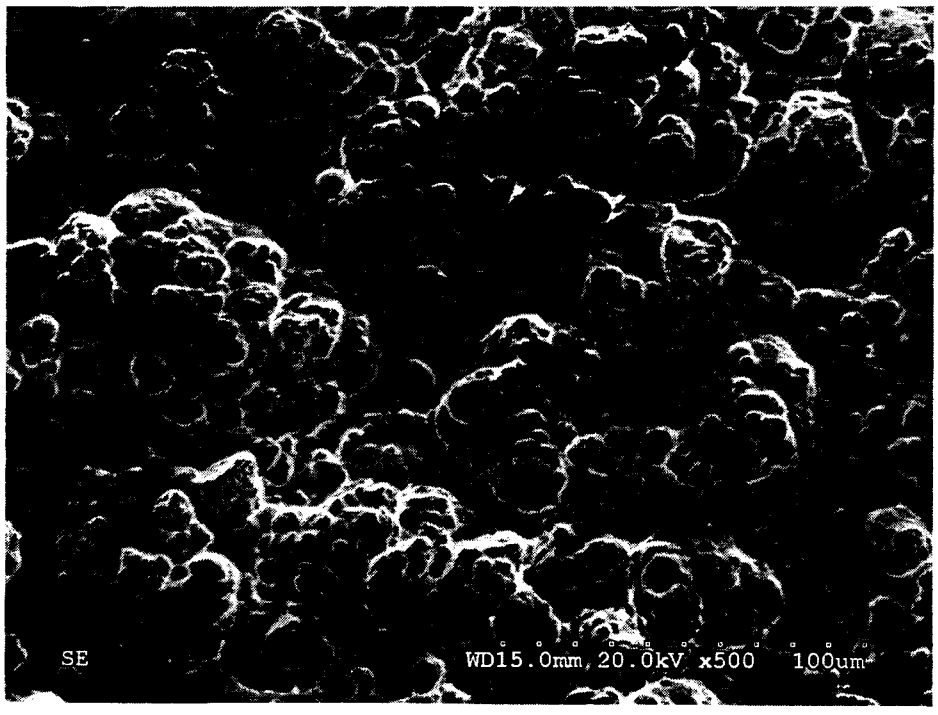

Figure 30: SEM micrograph. Ti grade 7. Sample 7.6 after 94 days immersion in 5 M H_2SO_4 with 10 gpl Cl addition. 20 kV, 500 x magnification.

The oxides present on the surface of the grade 7 samples have appeared in previous studies, which suggested the only way to remove these deposits to view the underlying metal is by sandblasting the area lightly.[10] The oxide growth theory is further supported by the change in colour of the solutions within the first week of immersion. Both solutions 5 and 6 took on a violet hue, with solution 6 much more brilliant (see Figure 31), although both solutions were essentially transparent. In solution 5 particularly, there was observed a tinge of violet in the static solution near the hanging samples. This shade of bright violet is the colour of Ti^{3+} as described in Pourbaix's Atlas of Electrochemical Equilibria in Aqueous Solutions[52] and has been seen in the output of WA AC. When the stoppers were removed for weighing of samples, the violet colour disappeared and the solutions were again transparent. Exposing the solutions

to air causes the oxidation of the Ti^{3+} to Ti^{4+}, which is pale yellow and essentially colourless. The violet colour did not reappear again until the solutions were refreshed at the 86-day mark. It is well known that small concentrations of oxidizing species effectively increase titanium's corrosion resistance in reducing acids by positively polarizing the metal. The accumulation of Ti^{4+} ions from the oxidation of the initial Ti^{3+} leads to a more protective, dehydrated titanium oxide layer.[10] Given the obvious presence of Ti^{3+} in the immersion solutions immediately after being refreshed, this explains the eventual stability of the samples.

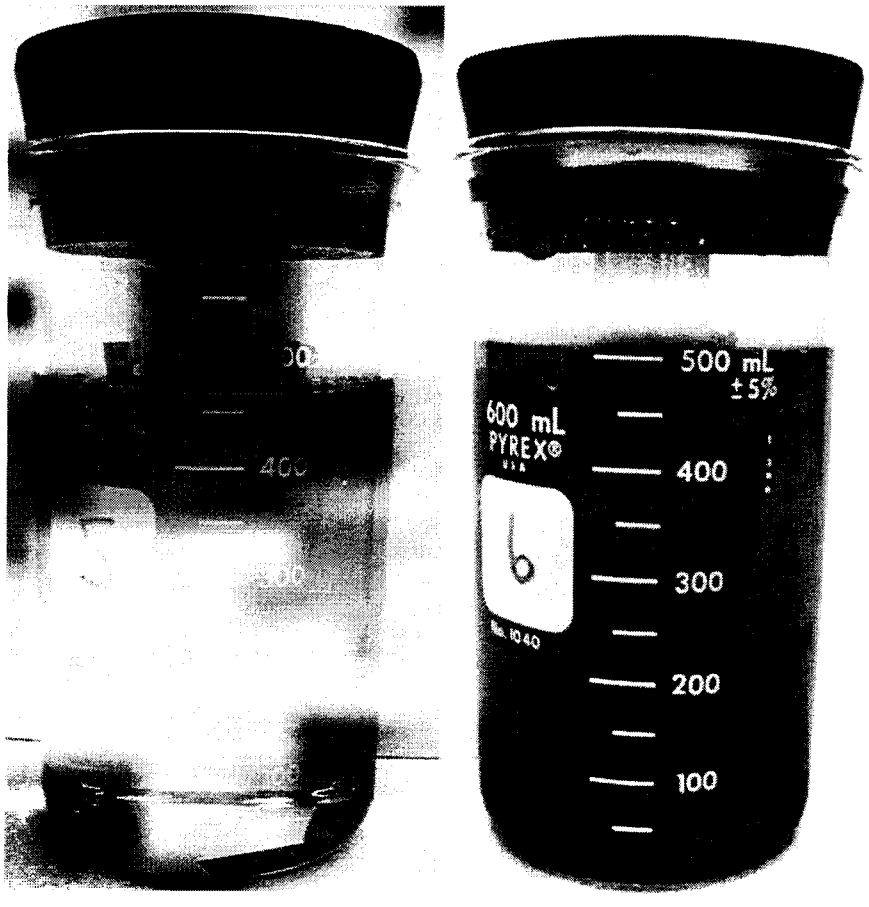

Figure 31: 5M H_2SO_4 immersion solutions after 14 days immersion. The beaker on the right contains no Cl- ions, while the beaker on the left has 10 gpl Cl-.

Penetration rates calculated from weight loss data are summarized in Table 4. These results are slightly lower than those found in previous studies of corrosion of impeller axles in AC that were constructed of the same material, however those studies replaced solutions with fresh acid every 12 days.[51] Samples that gained mass via oxide growth are recorded as a negative penetration rate. Ti grade 2 in 5M H_2SO_4 with 10 gpl Cl^- ion additions showed the highest penetration rates while grade 2 in 1M H_2SO_4 was the most resilient with the highest negative penetration rate, or the highest rate of oxide growth. It was quite obvious, however, that the grade 7 alloy showed marked improvement in corrosion resistance in all conditions tested.

Table 4: Penetration Rates for Ti grades 2 and 7 after long term immersion in H2SO4.

Sample (grade. #)	**Solution**	**Immersion Time (days)**	**Penetration Rate (mm/yr)**	**Penetration Rate (mpy)**
2.1	0.1 M	118	-0.0011	-0.043
2.2	0.1 M, Cl	118	-0.0010	-0.038
2.3	1 M	118	-0.0013	-0.052
2.4	1 M, Cl	118	0.040	1.56
2.5	5 M	94	0.22	8.64
2.6	5 M, Cl	94	0.64	25.4
7.1	0.1 M	118	-0.0010	-0.040
7.2	0.1 M, Cl	118	-0.0012	-0.048
7.3	1 M	118	-0.0012	-0.047
7.4	1 M, Cl	118	-0.00070	-0.029
7.5	5 M	94	0.0051	0.20
7.6	5 M, Cl	94	0.17	6.51

4.2 DC Polarization Testing

4.2.1 Calculation for Liquid Junction Potentials

The potential values obtained for all electrochemical tests were corrected for liquid junction potentials (LJP), or $\Phi^{I} - \Phi^{II}$. This junction existed because of the concentration difference in sulphate solutions on either side of the solution boundary (a glass frit); the H_2SO_4 concentration in the electrolyte and the K_2SO_4 concentration in the reference electrode. Table 5 shows the correction values calculated for the different concentrations of acid used in the room and elevated temperature polarization testing. It was assumed that no appreciable thermal junctions were present due to the low temperature nature of the testing. The LJP between solution-I and solution-II were calculated by means of the Henderson equation as follows.[58]

$$\Phi^{I} - \Phi^{II} = \frac{RT}{F} \times A \times \frac{\ln(\frac{B^{I}}{B^{II}})}{B^{I} - B^{II}} \qquad (12)$$

Where Φ_I is the potential of solution I, Φ_{II} is the potential of solution II, R represents the gas constant, T the absolute temperature (K), and F is Faraday's constant. The coefficients A and B are summations with respect to mobility μ_i and the ionic charge z_i of the species in solution I or II:

$$A = \Sigma z_i u_i (c_i^{I} - c_i^{II}) \quad (13)$$

$$B^{I} = \Sigma z_i^2 u_i c_i^{I} \quad (14)$$

$$B^{II} = \Sigma z_i^2 u_i c_i^{II} \quad (15)$$

The concentration of ions in the solution (c_i) has already considered the effect of the second dissociation constant of sulphuric acid:[60]

$$HSO_4^- \rightarrow SO_4^{--} + H^+ \quad (16)$$

By assuming infinite dilution, the values of ion mobility (u_i) can be replaced with values for ion diffusivities.[58] The thermodynamic data for these calculations can be found in Appendix C: Data for Calculation of Liquid Junction Potentials.

Table 5: Correction factors for liquid junction potential differences.

Conc. H_2SO_4 vs. sat. K_2SO_4 ref. Electrode	Correction Factor (mV)
0.3	9.1
1	23.4
5	47.5
0.6 HCl	9.7

4.2.2 Open-Circuit Potential Measurements

The results of measuring and recording the open circuit potential (Figure 32) show a rapid fall in potential as the metal, oxide film and electrolyte converge on an equilibrium potential.

The commercially pure grades came to rest within 100 mV of each other at around -0.50 V_{SHE}, while Ti grade 7 open circuit potential was measured to be much greater (approximately 0.07 V_{SHE}). The overvoltage required to initiate the HER is known to be less on the surface of Pd than on Ti, and the resulting mixed potential comes to rest at more noble values. It is possible the observed increase in potential before reaching a steady state value is because of this and would explain why grade 7 typically exhibits better corrosion resistance, by fostering more oxidizing potentials.

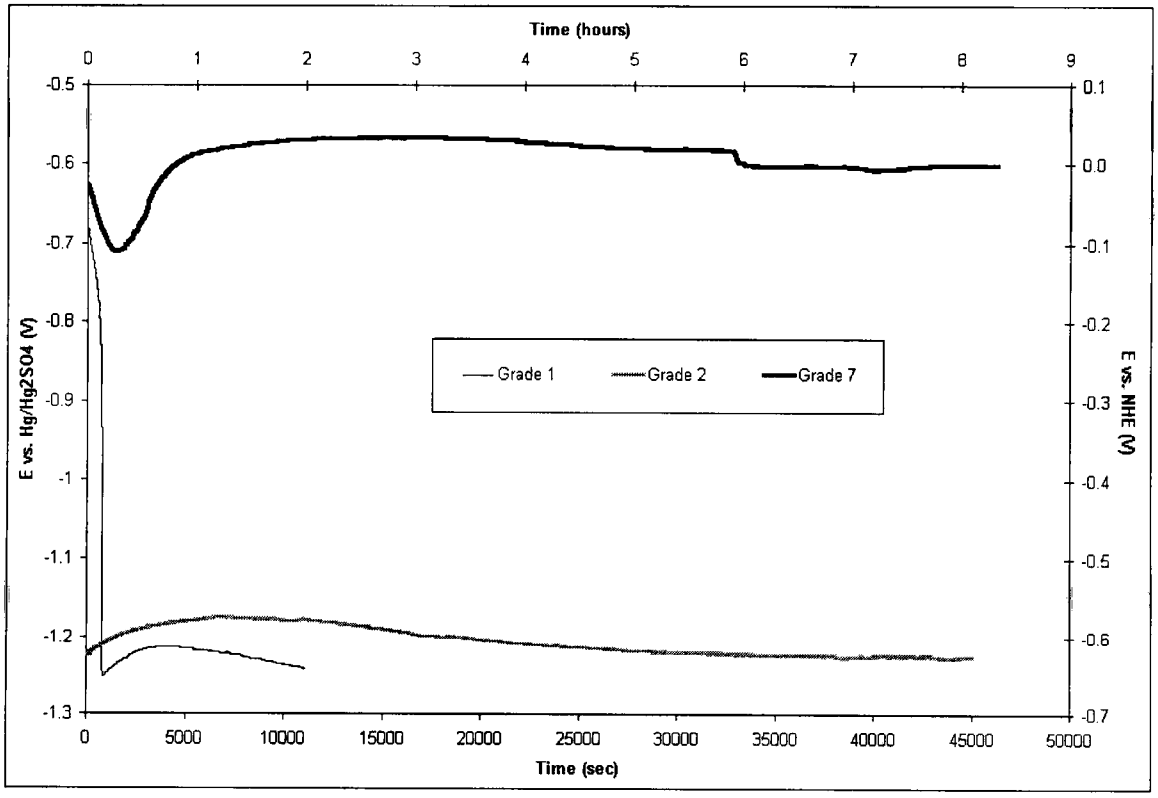

Figure 32: Open circuit potential measurements for Ti grades 1, 2, and 7 at 50°C in 1 M H_2SO_4.

Blackwood et. al. have reported breakdown periods of 4 hours on porous Ti samples in 3 M H_2SO_4 at 37°C, but they also reported stable potentials more than 300 mV less than those shown above.[17] The discrepancy is most likely due to the localized corrosion mechanisms occurring within the pores. Even after 8 hours of observation, the samples did not exhibit anything characteristic of film breakdown, and surfaces appeared almost completely unaffected.

4.2.3 Effect of Alloying Additions

Figure 33 is a comparison of the electrochemical characteristics of the three Ti grades used in this study. The corrosion rates of Ti grades 1 and 2 are very similar but grade 7 shows a slightly increased current density. Given that this is the corrosion resistant alloy, it would suggest the passage of current is not between the metal and electrolyte, but instead between the outer layer of the oxide and the electrolyte. Dissolution of the oxide film on solid Ti can be accelerated by the application of a cathodic current:[17]

$$TiO_2 + 3H^+ + e^- \rightarrow Ti(OH)^{2+} + H_2O \qquad (17)$$

However, samples cathodically polarized for in excess of 20 minutes showed no different results and therefore it is assumed the oxide formed quickly in the active region is sufficient to

protect the metal from further oxidation. Knowing the presence of an oxide is inevitable, there are now two possible routes for electron transfer[64][66]:

(i) If the film is sufficiently thin, an electron is exchanged between the underlying metal and the electrolyte. In this case the film acts as a potential barrier and current decreases dramatically with film thickness. This is typically the situation with films in the range of 0.4 - 3 nm thick.

(ii) If the film is thicker (> 3 nm) an electron is exchanged between the electrolyte and the oxide layer itself. In this case the electrode behaves like an ordinary semiconductor or insulator, and current is relatively independent of film thickness. In this case however, the film has much more control over the potential and current.

For this investigation, the charge passed during the potentiodynamic scan was assumed to be consumed by oxide thickening and the small change decrease in current density as the oxide layer grows means the films formed can be considered thick (> 3nm). This assumption agrees with reports of previous studies on Ti that confirm this alloy is a thick film electrode and typically reacts via the conduction band mechanism.[10][67]

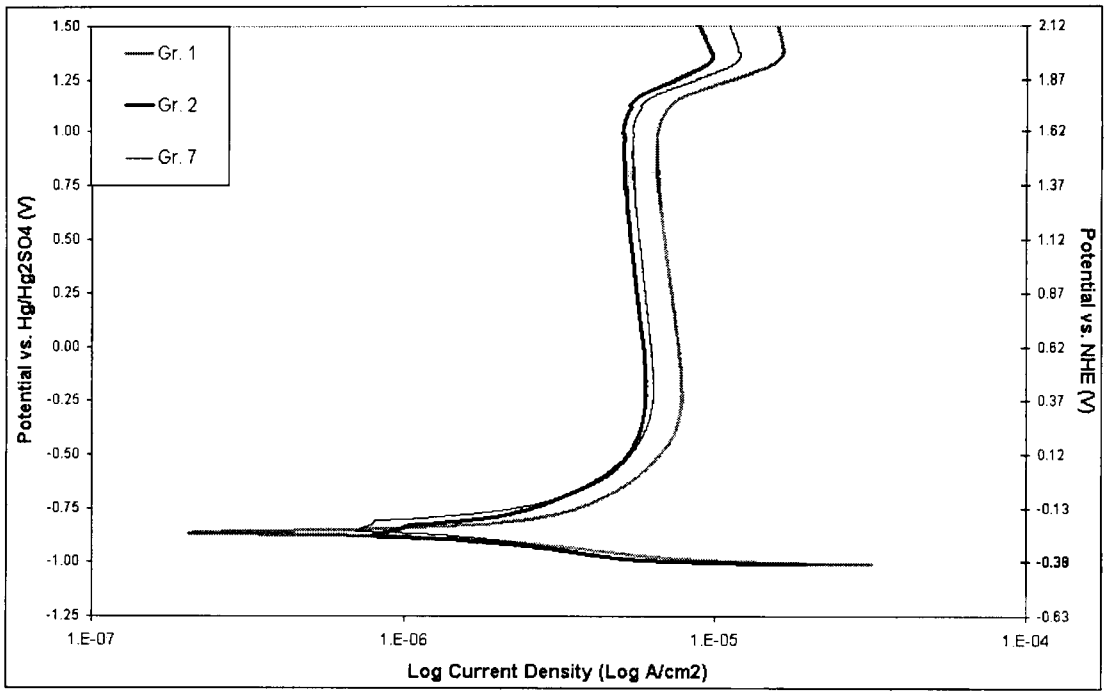

Figure 33: Potentiodynamic scans of Ti grades 1, 2, and 7 in 0.3 M H_2SO_4 at room temperature, scan rate 0.5 mV/s.

The electrochemical films grown during testing were assumed to be amorphous and hydrated based on information provided by previous research. Passive films in general are amorphous when grown at low potentials, and in aqueous solutions, hydrated oxides are expected to form.[17][22][29][35][61] Anodized films that are hydrated do not protect as well as films grown naturally by heating in air or water, even though they may also be composed of both the crystalline and amorphous structures of TiO_2.[35]

After reaching approximately 1.7 V_{SHE} during the potentiodynamic scans, all samples in all conditions exhibited a half-decade increase in current density. This potential corresponds well to the dissolution of the oxide surface to TiO_2^{2+}, a colourless ion. This ion could then form

soluble complexes with sulphates such as $TiOSO_4$[32] and chlorides such as $TiOCl_2$[33] in solution according to the following reactions:

$$TiO_2 \rightarrow TiO_2^{2+} + 2\,e^- \quad (18)$$

$$TiO_2^{2+} + SO_4^{2-} \rightarrow TiOSO_{4(a)} + 1/2\,O_2 \quad (19)$$

And similarly for chlorides:

$$TiO_2^{2+} + 2Cl^- \rightarrow TiOCl_{2(a)} + 1/2\,O_2 \quad (20)$$

As the solubility of the oxidized ions is exceeded, they will precipitate out as naturally occurring minerals, titanium oxide sulphate or titanium oxide chloride, and the current resumes a plateau.

Following potentiodynamic scanning, a dull grey film appeared on the exposed surfaces of the specimens, corresponding to the results of previous work.[29] Figure 34 depicts an SEM micrograph of the surface of Ti grade 1 following a potentiodynamic scan from -1.5 $V_{Hg/Hg2SO4}$ to 2.0 $V_{Hg/Hg2SO4}$ at room temperature in 0.3 M sulphuric acid using a scan rate of 0.5 mV/s. The surface appears very similar to that of the immersion samples following 3 months of immersion in the same solution. The increased overpotential applied to the surface of the specimen accelerates the reducing effects of the electrolyte and produces slightly more aggressive attack, apparent from the grain sized depressions uniformly covering the surface.

The appearance of the deep grain-sized holes again suggests preferential attack at the grain boundaries.

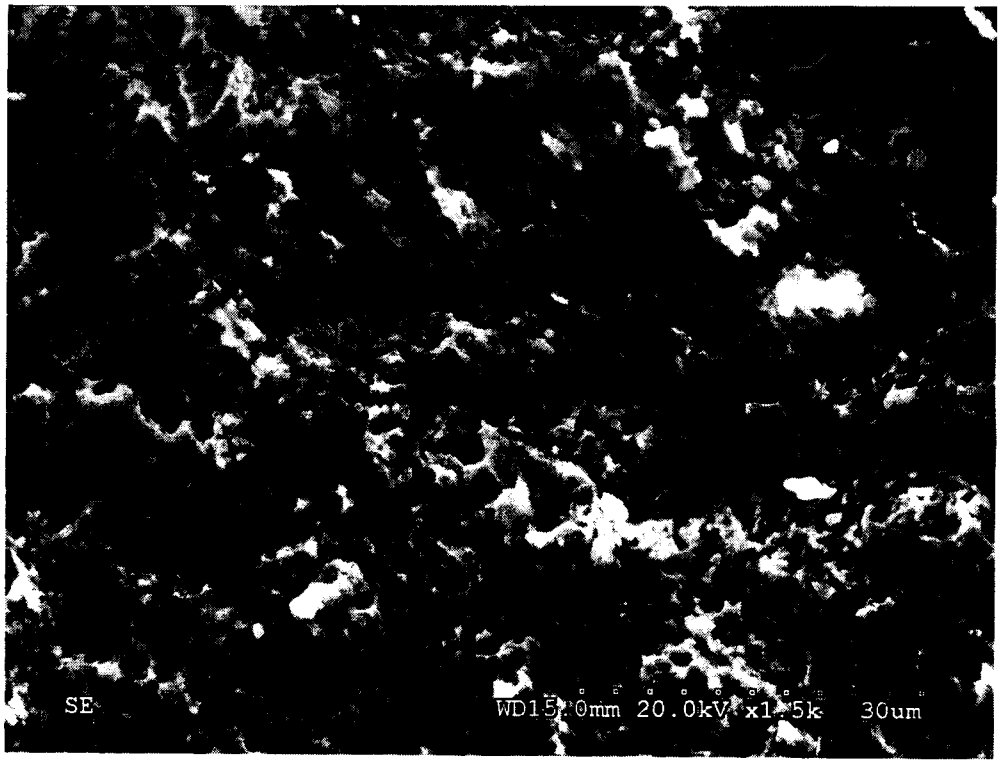

Figure 34: SEM micrograph, Grade 1 after potentiodynamic scan in 0.3 M H_2SO_4 at 0.5 mV/s.

4.2.4 Effect of Electrolyte pH

The effects of acid type and concentration are summarised in Figure 35. There are three regions of interest on this curve, the portion of the curve corresponding to metal dissolution, the region of oxide thickening as indicated by the plateau portion of the curve, and the previously discussed region of oxide layer oxidation. The concentration and type of acid

affects only the first two regions, leaving the shift in current density of the third unchanged. As the acid concentration is increased the maximum anodic current also increases, creating a "nose" immediately prior to the oxide growth. The sharp decrease in current from the maximum anodic current density to the plateau current density corresponds to the attainment of a potential range in which an insoluble corrosion product forms, significantly lowering the rate at which the metal corrodes. Increases in the maximum anodic current densities represent an increased rate of metal dissolution while the system approaches equilibrium with the oxide layer. Once the scan passes this point there is little change in the plateau current density. Interestingly, the same experiment performed using 0.62 M HCl electrolyte (with the same concentration of H^+ ions as 0.3M H_2SO_4 electrolyte) produced the same plateau current density as that of the 5 M H_2SO_4 solution, again suggesting Cl^- ions are responsible for increased attack on the specimens. The maximum anodic current density increases with decrease in pH corresponding to results obtained by Thomas and Nobe.[40]

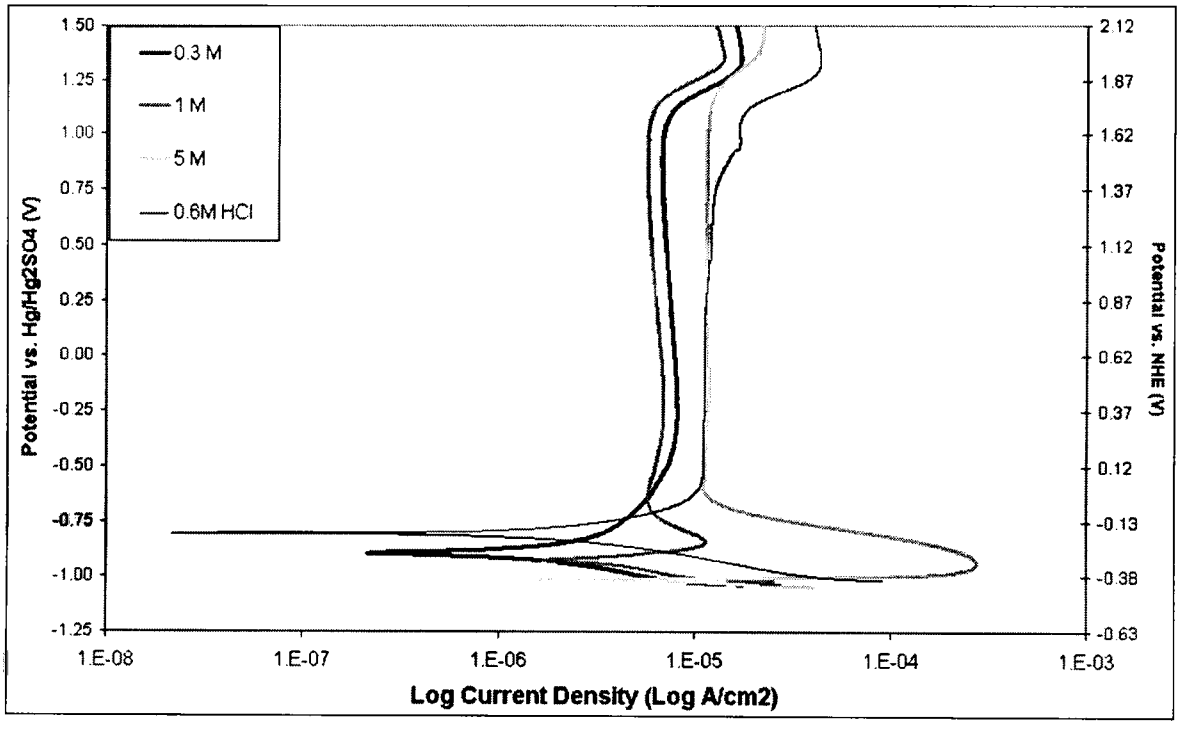

Figure 35: Effect of acid concentration on Ti grade 1 potentiodynamic scans at room temperature in H_2SO_4 and HCl, scan rate 0.5 mV/s.

4.2.5 Effect of Scan Rate

Although ASTM standards recommend a scan rate of 0.5 mV/s for most DC polarization testing procedures, the effects of the scan rate itself were also examined. The results of this testing are shown in Figure 36. Again, the characteristic shift in current density in the upper region of the curves exists, but more noticeable is the effect on the limiting plateau current density. The slower scan rates allowed more time for the samples to build a protective oxide layer. As the scan rate was increased from 0.1 mV/s to 10 mV/s the plateau current density increased more than two orders of magnitude. The corresponding values of charge passed,

calculated by taking the area under the current density vs. potential curve, was estimated and reported for these tests in

Table 6. As the scan rate increased, the amount of charge passed during testing decreased, with the greatest amount of charge being passed by the lowest scan rate.

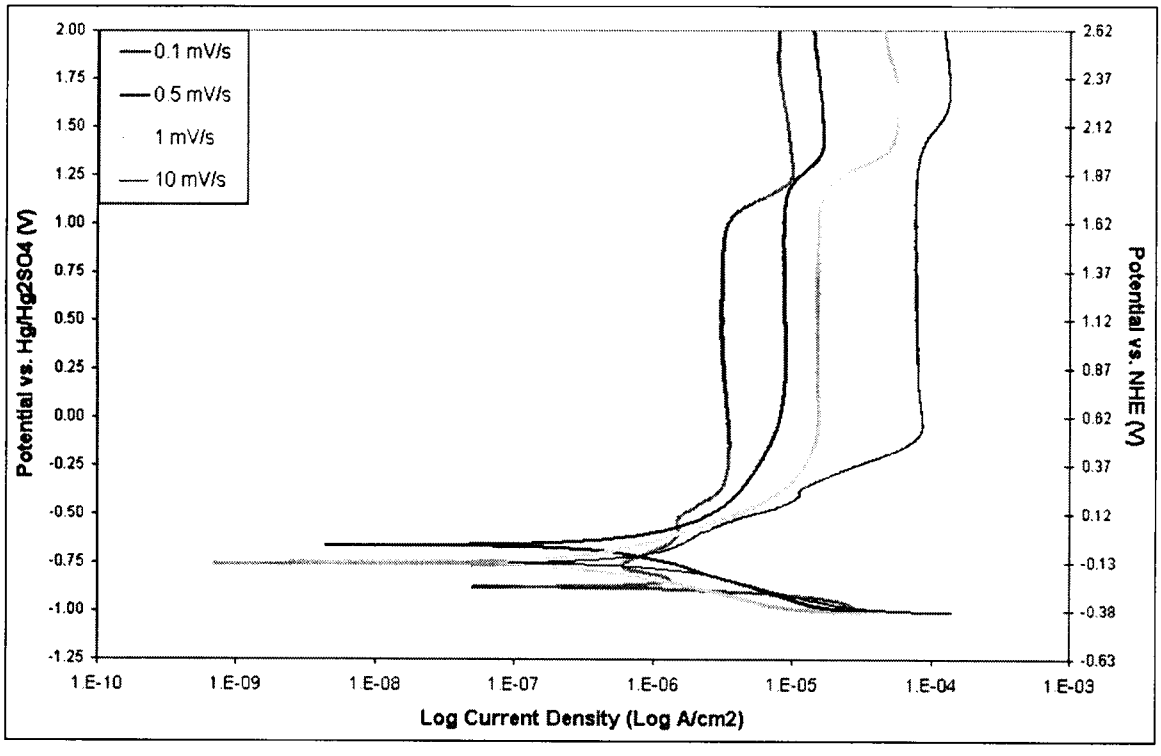

Figure 36: Effect of scan rate on the potentiodynamic behaviour of Ti grade 1 at room temperature in 0.3 M H_2SO_4, scan rate as labelled.

The additional charge passed in the lower scan rate results in a thicker, more ordered oxide forming on the surface. This was also the case as found by other researchers who concluded that films grown using slow potentiodynamic sweeps are more stable than rapidly grown films.[17] Theoretically the crystalline oxide will provide better protection from corrosion than

an amorphous coating, although weaker mechanically, and the plateau currents corresponding to the low scan rates are much smaller. Another possible explanation for this behaviour would be a change in the resistance polarization with scan rate, causing increased currents at the same potentials. The effects of polarization resistance, however, are beyond the scope of this study.

Table 6: Charge passed as a function of scan rate on potentiodynamic scans of Ti grade 1 in 0.3M H_2SO_4.

Scan Rate (mV/s)	Charge Passed ($x10^{-2}$ C)
0.1	5.49
0.5	3.70
1	2.33
10	1.69

4.2.6 Effect of Chlorides

The effects of chlorides present in the electrolyte are more difficult to explain. Figure 37 compares the results of increasing Cl^- ions from 0 to 1.1 M. Although there is little difference between these tests themselves until 1.1 M, the plateau current has increased by a decade over the previous testing without the anions present (Figure 35). After increasing the concentration to 1.1 M, the protective oxide layer began to show signs of localized breakdown, but at a lower plateau current density. In all tests with 1.1 M Cl^- additions, the breakdown point was around 0.5 V_{SHE}, past this potential the behaviour cannot be predicted.

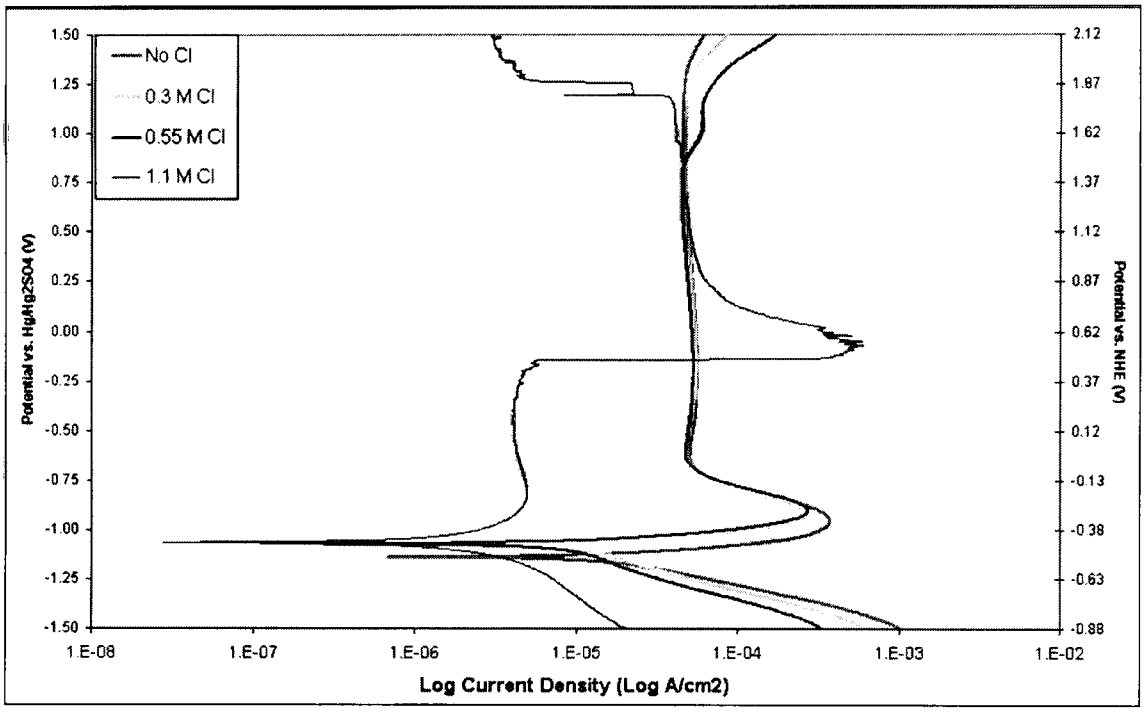

Figure 37: Effect of Cl ion content on the potentiodynamic behaviour of Ti grade 1 at room temperature in 5 M H_2SO_4, scan rate 0.5 mV/s.

The repeated spikes in current on the 1.1 M chloride graphs (Figure 38) are the result of a localized breakdown and repair events occurring on the protective film, followed by precipitation of the corrosion product as the solubility product is reached. The current then returns to the plateau, until higher potentials when breakdown occurs again. The potentials observed for the localized breakdown are well within the region of TiO^{2+} stability at pH = 0.3. The potentials corresponding to the current spikes seem quite low in comparison with similar work by Been and Grauman who have found pitting potentials in excess of +5 V_{SCE} in saturated NaCl at boiling, and pitting potentials of Ti in sulphate and phosphate media are reported to be in excess of +80 V_{SCE}.[10]

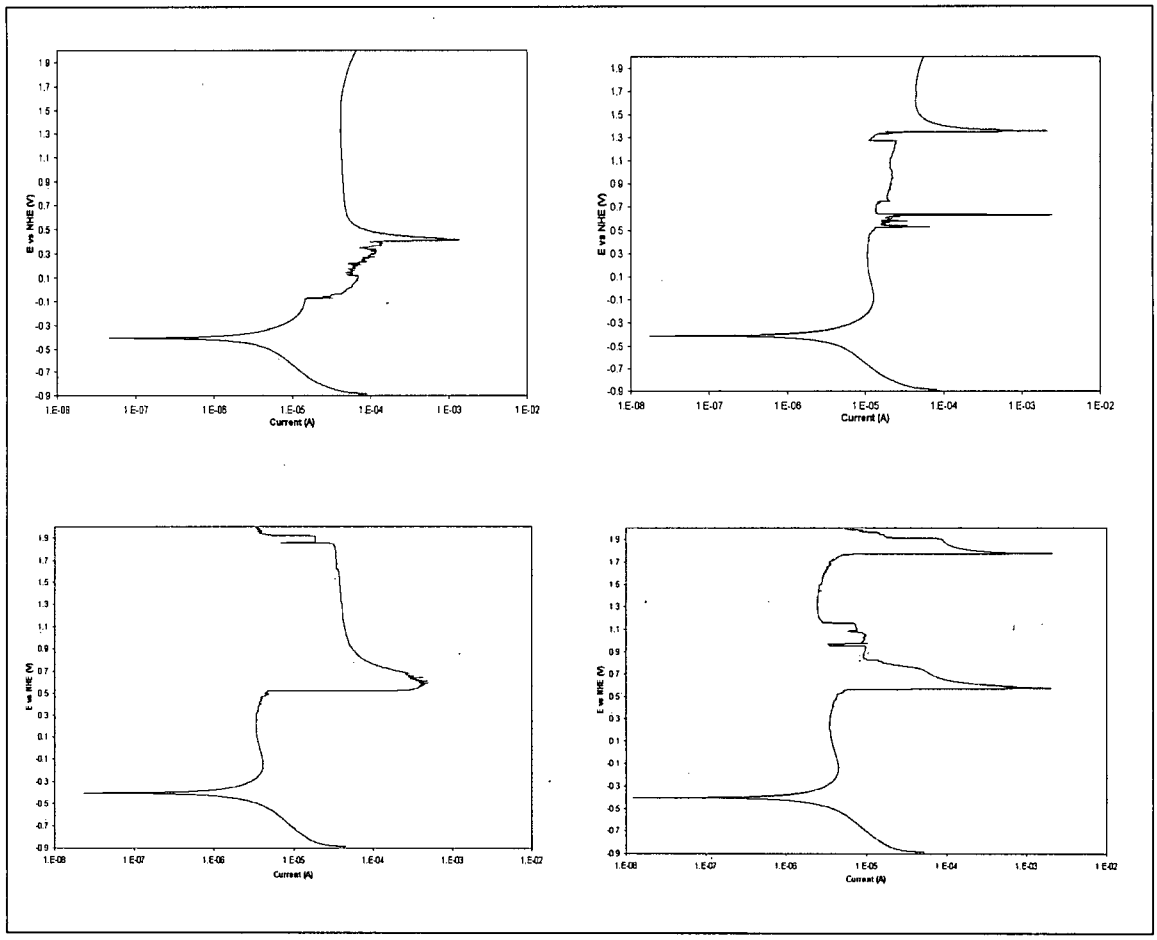

Figure 38: Effect of 1.1 M chloride additions on the potentiodynamic behaviour of Ti. Ti grade 1 in 5M H_2SO_4 at room temperature, scan rate 0.5 mV/s.

These graphs do not show the familiar half-decade shift in current that is present in all of the other graphs. The reason for this is unclear; however the absence may be due to the corrosion inhibiting properties of the Cl^- ion when present in the bulk solution where concentration gradients control the flow of ions and not the driving force to reach electroneutrality. Previous work has found crevice attack to be more severe at higher chloride levels if solution aeration is maintained, but without aeration oxygen solubility is so poor at higher Cl^- concentrations that crevice attack can be stifled.[10] Chloride solutions of 1.1 M are

very artificial and are often observed only in tight crevices, hence these solutions are considered to be high chloride levels. Additionally, solutions were purged with N_2 to de-aerate so little or no oxygen was present in the electrolyte unless as a product of the breakdown of water. The author proposes that the high Cl^- concentration and low O_2 concentration serve to slow the oxidation reaction at the oxide/solution interface, thus avoiding the increased dissolution current.

4.2.7 Effect of Temperature

Studies into the effects of temperature on the potentiodynamic behaviour of Ti alloys were attempted, however the results were quite random and no patterns emerged. Testing on the commercially pure grades were not as inconsistent as testing performed on the crevice corrosion resistant Ti grade 7, but showed opposite trends in corrosion potential and plateau current density from each other, as well as a general lack of reproducibility, making analysis difficult. Upon closer examination of the working electrode surface, small chunks of high fluoride concentration were found randomly scattered on the surface. These appear as the white flakes present in smaller quantities on Ti grade 1 at room temperature (Figure 34). It is known that some fluorocarbon polymers can release fluoride ions into aggressive crevice environments, thereby interfering with test results.[10] Given the constituents of the sample holder itself (Tefzel®) and the crevice free washer designed to eliminate crevice effects

(Teflon®), the results appear to have been tainted and future studies should instead use a working electrode mounted in a more inert material.

4.2.8 Calculation of Corrosion Rates

Calculation of a corrosion rate (R) in mm/y from the potentiodynamic experiments was made using Faraday's Law (Equation 21), with the current taken from the passive region of the curve. This was done because Ti does not exhibit anodic Tafel behaviour due to the formation of an insoluble oxide layer.[61] Instead, the corrosion current (i_{corr}) was taken from the limiting plateau current in the passive region.

$$R = X\frac{i_{corr}W}{\rho F} \tag{21}$$

Where W is the equivalent weight (11.98 g for $Ti^{(IV)}$)[29], ρ is the density of the metal (4.5 g/cm^3)[10][35][57][61] and X is a conversion factor (31,536) for time and distance units.

Table 7 shows the results of these calculations for corrosion currents encountered during this investigation.

Table 7: Calculated corrosion rates for potentiodynamic testing at room temperature for all conditions.

Test Condition			Plateau Current	R x 10^{-6}	R x 10^{-4}
Grade	Acid (M)	Cl^- (M)	(10^X A/cm2)	(mm/yr)	(mpy)
1	0.3	0	-5.20	5.49	2.16
2	0.3	0	-5.25	4.89	1.93
7	0.3	0	-5.12	6.52	2.57
1	1	0	-5.15	6.16	2.43
1	5	0	-5.00	8.70	3.43
1	5	0.28	-4.25	49.0	19.3
1	5	0.56	-4.25	49.0	19.3
1	5	0.85	-4.25	49.0	19.3
1	5	1.13	-5.25	49.0	19.3
1	0.63 M HCl	0.63	-5.00	8.70	3.43

The highest corrosion rates occurred in the experiments with medium strength chlorides present (0.56 and 0.85 M) in 5M H_2SO_4, and were calculated to be 8.7 x 10^{-6} mm/yr (3.4 x 10^{-4} mpy). The corrosion rate of Ti grade 1 in 0.6M HCl, with similar proton concentration as that found in the HPAL process, was determined to be 8.7 x 10^{-6} mm/yr (3.4 x 10^{-4} mpy). Other studies have found corrosion rates of 0.13 mm/yr in 26 wt.% HCl (7 M HCl) at room temperature.[10] According to these calculations, Ti grade 7 displayed the worst resistance to corrosion of the three alloys in the weakest acid solution. Overall, as the acid concentration and Cl^- ion concentration are increased, so is the attack on the metal.

4.2.9 The Effect of Electrode Material on the RedOx Characteristics of Iron

Figure 39 shows the Eh-pH diagram for the Fe-S-H_2O system as developed using HSC Chemistry software. In the potential and pH regions of this study there are several phase boundaries occurring if solid sulphates or sulphides are formed. However, if the assumption is made that all iron sulphates completely dissociate in the electrolyte, both the Fe^{3+} and Fe^{2+} ions are stable over the potential regions tested.

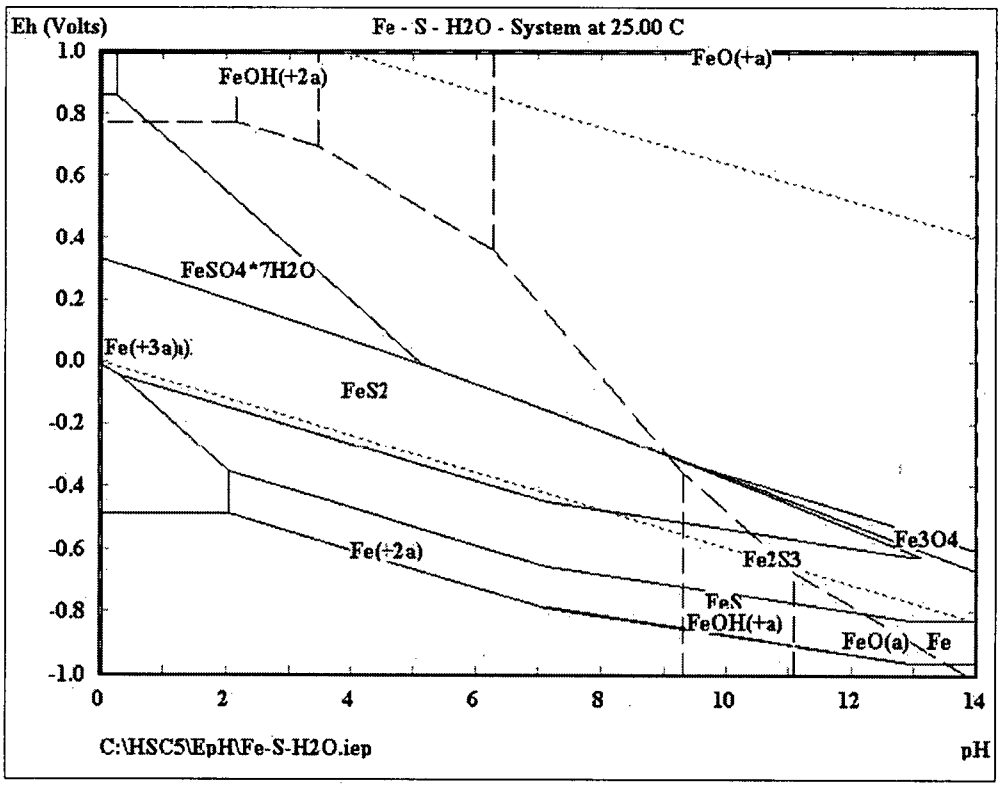

Figure 39: Eh-pH diagram for the Fe-S-H2O system at 25°C, with 0.41M Fe^{2+} and 0.3M H_2SO_4. Developed using HSC Chemistry software.

The open circuit potential (E_{oc}) for the iron redox reaction was calculated to be approximately 0.653 V_{SHE} for all tests using the following equation:

$$E_{oc} = E^{o} + 2.303\frac{RT}{nF}\log\left(\frac{[Fe^{3+}]}{[Fe^{2+}]}\right) \qquad (22)$$

Where E^{o} = 0.771 V_{SHE}[56] and $\log[Fe^{3+}]/[Fe^{2+}]$ = 0, -1, and -2. Both calculations and graphical interpretations are in agreement and both show little affect of cation concentration on the open circuit potential. It should be mentioned that E_{oc} was the same for both electrodes. The ferrous concentration seemed to only effect the kinetics of the iron redox reaction and had only a small effect on the thermodynamics.

Figure 40 depicts the results of iron redox testing on a Pt working electrode and these correspond well to work by Schmickler using similar conditions.[64] With no iron sulphate present in the electrolyte, E_{oc} is approximately 0.8 V_{SHE}, indication that the decomposition of H_2O is the only reaction occurring during polarization. Once Fe ions are introduced the potential drops and E_{oc} hovers around the calculated value of 0.6 V_{SHE} and those tests showing Tafel behaviour have relatively high slopes suggesting surface control mechanisms are responsible for current behaviour. Graphs would appear to be exhibiting concentration polarization: mass transfer or diffusion limited effects at the reacting metal surface. This is because a point is reached where increasing the driving force (i.e. potential) no longer has any effect on the rate of the reaction. The reaction rate instead becomes dependant on either the mass transport rate at which reactant species arrive at the electrode, or the rate at which the

products of the reaction can be removed from the vicinity of the electrode surface, and is essentially independent of potential.

All of the reduction curves show limiting currents due to concentration polarization and hence no Tafel data could be extracted, unfortunately the same was also true for the anodic curves taken from electrolytes with ferrous ions in excess of 0.04 M Fe^{2+}. The limiting anodic current was shown to increase with ferrous sulphate concentration suggesting it is the transport of ferrous ions to the electrode surface that is the rate-controlling step in the anodic reaction. At greater concentrations of ferrous ions, the removal of oxidized Fe^{3+} ions from the electrode surface may be slower than the oxidation kinetics and a limiting current based on concentration gradients may be formed. It is also possible that if the concentration of ferric ions becomes too large, oxide formation will occur.

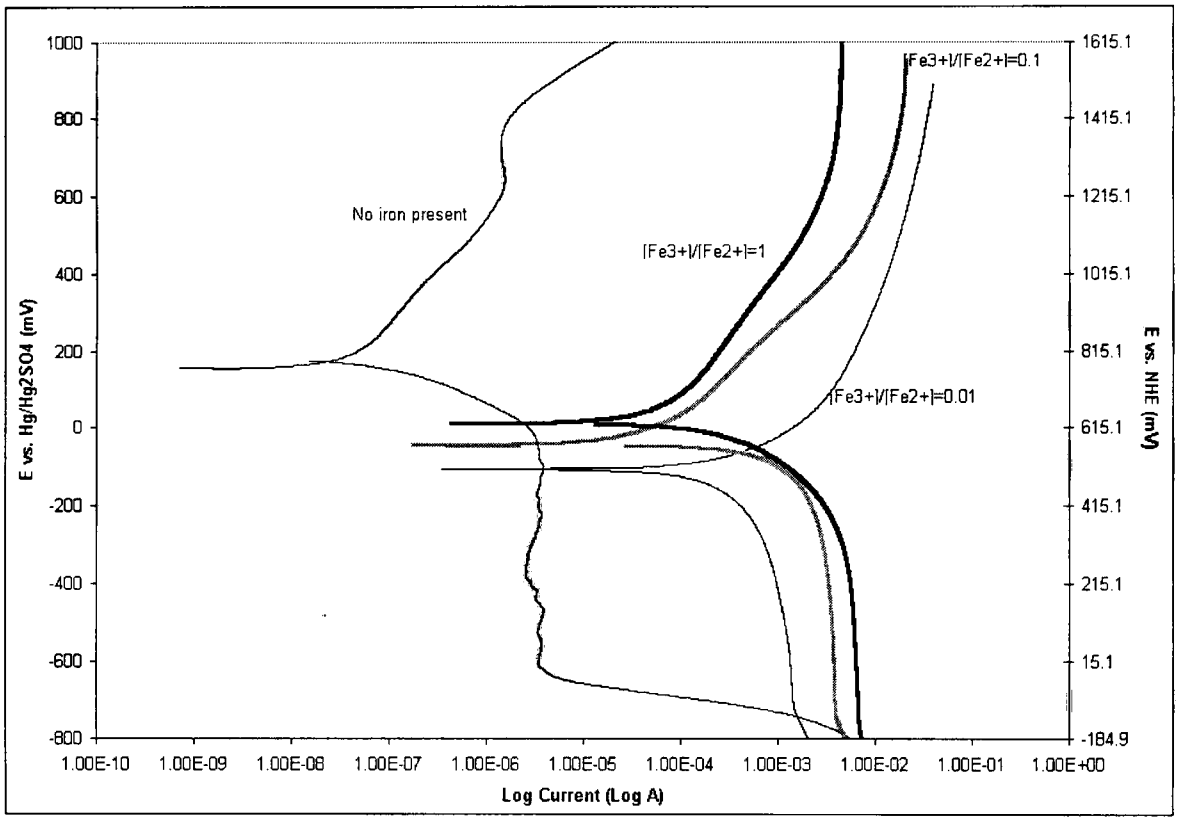

Figure 40: Effect of [Fe3+]/[Fe2+] ratio on a Pt electrode at room temperature in 0.3 M H2SO4, scan rate 0.5 mV/s.

Similarly, in Figure 41, only the anodic curves corresponding to the lower concentrations of ferrous ions were found to exhibit Tafel behaviour eventually going to concentration polarization. Again, the high concentration of ferrous in $[Fe^{3+}]/[Fe^{2+}] = 0.01$ reached a limiting current at lower overvoltage than the rest and at lower potentials, before any Tafel behaviour can occur. This information is again support of the theory that ferric diffusion away from, or ferrous diffusion to, the surface is the limiting step in the iron redox reaction. In terms of the HPAL environment this would suggest the concentration of ferric or ferrous ions from ores in slurry feed could be the controlling factors in the reduction and oxidation currents occurring on the Ti surface, thus controlling metal dissolution in creviced situations.

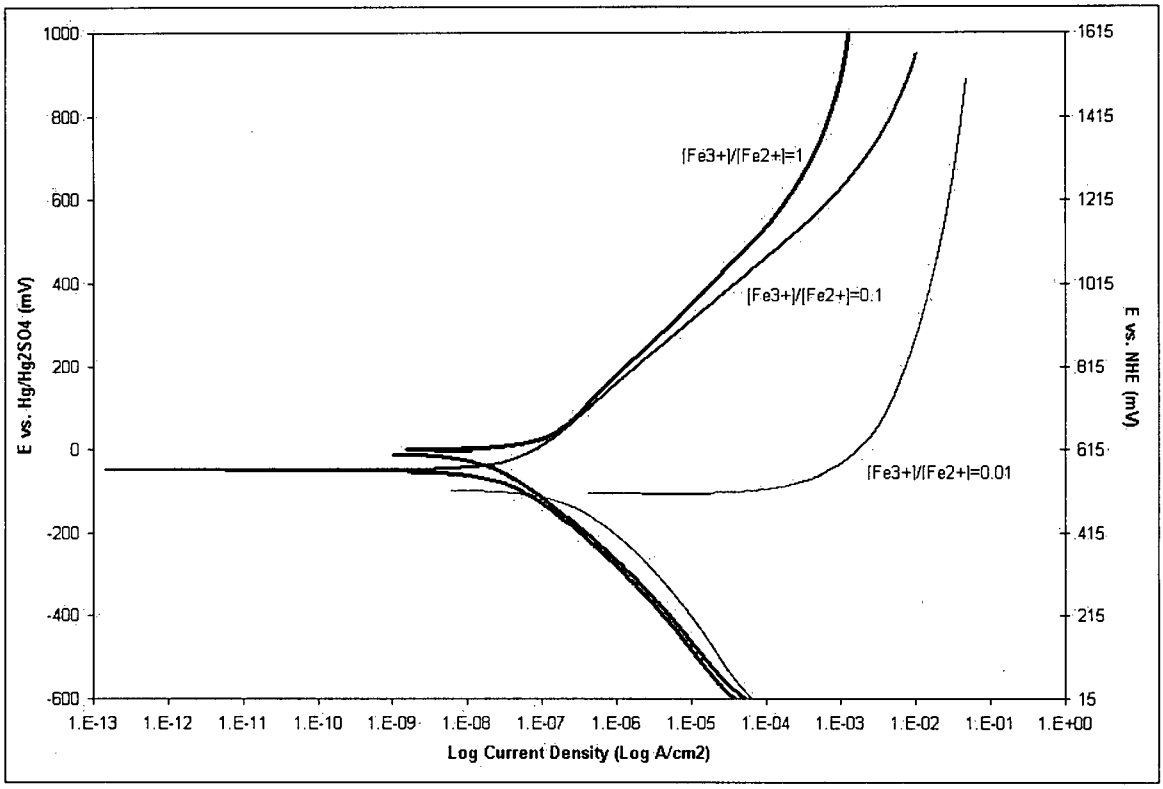

Figure 41: Effect of [Fe3+]/[Fe2+] ratio on a Ti electrode at room temperature in 0.3 M H2SO4, scan rate 0.5 mV/s.

4.2.10 Calculation of Iron Diffusion Coefficients and Limiting Anodic Current Densities

Using the results of the Fe redox scans the diffusion layer thickness (δ) on a rotating disc electrode can be calculated using the Levich Equation[31]:

$$\delta = 0.61 D^{\frac{1}{3}} \upsilon^{\frac{1}{6}} \omega^{-\frac{1}{2}} \qquad (23)$$

Where D is the diffusion coefficient of the ferric/ferrous ions (approximated to be 7.5 x 10^{-6} cm^2/s), ω is the angular velocity of the disc electrode (104.72 s^{-1}), and υ is the kinematic viscosity (1.02 x 10^{-2} cm^2/s) and is calculated from the dynamic viscosity (η) and the density (ρ) of the electrolyte:

$$\upsilon = \frac{\eta}{\rho} \tag{24}$$

This results in a diffusion layer thickness of 5.43 x 10^{-4} cm or 5.43 μm. In addition, the limiting anodic current can be calculated using equation 23 and compared to values found empirically:

$$i_{l,a} = 0.62nFAD^{\frac{2}{3}}\omega^{\frac{1}{2}}\upsilon^{-\frac{1}{6}}C^* \tag{25}$$

Where C^* is the concentration of ferrous ions in the bulk solution in mol/cm^3.

Table 8 shows the calculated values for the $i_{l,a}$ and compares them to those found during this study.

Table 8: Results of $[Fe^{3+}]/[Fe^{2+}]$ potentiodynamic scans on Pt and Ti electrodes in 0.3M H_2SO_4.

$[Fe^{3+}]/[Fe^{2+}]$	Electrode Material and Surface Area (cm^2)		Mass of Ferric (g)	Mass of Ferrous (g)	Conc. Of Ferric (x 10^{-5} M/cc)	Conc. Of Ferrous (x 10^{-5} M/cc)	$i_{l,a}$ Act. (x10^{-3} A)	$i_{l,a}$ Calc. (x10^{-3} A)
1	Pt	0.283	2.29	2.29	8.20	8.20	3.16	11.69
0.1	Pt	0.283	1.153	11.52	4.12	41.26	17.8	58.80
0.01	Pt	0.283	0.622	62.199	2.22	222.75	31.6	317.49
1	Ti	0.833	1.184	1.189	4.24	4.26	1	17.86
0.1	Ti	0.833	1.241	12.53	4.44	44.87	10	188.37
0.01	Ti	0.833	0.662	66.19	2.37	237.04	39.8	994.51

All calculated values were greater than those found during testing prompting investigation into the variables used for calculation. As the only approximated value was the assumed diffusion coefficient approximated. By rearranging equation 25 and solving for the diffusion coefficient, an average calculated value was found to be 4.65×10^{-7} cm^2/s; two orders of magnitude smaller than the assumed value. Further recalculation yielded a diffusion layer thickness of 2.15×10^{-4} cm or 2.15 μm, less than half of the value calculated originally. With such a low difusion coefficient and such a small diffusion layer thickness, it would be expected that mass transport effects at the surface of the electrode would be the limiting factor in redox kinetics and concentration polarization should be observed.

The graph in Figure 42 is a direct comparison between the Ti and Pt working electrode at $[Fe^{3+}]/[Fe^{2+}] = 0.1$ in 0.3M H_2SO_4 with approximately 0.04M ferric and 0.45M ferric ions at room temperature using a scan rate of 0.5 mV/s. From the graph it can be seen the Tafel slopes are very high leading to a concentration polarization mechanism at the more extreme potentials. In addition, the Tafel slope of the reaction occurring on the Ti working electrode

(175 mV/decade) is lower than that of the Pt working electrode (300 mV/decade). Tafel extrapolation to the $E_{Fe2+/Fe3+}$ reversible potentials showed the exchange current densities to be approximately 10^{-7} and 10^{-4} on the titanium and platinum surfaces respectively. The slower kinetics on the Ti electrode compared to the Pt electrode mean reduction occurs faster on the more noble Pt surface. Assuming the same is true for the Pd additions in the Ti grade 7 alloys, it would explain the improved corrosion resistance, particularly in a crevice situation. If the exchange current densities of the HER are greatest on the noble metals then the reversible potential of the H_2-H^+ couple is positive relative to the critical passivation potential at all pH.[61] Consequently, accumulation of Pd on the surface of the alloy, resulting from the preferential dissolution of Ti in a creviced geometry (or any other highly aggressive electrolyte), is accompanied by an increase in the effective cathodic current density due to the HER or in this case, the Fe reduction reaction. Metal dissolution taking place within a crevice requires a reduction reaction on the surface to consume the electrons produced by the other half of the reaction. Therefore, it should theoretically be possible to passivate Ti simply by increasing the effective cathodic current density at an active-state titanium surface.[61]

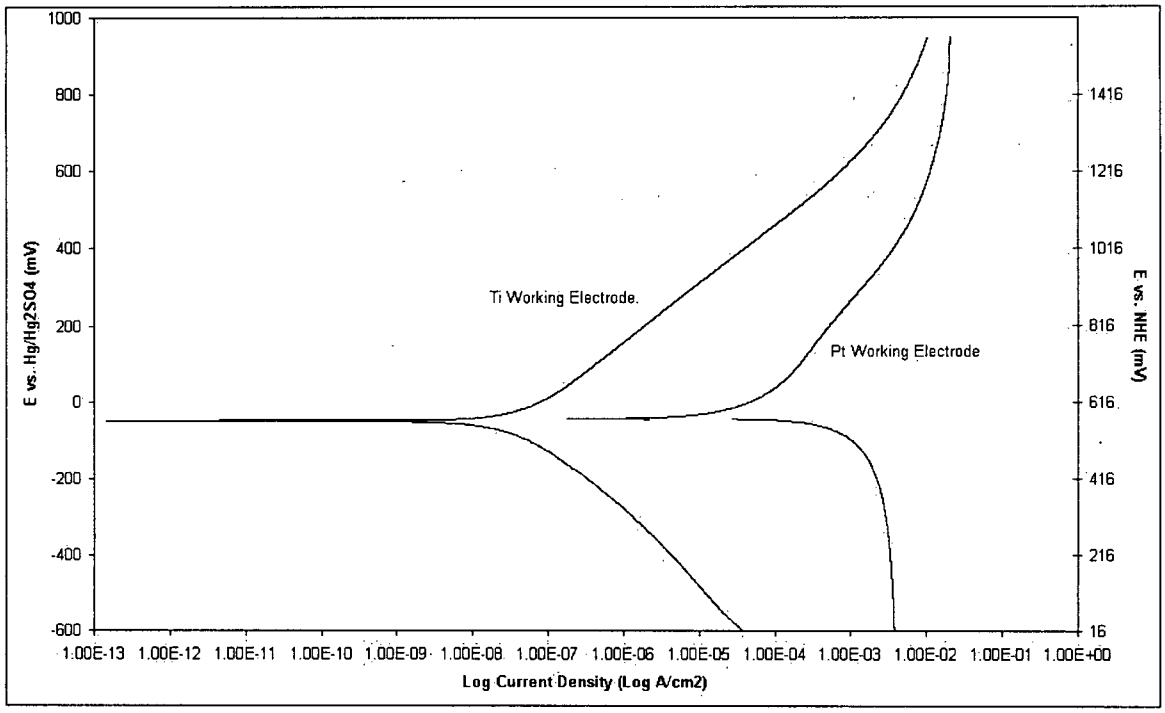

Figure 42: Comparison of reaction kinetics on Ti and Pd surfaces in 0.3 M H_2SO_4 with 0.08M ferric and ferrous sulphate, and 0.04M ferric and ferrous Sulphate respectively. [Fe3+]/[Fe2+] = 0.1.

Under typical oxide growth, electrons are consumed by the O_2 reduction reaction occurring on surfaces external to the crevice.[38] However, with the presence of ferrous ions on the surface in the form of scale, the O_2 reduction reaction would take the excess electrons from the ferrous oxidation and not the metal dissolution. If ferrous oxidation were to occur faster than the oxygen reduction, no Ti would be consumed within the crevice.

5 Conclusions and Recommendations

The corrosion of three commercially available Ti alloys (ASTM grades 1, 2, and 7) in aqueous sulphuric acid electrolytes (0.1, 0.3, 1, and 5M H_2SO_4) was studied using immersion testing over several months, open circuit potential measurements, and potentiondynamic polarization techniques. The effects of iron and chloride ions present in HPAL slurries were also examined using potentiodynamic polarization techniques and a RDE. Analysis of results and SEM micrographs have yielded interesting information concerning the nature of the oxide growth mechanisms and possible insight into corrosion problems for WA AC linings. Combining the results of this study with information gained from the literature review, the following conclusions can be made.

As discovered during long term immersion testing of Ti grades 2 and 7, the presence of even trace elements of oxidizing species, such as Ti^{3+} from Ti dissolution, can effectively inhibit corrosion by supporting oxide film growth or retarding the initiation phase of crevice corrosion. However all samples succumbed to a localized form of corrosion as a result of preferential attack on iron impurities, leaving small pits behind. The attack was shallow and sparsely distributed. Ti grade 7 showed obvious improvement in corrosion resistance over the commercially pure grades by forming a thick oxide layer on the exposed surface with more complete coverage than the other alloys. Pd additions proved to be helpful in preventing corrosion but less refined Ti grade 2 displays marginally better resistance in some situations

due to alloy inhibitor ions. In all cases the Ti coupons eventually became stable in the immersion solutions unless fresh solution was introduced.

Open circuit potential measurements place the Ti grade 7 rest potential in 0.3M H_2SO_4 at room temperature at approximately 0.07 V_{SHE}, while Ti grade 1 and Ti grade 2 have rest potentials in the same solution of approximately -0.50 V_{SHE}. The elevated potential found for Ti grade 7 is due to the Pd alloying additions, which increase the rate of the HER on the surface of the working electrode. It would be interesting to measure the potentials associated with the immersion testing over the longer trial periods. Combining a long term potentiostatic testing with more frequent weight loss measurements corresponding to changes in potentials would provide a valuable "map" of the corrosion events as they happen.

Ti alloys react to anodic polarization by thickening the amorphous, hydrated oxide layer. The oxide then thickens until the potential is raised above 1.8 V_{SHE} when there is a change in the oxidation state of the oxide cations. This corresponds to the formation of TiO^{2+} complexes with either Cl^- or SO_4^{2-} ions to form titanium oxide chloride or titanium oxide sulphate respectively. Eventually, the solubility of the complexes is reached and a new limiting plateau current is reached. The maximum corrosion rate obtained during testing was using Ti grade 1 in 5M H_2SO_4 with Cl^- ions and had a value of 4.9×10^{-5} mm/yr (0.002 mpy). However, due to the inevitable formation of oxides in this system, the corrosion rates calculated from the current plateau are exaggerated. The severity of attack was found to increase with a decrease in pH, but unfortunately the effects of temperature were very difficult to ascertain given the nature of

the testing equipment. Interestingly, the result of elevated temperature studies might have been a lower limiting current plateau due to bisulphate formation at increased temperature.

In all cases, corrosion rates were greater in solutions containing NaCl. Chlorides present in process solutions will selectively attack grain boundaries, eventually leading to grain fallout. This occurs over the entire surface of the material and results in a "general" corrosion of the metal. Spatially localized film breakdown was determined empirically to occur at potentials above 0.5 V_{SHE} in 5M H_2SO_4 at room temperature and 1.1 M anion concentration. The results of all experiments show an increase in the corrosion rate with Cl^- concentration and all maximum corrosion rates reported were for electrolytes containing chloride ions. Further examination into the combined effects of chlorides at temperature in the presence of ferrous ions would prove quite useful in predicting maximum corrosion rates of Ti components in service. If samples were immersed a short distance into hematite powder within the electrolyte the effects of scale formation on Ti in HPAL environments could be studied specifically.

The reduction and oxidation characteristics of the Fe^{2+}-Fe^{3+} were examined on RDE electrodes made from both Pt and Ti. All results show limiting currents to be controlled by concentration polarization, and the kinetics of the overall reactions were faster on the surface of the nobler Pt electrode. Cathodic Tafel slopes could not be determined without linear cathodic Tafel behaviour and the anodic Tafel behaviour occurred only at the lower concentrations of ferrous ions. Slopes were on the order of 150-300 mV/decade with exchange current densities of 10^{-7} and 10^{-4} for Ti and Pt respectively. In addition, as the concentration of ferrous ions increased the anodic Tafel slopes both decreased and reached limiting current

densities at lower potentials. The improved kinetics on the noble metal explains the use of Pd as an alloying element in Ti. By improving the speed of ferrous oxidation on the metal surface, reduction reactions are fed the necessary electrons required to halt crevice initiation.

Unfortunately for the HPAL process, the effects of ferrous ions in slurries on the commercially pure Ti grades will have the opposite effect. Porous scale formation on internal AC surfaces will trap solutions containing dissolved Cl^- ions against the Ti surface. As local chemistry changes, the pH will decrease and a crevice situation occurs. Without the Pd additions, the Ti retards the Fe redox reactions and the Ti is attacked via normal crevice corrosion mechanisms. Further investigations into the basis of this phenomenon and Ti's effect on the kinetics of other reactions occurring simultaneously would prove beneficial in the modelling the effects of the aggressive HPAL process streams.

Additional investigation of the general corrosion mechanisms of these alloys in aqueous sulphuric acid electrolyte should include significantly more aggressive environments involving higher temperatures and pressures. DC polarization testing should be concentrated in the active region between -0.3 and 0.1 V_{SHE} at low pH using slow scan rates or even potentiostatic methods if possible as this should be the region of most aggressive attack on α-phase alloys. Specific studies on Ti applications in the HPAL process would be best achieved by placing corrosion coupons in direct contact with process streams and slurries. Simultaneously monitoring weight loss and measuring the surface potentials relative to the surrounding lining, allows the erosion and crevice corrosion effects to be treated separately to observe the mode of crevice formation (erosion or H^+ induced cracking). Finally, forensic evaluation of actual AC

linings using XPS, SEM, and optical microscopy would be a most effective method for determining the corrosion mechanisms at work.

6 Nomenclature

TDS	Total Dissolved Solids
CPI	Chemical Process Industry
α	hcp phase
β	bcc phase
AC	Autoclave
WA	Western Australia
XPS	X-ray Photoelectron Spectroscopy
XRD	X-ray Diffraction
SEM	Scanning Electron Microscope
EDS	Electron Diffraction Spectroscopy
DI	De-Ionized Water
Δm	Change in mass (g)
HPAL	High Pressure Acid Leach Process
ϕ^I	Potential of Solution I
ϕ^{II}	Potential of Solution II
A	Surface area (cm^2)
ρ	Density (g/cm^3)
R	Corrosion rate (mm/yr or mpy)
PAR	Princeton Applied Reasearch
RDE	Rotating Disc Electrode
a_{H+}	Activity of hydrogen ions
ΔG	Change in free energy (J/mol)
n	no. of electrons transferred
E	Potential (V)
LJP	Liquid Junction Potential (V)
W	Equivalent weight
V_d	Explosive detonation velocity
V_c	Impact point velocity
V_p	Plate collision velocity

7 References

(1) Grauman, J.S. and Say, T. "Titanium for Hydrometallurgical Extraction Equipment," Advanced Materials and Processes, March 2000, pp. 25-29.

(2) Czerny, C.J. and Whittington, B. "Scale Formation in the Pressure Acid Leach Process," courtesy of Oretest Pty. Ltd., provided by Timet.

(3) Kyle, J.H. "Water Quality in Nickel Laterite Processing," courtesy of Oretest Pty. Ltd, provided by Timet.

(4) Banker, J.G. "Hydrometallurgical Applications of Titanium Clad Steel" Website: Cladinc.com.

(5) Yao, L-A. et. al. "Microelectrode Monitoring the Crevice Corrosion of Titanium," Corrosion, Vol. 47, No. 6, pp. 420-423 (1991).

(6) McKay, P. and Mitton, D.B. "An Electrochemical Investigation of Localized Corrosion of Titanium in Chloride Environments," Corrosion, Vol. 41, No. 1, pp. 52-62 (1985).

(7) Perdikis, P. and Papangelakis, G. "Scale Formation in a Batch Reactor Under Pressure Acid Leaching of a Limonitic Laterite," CMQ, Vol. 37 no. 5 (1998).

(8) Kyle, J.H. and Corrans, I.J. "Pilot Plant Testing of Nickel Laterites," courtesy of Oretest Pty. Ltd., provided by Timet.

(9) Rubisov, D.H. and Papangelakis, V.G. "The effect of acidity 'at temperature' on the morphology of precipitates and scale during sulphuric acid pressure leaching of laterites," CIM Bulletin Vol. 93, no. 1041 (2000).

(10) Been, J. and Grauman, J.S., "Titanium and Titanium Alloys," Uhlig's Corrosion Handbook, 2nd ed., R.W. Revie Ed., John Wiley and Sons, Inc. (2000).

(11) Mountford, J.A. Jr. "Titanium Alloys for the CPI," Advanced Materials and Processes, June 2001, pp. 55-58.

(12) Nobili, A. "Explosion Bonding Process" NOBELCLAD Technical Bulletin, (1999).

(13) Collings, E.W. Applied Superconductivity, Metallurgy and Physics of Titanium Alloys. New York, Plenum Press (1986).

(14) Tromans, D. "Modeling Oxygen Solubility in Water and Electrolyte Solutions," Industrial Engineering and Chemistry Research, Vol. 39, no. 3 (2000).

(15) McKay, P. and Mitton, D.B. "An electrochemical Investigation of Localized Corrosion on Titanium in Chloride Environments," Corrosion, Vol. 41, no. 1, NACE (1985)

(16) Ding, X. and Liu, X. "Synthesis and microstructure control of nanocrystalline titania powders via a sol-gel process," Materials Science & Engineering A, vol. 224 p. 210-215, 1997.

(17) Blackwood, D.J. nad Chooi, S.K.M., "Stability of protective oxide films formed on a porous titanium," Corrosion Science 44 (2002).

(18) Neville, A. and Xu, J. "An assessment of the instability of Ti and its alloys in acidic environments at elevated temperature," Journal of Light Metals 1 (2001).

(19) Pang, M. et. al. "Structural and Mechanical Characteristics of Anodic Oxide Films on Titanium," Corrosion, Vol. 57, No. 6, pp. 523-531.

(20) Schutz, R.W. "Understanding and Preventing Crevice Corrosion of Titanium Alloys Parts 1 & 2," Materials Performance, October and November 1992.

(21) Kobayashi, M. et. al. "Study on Crevice Corrosion of Titanium," Nippon Stainless Steel Co., Ltd. Joetsu Japan, provided by TIMET.

(22) Noel, J.J., "The Electrochemistry of Titanium," PhD thesis, University of Manitoba (2000).

(23) Cecile, B. et. al. "Contribution to the Study of the Behaviour of Titanium in Sulphuric Acid Solution at High temperature and Pressure," Department Mineralurgie BRGM, Orleans Cedex, France, Provided by TIMET Corp.

(24) Mountford, J.A. Jr. Titanium-"Properties, advantages and applications: Solving the corrosion problem in marine service," Provided by: Tico Titanium, Inc. New Hudson Michigan, U.S.A.

(25) Grauman, J.S. and Say, T. "Understanding the Behaviour and Preventing Problems with Titanium in Hydrometallurgical Pressure Leaching Equipment," ALTA Hydrometallurgy Forum (1999).

(26) Whittington, B.I. and Muir, D. "Pressure Acid Leaching of Nickel Laterites: A Review," Min. Pro. Met. Rev., Vol. 21 (2000).

(27) Moulder, J.F. Handbook of X-ray Photoelectron Spectroscopy. Perkin Elmer Corp. (1992).

(28) Czerny, C.J. and Whittington, B. "Scale Formation in the Pressure Acid Leach Process," Oretest Pty. Ltd., Kewdale Western Australia and CSIRO Division of Minerals, Waterford Western Australia, provided by TIMET.

(29) Been, J. "Titanium Corrosion in Alkaline Hydrogen Peroxide Environments," PhD. Thesis, UBC, Oct 1998.

(30) Blackburn, M.J., Williams, J.C. "The preparation of thin films of titanium alloys," Trans. Of the Met. Soc. Of AIME. No. 239 (1967)

(31) Levich, V.G., Physicochemical Hydrodynamics. Prentice-Hall, NJ (1962).

(32) Yamabi, S. and Imai, H. "Synthesis of Rutile and Anatase Films with High Surface Areas in Aqueous Solutions Containing Urea," Thin Solid Films 434 (1-2) (2003).

(33) Song, J.S. et al. "Redox Abilities of Rutile TiO_2 Ultrafine Powder in Aqueous Solutions," Metals and Materials International, Vol. 8 (2002).

(34) ASTM G 31 9.1 Standard Recommended Practice for Laboratory Immersion Testing of Metals

(35) Been, J. and Tromans, D., "Titanium Corrosion in Alkaline Hydrogen Peroxide," Corrosion, Vol. 56, no. 8 (2000).

(36) Bard, A.J. and Faulkner, L.R. Electrochemical Methods: Fundamentals and Applications. 2nd ed. John Wiley and Sons, New York (2001).

(37) Criss, C.M. and Cobble, J.W., "The Thermodynamic Properties of High Temperature Aqueous Solutions. IV. Entropies of the Ions up to 200°C and the Correspondence Principle", J. Am. Chem. Soc., Vol. 86 (1964).

(38) He, X., Noel, J.J. and Shoesmith, D.W. "Temperature dependence of Crevice Initiation on Ti Grade-2" Journal of the Electrochemical Society, Vol. 149, no. 9 (2002).

(39) Betts, A.J. and Boulton, L.H. "Crevice Corrosion: review of mechanisms, modeling and mitigation," British Corrosion Journal, Vol. 28, No. 4. 1993, pp. 279-295.

(40) Thomas, N.T. and Nobe, K. "The electrochemical Behaviour of Titanium: Effect of pH and Chloride ions." J. Electrochem. Soc.: Electrochemical Technology, Vol. 116, No. 12 (1969).

(41) Metals Handbook 9th Ed., Vol. 13: Corrosion (1992).

(42) Perdikis, P. and Papangelakis, V.G. "Scale Formation in a Batch Reactor Under Pressure Acid Leaching of a Limonitic Laterite," Canadian Metallurgical Quarterly, Vol. 37, No. 5, pp. 429-440 (1998).

(43) Grauman, J.S. and Willey, B. "Shedding New Light on Titanium in CPI Construction," Titanium Metals Corp. and Titanium Fabrication Corp.

(44) Yonghong, Y. et. al. "Electrochromism of titanium oxide thin films," Thin Solid Films, vol. 298 p. 197-199, 1997.

(45) ASTM G48-92 "Standard Test Methods for Pitting and Crevice Corrosion Resistance of Stainless Steels and Related Alloys by Use of Ferric Chloride Solution (1992).

(46) Jenner, G. "Design of Autoclaves for Corrosive Media," Physica 139 & 140B (1986).

(47) Lamb, S. and Thayer, M.J. "Materials for the Hydrometallurgical Industry," Paper 01346 NACE (2001)

(48) Kritzer, P., Boukis, N. and Dinjus, E. "Factors controlling corrosion in high temperature aqueous solutions: a contribution to the dissociation and solubility data influencing corrosion processes," Journal of Supercritical Fluids, Vol. 15 (1999).

(49) Cservenyak, I., Kelsall, G.H. and Wang, W. "Reduction of Ti IV Species in Aqueous Sulphuric Acid and Hydrochloric Acids I. Titanium Speciation," Electrochemica Acta Vol. 41 no. 4 (1996).

(50) Seagle, S.R. and Thomas, D.E. "Status of Titanium Technology," Chemical Engineering Progress, June (1986).

(51) Takamura, A. "Corrosion Resistance of Ti and Ti-Pd Alloy in Hot, Concentrated Sodium Chloride Solutions," NACE (1967).

(52) Pourbaix, M. Atlas of Electrochemical Equilibria in Aqueous Solutions. Pergamon Press, Toronto (1966).

(53) Metals Handbook, Ninth ed. Volume 13, Corrosion (1992).

(54) Bard, A.J., Parsons, R. and Jordan, J. Standard Potentials in Aqueous Solutions "Titanium, Zirconium, and Hafnium." IUPAC (1983).

(55) Technical bulletin 51 – Impeller Axle Corrosion and Wear Resistance. Data Industrial Corp. www.dataindustrial.com.

(56) Pourbaix, M., Atlas of Electrochemical Equilibria in Aqueous Solutions. Chapter 4, Section 8.1, Pergamon Press (1966).

(57) Schutz, R.W. "Utilising Titanium to Successfully Handle Chloride Process Environments," METSOC, Chloride Metallurgy Volume 1 pp. 85-88 (2002).

(58) Newman, J.S. Electrochemical Systems. Prentice Hall N.J. (1973).

(59) Tromans, D. "Modeling Oxygen Solubility in Water and Electrolyte Solutions" Ind. Eng. Chem. Res., Vol. 39, No. 3 pp. 805-812 (2000).

(60) Staples, B. R. Holcomb, G. R. Cramer, S. D. "Calculation of pH for high-temperature sulfate solutions at high ionic strengths," Corrosion, Houston, TX pp. 35-41 (1992).

(61) Kelly, E.J., "Electrochemical Behaviour of Titanium," Modern Aspects of Electrochemistry, Vol. 14 pp.319-423 (1982).

(62) Lumsden, J.B. and Staehle, R.W., Temperature Dependence of the Film Covered Electrode," Dept. of Metallurgical Engineering, The Ohio State University, Columbus, (1992).

(63) Tromans, D. and Frederick, L., "Electrochemical Studies of Crevice Corrosion Rates on Stainless Steels," Corrosion, Vol. 39, no. 8 pp.306-311 (1983).

(64) Schmickler, W. and Schultze, J.W., "Electron Transfer Reactions on Oxide-Covered Metal Electrodes," Modern Aspects of Electrochemstry, Vol. 17, pp.357-407 (1986).

(65) Kelly, E.J., "Anodic Dissolution and Passivation of Titanium in Acidic Media," J. Electrochem. Soc.: Electrochemical Science and Technology pp.2064-2074 (1979).

(66) Clarke, C.F., Ikeda, B.M. and Hardle, D., "Effect of Crevice Corrosion on Hydrogen Embrittlement of Titanium," EICM Proceedings Provided by TIMET Corp.

(67) Schmickler, W. and Mohr, J., "The rate of electrochemical electron-transfer reactions," Journal of Chemical Physics, Vol. 117, no. 6, pp. 2867-2872 (2002).

(68) Hua, F., Sarver, J.M., and Jevec, J.M. "General Corrosion Studies of Candidate Container Materials in Environments Relevant to Nuclear Waste Repository." NACE International CORROSION Conference Proceedings Apr. 7-11 (2002).

(69) ASTM B265 Grade Designation.

(70) Fontana, M.G. Corrosion Engineering 3rd ed. McGraw Hill, New York (1986).

Appendix A: Thermodynamic Data for E-pH Diagrams

The following table of thermodynamic data (Table 9) was used to construct the E-pH diagrams found in section 3.1. Below this is a summary of the Excel calculations generated (Table 10). In each case: n represents the number of electrons consumed and m the number of protons. If m is a negative value, protons are produced during the reaction. The data shown here is for metal ion activity of 10^6. Y1, Y2, X1 and X2 are the intercepts associated with each reaction at both extremes. Ti data from J. Been[29] and S data from HSC Chemistry Software.

Table 9: Thermodynamic data for calculation of E-pH diagrams at 298K.

Species	State	G° (KJ/gmol)	Species	State	G° (KJ/gmol)	S° (J/gmol-K)
H+	aq	0.00	H+	aq	0.00	0.00
H2O(l)	l	-237.14	H2O(l)	l	-237.14	69.95
O2(g)	g	0.00	O2(g)	g	0.00	205.15
H2(g)	g	0.00	H2(g)	g	0.00	130.68
Ti	c	0.00	Ti	c	0.00	30.29
TiO	c	-513.63	TiO	c	-513.63	34.77
TiO2	c	-890.01	TiO2	c	-890.01	50.25
TiO2.H2O	c	-1058.50	TiO2.H2O	c	-1058.50	90.00
Ti2O3	c	-1434.73	Ti2O3	c	-1434.73	78.78
Ti(OH)3	c	-1049.80	Ti3O2	c	-1028.94	
Ti++	aq	-314.00	Ti(OH)3	c	-1049.80	80.00
Ti+++	aq	-350.00	Ti++	aq	-314.00	-58.40
TiO++	aq	-577.40	Ti+++	aq	-350.00	-242.00
TiO2++	aq	-467.20	TiO++	aq	-577.40	-135.20
TiH2	c	-4.90	TiO2++	aq	-467.20	-123.50
HTiO3-	aq	-955.90	TiH2	c	-4.90	29.70
HSO4-	aq	-756.17	HTiO3-	aq	-955.90	116.00
SO4--	aq	-744.86	HSO4-	aq	-756.17	
HS-	aq	12.07	SO4--	aq	-744.86	
S--	aq	85.80	HS-	aq	12.07	
S	c	0.00	S--	aq	85.80	
H2S	aq	-28.57	S	c	0.00	
TiO(SO4)2--	aq	-12167.25	TiS	c	-264.94	
			Ti2S3	c	-369.09	
			TiS2	c	-430.47	
			Ti2S	c	-282.58	

			H2S	aq	-28.57	78.37
			TiO(SO4)2--	aq	-12167.25101	

Table 10: Thermodynamic calculations used for E-pH diagrams.

Non Electrochemical Reactions:	**pH**	**n**	**m**	**ΔGo**	**E**
TiO++ + 2H2O --> HTiO3- + 3H+	5.60	0	3	95782	1.88
Ti++ + H2O --> TiO + 2H+	4.816	0	2	37841	5.46
TiO++ + H2O --> TiO2 + 2H+	-4.97	0	2	-73859	6.47
TiO++ + 2H2O --> TiO2.H2O+ 2H+	0.90	0	2	-6818	0.59
HTiO3- + H+ -->TiO2 + + H2O	26.73	0	-1	-169641	29.76
HTiO3- + H+ -->TiO2.H2O	14.98	0	-1	-102600	18.00
Ti+++ + 3H2O --> Ti(OH)3 + 3H+	1.68	0	3	11623	18.00
TiO++ + 2HSO4- --> TiO(SO4)2-- + 2H+	-816.8	0	2	-9321329	
TiO(SO4)2-- + H2O --> TiO.H2O + 2SO4--		0	0	9856	
Oxygen evolution	**Slope**	**n**	**m**	**Eo**	**E**
O2 + 4H+ + 4e --> 2H2O	-0.06	4	4	1.229	1.23
Hydrogen evolution	**Slope**	**n**	**m**	**Eo**	**E**
2H+ + 2e --> H2	-0.06	2	2	0.000	0.00
Sulfur	**pH**	**n**	**m**	**ΔGo**	**E**
HSO4- --> H+ + SO4--	1.98	0	1	11313	11313
H2S --> HS- + H+	7.12	0	1	40646	40646
HS- --> S-- + H+	12.92	0	1	73728	73728
Sulfur	**Slope**	**n**	**m**	**Eo**	**E**
HSO4- + 7H+ + 6e --> S + 4H2O	-0.07	6	7	0.332	0.33
SO4-- + 8H+ + 6e --> S + 4H2O	-0.08	6	8	0.352	0.35
SO4-- + 9H+ 8e --> HS- + 4H2O	-0.07	8	9	0.248	0.25
SO4-- 8H+ + 8e --> S-- + 4H2O	-0.06	8	8	0.153	0.15
S + 2H+ + 2e --> H2S	-0.06	2	2	0.148	0.15

Electrochemical Reactions:	Slope	n	m	Eo	E
Ti3+ +3e --> Ti	0.000	3	0	-1.209	-1.268
Ti2+ +2e --> Ti	0.000	2	0	-1.627	-1.716
TiO++ + 2H+ + 4e --> Ti + H2O	-0.030	4	2	-0.882	-0.926
TiO++ +2H+ +2e --> Ti++ + H2O	-0.059	2	2	-0.136	-0.136
HTiO3- + 5H+ +2e -->Ti2+ +3H2O	-0.148	2	5	0.360	0.360
TiO + 2H+ +2e --> Ti + H2O	-0.059	2	2	-1.431	-1.431
TiO2 + 4H+ + 2e --> Ti++ + 2H2O	-0.118	2	4	-0.519	-0.430
TiO2.H2O + 4H+ + 2e --> Ti++ + 3H2O	-0.118	2	4	-0.171	-0.083
TiO2 + 4H+ + e --> Ti+++ + 2H2O	-0.237	1	4	-0.664	-0.487
Ti + 2H+ + 2e --> TiH2	-0.059	2	2	0.051	0.051
TiO2.H2O + 6H+ + 6e --> TiH2 + 3H2O	-0.059	6	6	-0.608	-0.608
TiO2++ +H2O +2e --> HTiO3- + H+	0.030	2	-1	1.303	1.30
TiO2++ +2H+ +2e --> TiO++ + H2O	-0.059	2	2	1.800	1.80
TiO2++ + 2e + H2O --> TiO2.H2O	0.000	2	0	1.835	1.75
Ti+++ +e --> Ti++	0.000	1	0	-0.373	-0.37
Ti(OH)3 + H+ + e --> TiO + 2H2O	-0.059	1	1	-0.645	-0.64
Ti(OH)3 + 3H+ + e --> Ti++ + 3H2O	-0.177	1	3	-0.253	-0.08
TiO2.H2O+ H+ + e --> Ti(OH)3	-0.059	1	1	-0.090	-0.09
TiO2.H2O + 4H+ + e --> Ti+++ + 3H2O	-0.237	1	4	0.030	0.21
TiO++ +2H+ +e --> Ti+++ + H2O	-0.118	1	2	0.101	0.10
HTiO3- + 2H+ + e --> Ti(OH)3	-0.118	1	2	0.973	0.80
TiO + 4H+ +4e --> TiH2 + H2O	-0.059	4	4	-0.703	-0.70
Ti+++ + 2H+ +5e --> TiH2	-0.024	5	2	-0.715	-0.75

Appendix B: Materials Characterisation

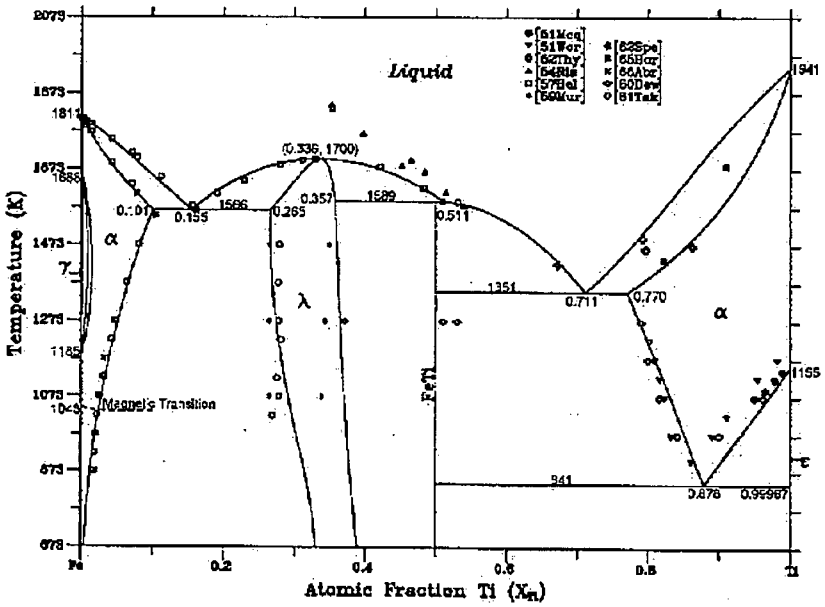

Figure 43: Phase diagram for Fe-Ti alloys.

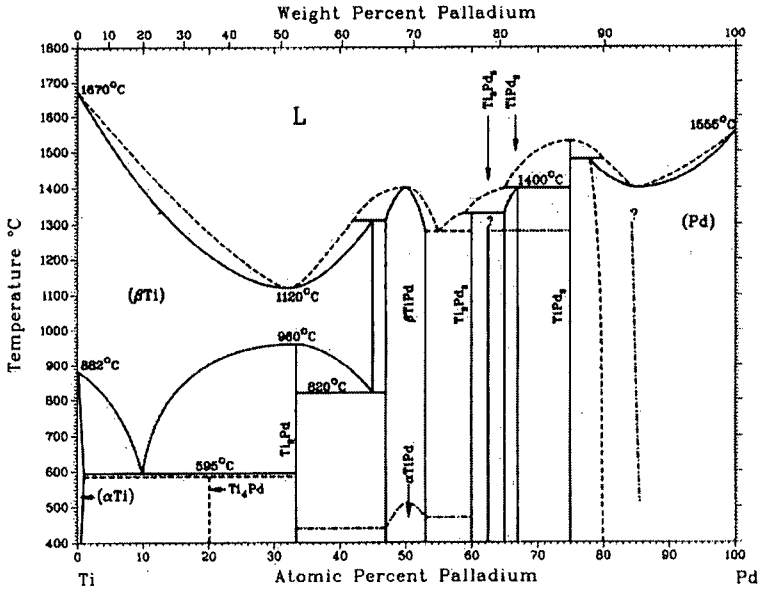

Figure 44: Phase diagram for Pd-Ti alloys.

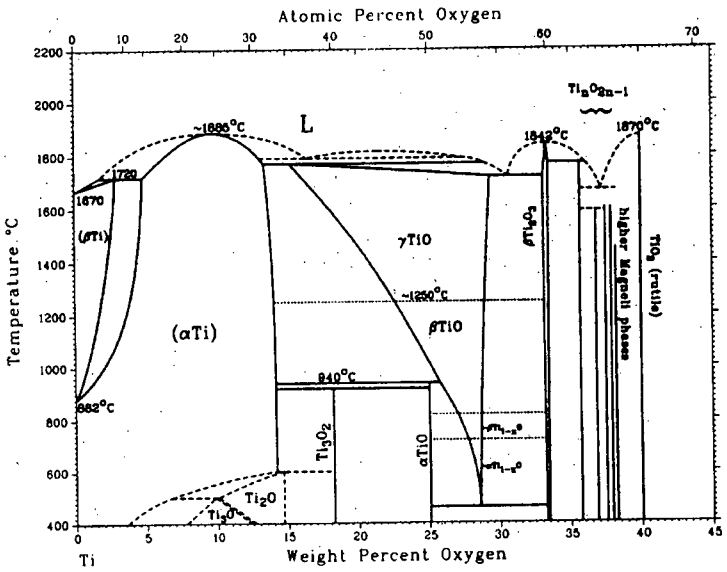

Figure 45: Phase Diagram for Ti-O alloys.

EDS Results:

Grade 1

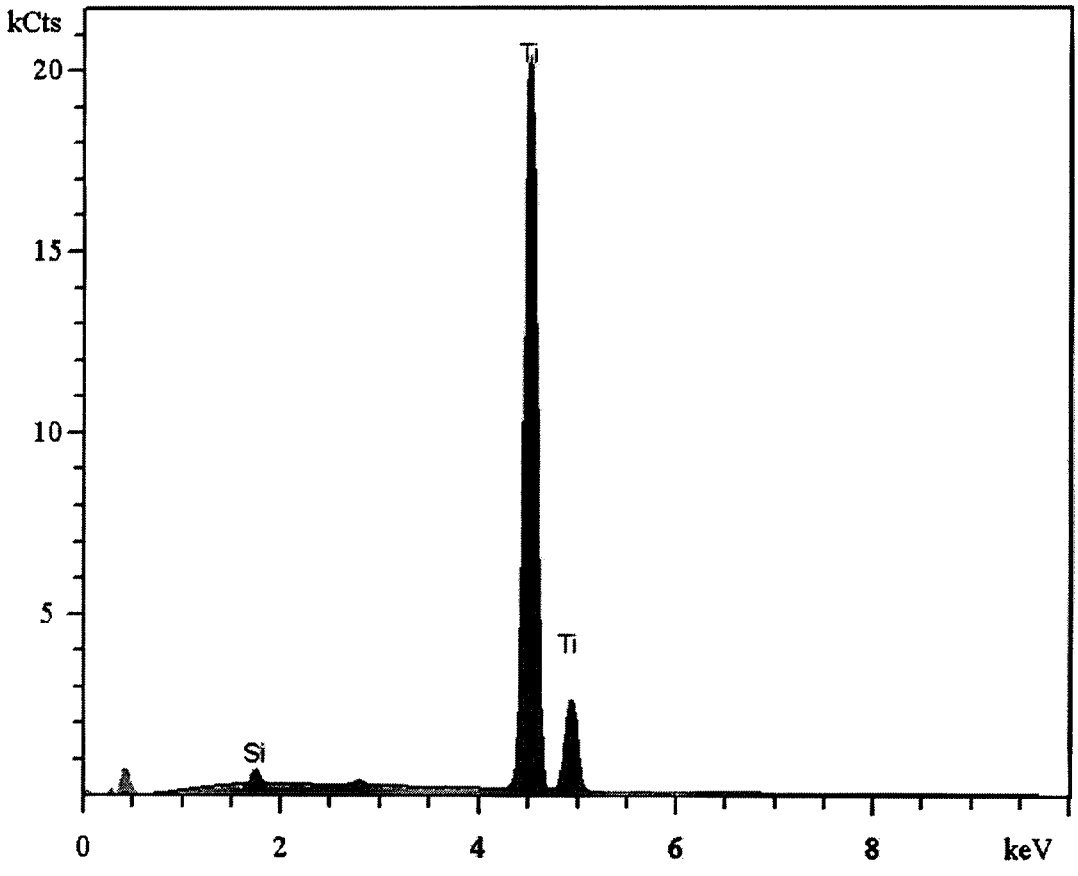

EDS Spectrum Ti grade 1

	Concentration
Silicon	0.96 wt%
Titanium	99.04 wt%

Element	Line	Method	Intensity	KRatio	ZAF	Concentration	2Sigma	Z	A	F
Si	KA	PRZ	19.14	0.007	1.452	0.96 wt%	0.055 wt%	0.876	1.670	0.992
Ti	KA	PRZ	1309.87	0.988	1.003	99.04 wt%	0.374 wt%	1.001	1.001	1.000

Grade 2

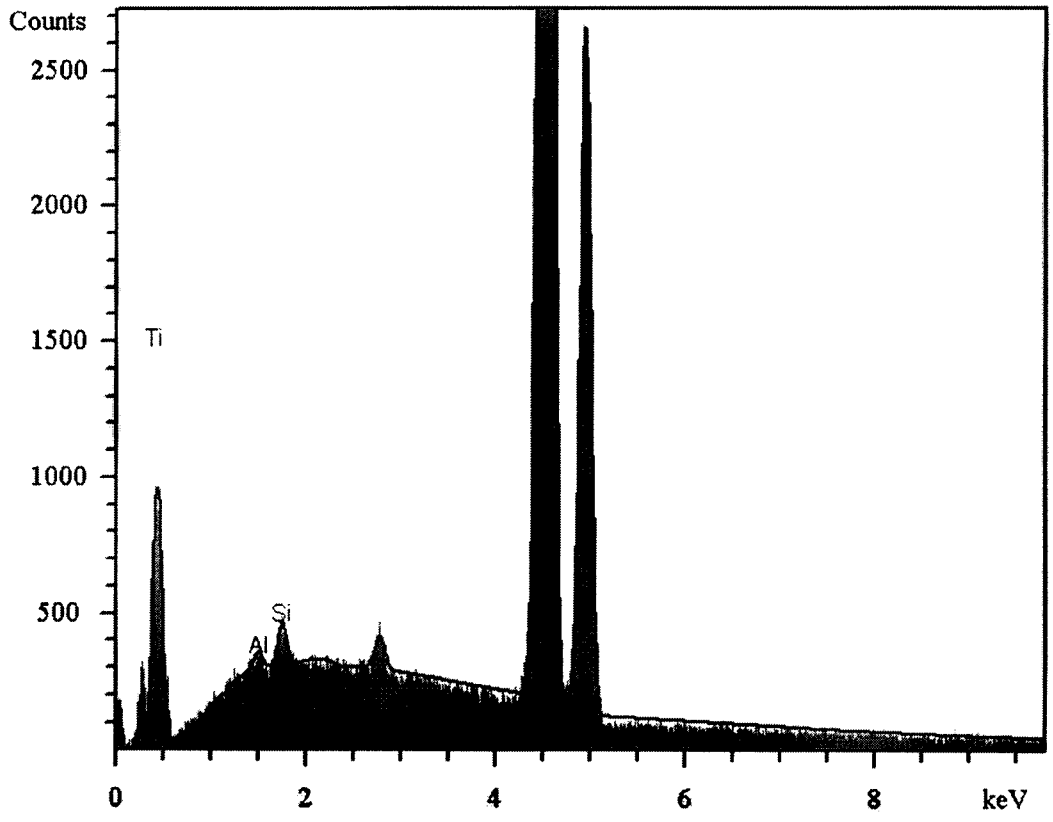

EDS Spectrum Ti grade 2

	Concentration
Silicon	2.78 wt%
Titanium	97.22 wt%
Iron	0.00 wt%

Element	Line	Method	Intensity	KRatio	ZAF	Concentration	2Sigma	Z	A	F
Si	KA	PRZ	60.59	0.019	1.444	2.78 wt%	0.054 wt%	0.878	1.656	0.992
Ti	KA	PRZ	1385.44	0.965	1.007	97.22 wt%	0.291 wt%	1.004	1.003	1.000
Fe	KA1	PRZ	0.00	0.000	1.000	0.00 wt%	0.000 wt%	1.000	1.000	1.000

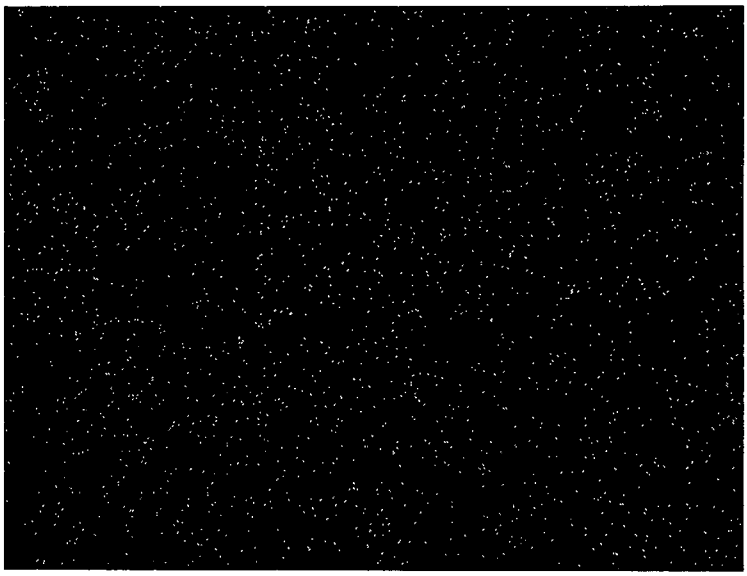

EDS Map of Fe content in Ti grade 2.

Grade 7

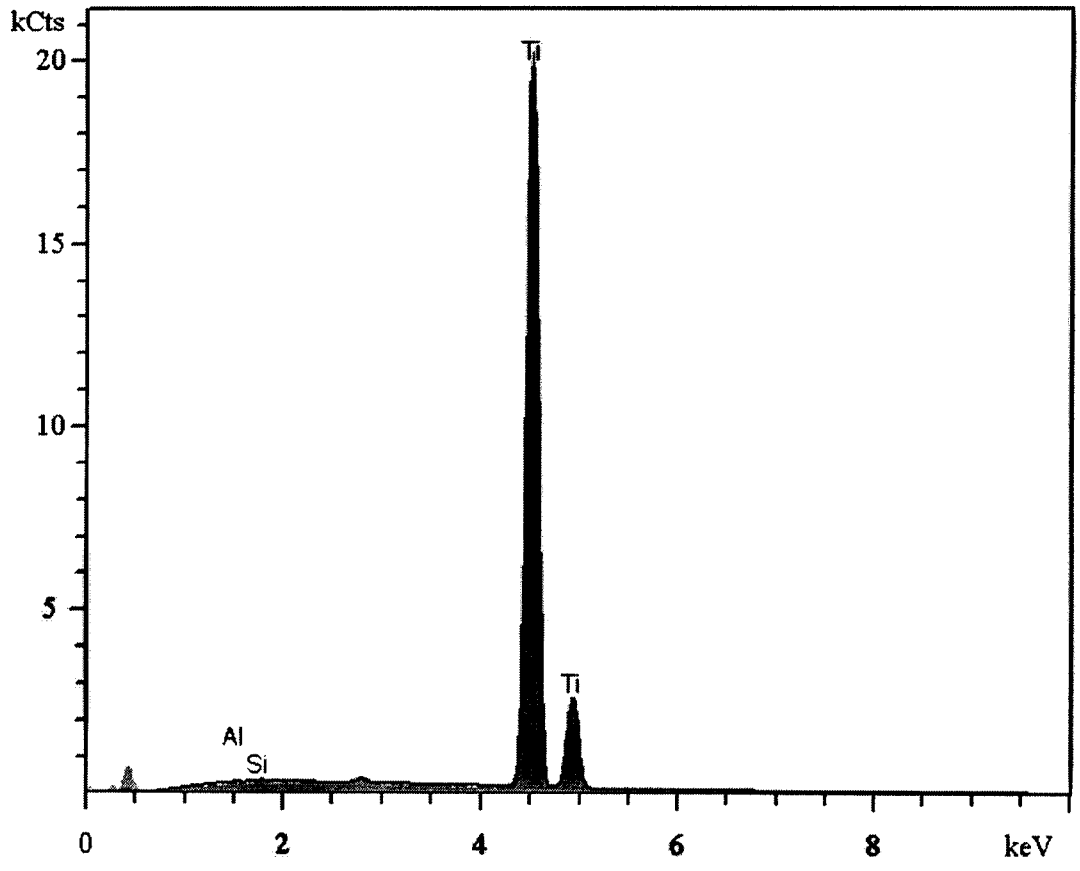

EDS Spectrum for T grade 7.

	Concentration
Aluminum	0.00 wt%
Silicon	0.08 wt%
Titanium	99.92 wt%

Element	Line	Method	Intensity	KRatio	ZAF	Concentration	2Sigma	Z	A	F
Al	KA	PRZ	0.00	0.000	1.000	0.00 wt%	0.000 wt%	1.000	1.000	1.000
Si	KA	PRZ	1.52	0.001	1.456	0.08 wt%	0.050 wt%	0.875	1.677	0.992
Ti	KA	PRZ	1299.30	0.999	1.000	99.92 wt%	0.379 wt%	1.000	1.000	1.000

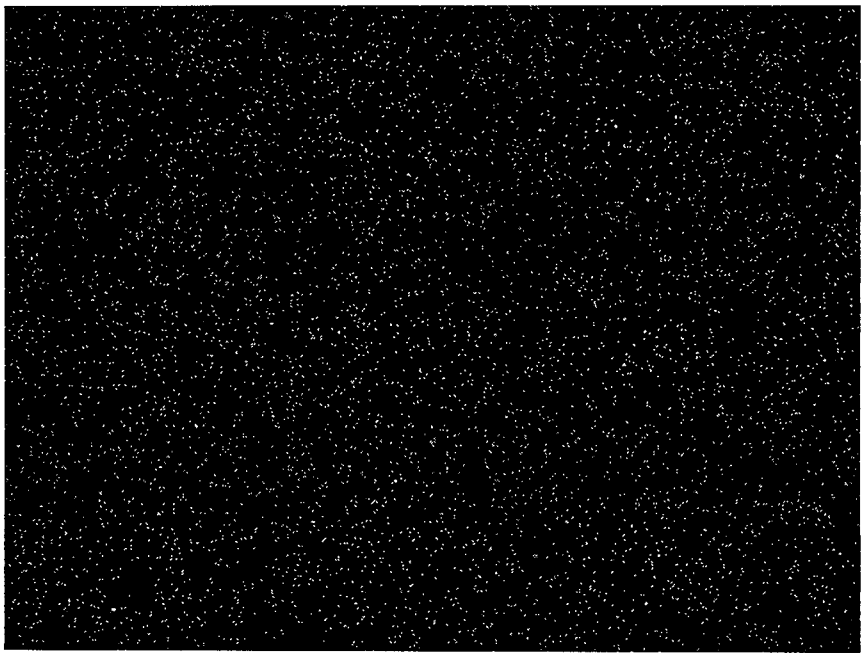

EDS Map of Pd content in Ti grade 7.

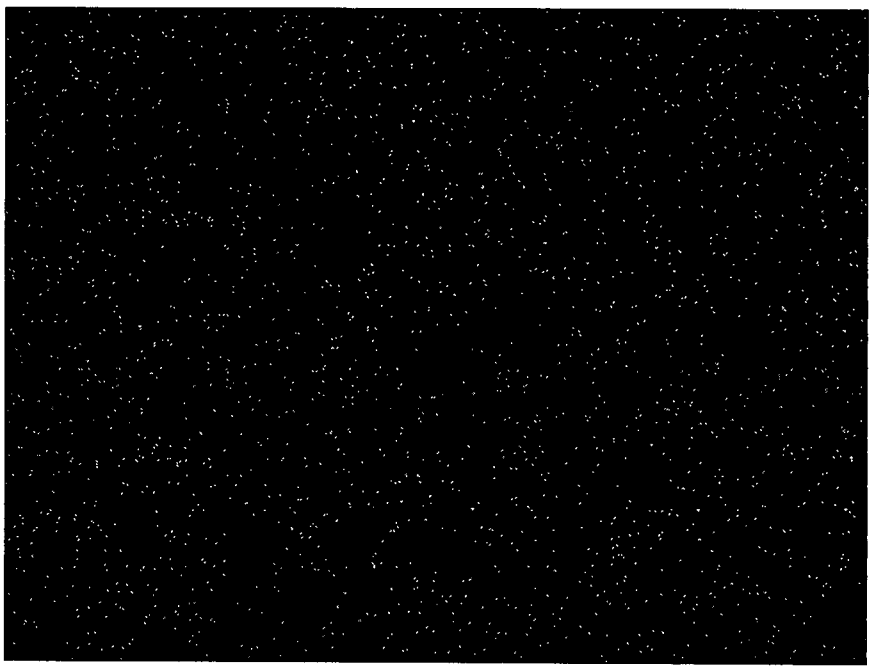

EDS Map of Fe content in Ti grade 7.

Appendix C: Data for Calculation of Liquid Junction Potentials

Table 11: Data for calculation of LJP in H2SO4 at 23°C.

	0.3 M	1 M	5 M	
zi,iv	1	1	1	H+,K+
zii,v	-1	-1	-1	HSO4-
ziii	-2	-2	-2	SO4--
ci	0.360648	1.116391	5.2691200	H+
cii	2.45E-01	9.03E-01	4.83E+00	HSO4-
ciii	6.06E-02	1.16E-01	2.69E-01	SO4--
civ	1.38E-01	1.38E-01	1.38E-01	K+
cv	6.89E-02	6.89E-02	6.89E-02	SO4--
ui	9.31E-05	9.31E-05	9.31E-05	H+
uii	1.33E-05	1.33E-05	1.33E-05	HSO4-
uiii	1.07E-05	1.07E-05	1.07E-05	SO4--

Table 12: Data for calculation of LJP in H2SO4 at 50°C.

	0.3 M	1 M	5 M	
zi,iv	1	1	1	H+,K+
zii,v	-1	-1	-1	HSO4-
ziii	-2	-2	-2	SO4--
ci	0.338415	1.072297	5.1649799	H+
cii	2.68E-01	9.47E-01	4.93E+00	HSO4-
ciii	3.84E-02	7.23E-02	1.65E-01	SO4--
civ	1.38E-01	1.38E-01	1.38E-01	K+
cv	6.89E-02	6.89E-02	6.89E-02	SO4--
ui	1.64E-04	1.64E-04	1.64E-04	H+
uii	2.34E-05	2.34E-05	2.34E-05	HSO4-
uiii	1.88E-05	1.88E-05	1.87E-05	SO4--

Table 13: Data for calculation of LJP in 0.6 M HCl at 23°C.

zi,iv	1	H+,K+
zii,v	-1	Cl-
ziii	0	SO4--
ci	0.6	H+
cii	0.6	Cl-
ciii	0	SO4--
civ	1.38E+00	K+
cv	6.89E-01	SO4--
ui	0.00009312	H+
uii	0.00002032	Cl-
uiii	0.00001065	SO4--